

(7) 131  
YN

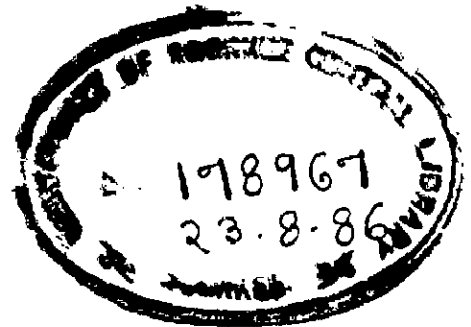
# **THERMOMECHANICAL AGEING OF 2014 ALUMINIUM ALLOY**

**A THESIS**

submitted in fulfilment of the  
requirements for the award of the degree  
of  
**DOCTOR OF PHILOSOPHY**  
in  
**METALLURGICAL ENGINEERING**

By

**SURENDRA SINGH**



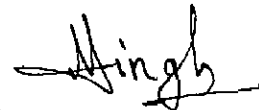
**DEPARTMENT OF METALLURGICAL ENGINEERING  
UNIVERSITY OF ROORKEE  
ROORKEE-247 667 (INDIA)**

October, 1985

## CANDIDATE'S DECLARATION


I hereby certify that the work which is being presented in the thesis entitled **THERMOMECHANICAL AGEING OF 2014 ALUMINIUM ALLOY** in fulfilment of the requirement for the award of the Degree of Doctor of Philosophy, submitted in the Department of **METALLURGICAL ENGINEERING** of the university is an authentic record of my own work carried out during a period from March, 1977 to August, 1985 under the supervision of Dr.D.B.GOEL.

The matter embodied in this thesis has not been submitted by me for the award of any other degree.



(SURENDRA SINGH)  
Lecturer,  
Dept. of Metallurgical Eng.,

This is to certify that the above statement made by the candidate is correct to the best of my knowledge.



(D.B. GOEL)  
Prof. and Head  
Dept. of Metallurgical Eng.,  
University of Roorkee,  
Roorkee (INDIA)

DATE: 14.10.1985

## ACKNOWLEDGEMENT

The author is highly indebted to Dr. D. B. Goel, Professor and Head, Department of Metallurgical Engineering, University of Roorkee, Roorkee, for his expert guidance and unfailing inspiration throughout the course of this investigation and preparation of the thesis. His valuable suggestions at various stages and thought provoking discussions have immensely contributed to this thesis for which the author wishes to record his deep sense of gratitude to him.

Thanks are due to Prof. Kailash Chandra, Director, USIC, University of Roorkee, for providing the facilities for transmission and scanning electron microscopic studies.

A very keen interest shown by Dr. E. S. Dwarakadasa, Professor, Department of Metallurgy, Indian Institute of Science, Bangalore, in this work and his valuable suggestions for fractographic studies are gratefully acknowledged.

The author is grateful to Dr. P. S. Misra, Reader, Department of Metallurgical Engineering, University of Roorkee and Mr. K. K. Sharma, Scientist, DMRL, Hyderabad, for their help in the Electron Probe Microanalyses.


The author wishes to record his appreciation for the help rendered by Mr. M. E. Haque, Reader, School of Hydrology, University of Roorkee, in preparation of this thesis. The author also wishes to thank all his colleagues and friends, who have directly or indirectly helped at various stages during this work.

It remains to express the sincere thanks for the assistance and active cooperation rendered by the technical staff, particularly M/S N. K. Saini (USIC), S. C. Kaushik, S. P. Kush

and S.K. Seth during experimentation, and for the excellent draftsmanship of Mr. M.C. Vaish as also for the flawless typing by Mr. R.C. Sharma.

The author is also thankful to his wife and children who have shown extreme perseverance and made him free from various family obligations during the course of this research work.

Roorkee, Oct. 14, 1985.

  
(SURENDRA SINGH)

ABSTRACT

The 2014 Al-alloy has a nominal composition: 4.40 Cu, 0.40 Mg, 0.80 Si, 0.80 Mn (Wt.pct.) and Fe as impurity element. Although this alloy has its own importance in the aircraft industry due to high hardness and high strength, its effective application is significantly hampered because of the poor secondary properties like fatigue strength and fracture toughness. The results reported in the literature on the influence of thermomechanical ageing (TMA) on fatigue properties of this alloy are not consistent. As far as the fracture toughness is concerned the presence of dispersoids/inclusions is reported to be detrimental. Combined influence of dispersoids and the microstructure developed as a result of TMA, however, has not been studied systematically to date. The present investigation has, therefore, been undertaken to explore the best combination of thermal and mechanical treatments, which may eliminate or minimise the density of dispersoids and modify suitably the microstructure so as to cause an overall improvement of primary as well as secondary mechanical properties.

The 2014 Al-alloy of commercial purity was prepared, homogenised at 500°C and hot rolled at 425 °C to desired cross sections. Various properties were measured in the following conditions:

- (i) As Quenched (AQ): solution treatment at 500°C, followed by ageing.

- (ii) Peak ageing (PA): artificial ageing of as quenched (AQ) alloy at 160°C to peak hardness level.
- (iii) TMA I            a : 25 pct. preageing (ageing for a period corresponding to a hardness which is 25 pct. of the peak hardness obtained in PA treatment), followed by 10 pct. warm rolling (i.e. 10 pct. reduction in thickness), followed by further ageing upto peak hardness value.
- b : 25 pct. preageing, followed by 20 pct. warm rolling, followed by further ageing upto peak hardness value.
- (iv) TMA II            a : 50 pct. preageing, followed by 10 pct. warm rolling, followed by further ageing upto peak hardness value.
- b : 50 pct. preageing, followed by 20 pct. warm rolling, followed by further ageing upto peak hardness value.

In all the above treatments, warm rolling and ageing were carried out at 160°C.

Tests were conducted to determine hardness, tensile properties, fatigue properties and fracture toughness after various treatments. Optical and transmission electron microscopic (TEM) studies were conducted to study the effect of various thermomechanical ageing treatments on the structural changes and the density of dispersoids. Scanning electron microscopy (SEM) was used to study the characteristics of fracture surfaces after fatigue failure and the

role played by the dispersoids on the crack initiation during fatigue of samples after different TMA treatments.

TEM studies reveal the formation of  $\theta''$  and  $\theta'$  during peakageing. Formation of  $\theta''$  is suppressed by the TMA treatments. Optical microscopy and electron probe microanalysis (EPMA) show two types of dispersoids: (i) dark etching, irregular shaped  $Al_{12}(Fe, Mn)_3Si$  and (ii) light etching nearly rounded  $Al_4CuMg_5Si_4$ . The TMA treatments reduce the density of these dispersoids.

A significant improvement in the various mechanical properties is observed after various thermomechanical ageing treatments. It is observed, for both 10 and 20 pct. deformations, that the peak hardness increases with pre-ageing, attains maximum at 50 pct. preageing. At 75 pct. preageing it again decreases. The effect of thermomechanical treatment on mechanical properties has, therefore, been studied only for 25 pct. preaged (TMA Ia and TMA Ib) and 50 pct. preaged (TMA IIa and TMA IIb) conditions in the present investigation. Among all the TMA treatments the maximum improvement in the hardness, tensile strength and fracture toughness has been achieved through TMA IIb treatment. It is also seen that the TMA IIb treatment not only imparts maximum improvement but also provides maximum stability to tensile properties when exposed to higher working temperatures.

The fatigue properties for as quenched, peak aged

and thermomechanically aged samples have been studied for various stress levels ranging from  $98 \text{ N/mm}^2$  to  $177 \text{ N/mm}^2$ . It is observed that at any stress level the alloy in the PA condition has lower fatigue life than in AQ condition. Further it is also observed that at any stress level the fatigue life is higher for thermomechanically aged specimen as compared to AQ and PA specimens. The best fatigue properties are observed in the alloy after TMA Ib treatment. It is also seen that for any value of fatigue life the corresponding endurance limit after TMA Ib treatment is constantly higher by a margin of 25 to 35  $\text{N/mm}^2$  from the values obtained in the peak aged condition, throughout the range of investigation.

It is observed that the TMA Ib and TMA IIB treatments enhance the  $K_{IC}$  value from peak aged condition by about 30 pct. In case of V-notch Charpy test for dynamic fracture toughness ( $K_{Id}$ ), however, the TMA IIB treatment is more effective than TMA Ib. The  $K_{Id}$  value obtained after TMA Ib is  $1060.00 \text{ N/mm}^{3/2}$ , whereas after TMA IIB treatment it is  $1168.00 \text{ N/mm}^{3/2}$ . The effect of the amount of deformation on  $K_{IC}$  and  $K_{Id}$  values is almost similar; but in general the  $K_{Id}$  values are higher than  $K_{IC}$  values after any TMA treatment.

The TMA treatments have been observed to affect substantially the ageing characteristics and the resultant microscopic structure of the alloy. The maximum effect on  $e'$



nucleation appears to be in the TMA Ib treatment which yields finest  $\theta'$  needles having the longitudinal dimension of approximately  $400 \overset{\circ}{\text{A}}$ . The TMA IIb treatment yields  $\theta'$  of intermediate fineness ( $600 \overset{\circ}{\text{A}}$ ). It is also observed that all the TMA treatments suppress the formation of  $\theta''$  platelets.

The TMA I and TMA II treatments, besides affecting the ageing kinetics, also lead to precipitate-dislocation networks of different magnitudes, which affect the resultant mechanical properties of the alloy. In the present study it is observed that TMA IIb treatment results in thickest dislocation-precipitate tangles among all the thermomechanical treatments.

The SEM studies show all fatigue fractures to be apparently transcrystalline and there is no instance of intergranular failure. The present investigation reveals that in high cycle fatigue the failure occurs by (i) formation and interaction of surface striations and (ii) dispersoid/matrix decohesion.

The results of the present investigation are observed to be influenced by the presence of dispersoids and by the size, shape and distribution of precipitates formed during various treatments. The increase in hardness and tensile properties as a result of TMA treatment is observed due to (i) reduction in density of dispersoids, (ii) increase of nucleation sites for  $\theta'$  precipitation leading to a fine distribution of  $\theta'$  and (iii) formation of dislocation-particle

tangles.

Best fatigue properties are observed in TMA Ib treated sample, as this treatment results in the finest distribution of  $\theta'$  and minimum density of dispersoids. The  $\theta'$  particles restrict the growth of fatigue crack fronts. The failure due to dispersoid-matrix decohesion is also greatly reduced after this treatment due to a very low density and a fine size of dispersoids.

The various structural parameters, which are observed to affect fracture toughness, are (i)  $\theta'$ ; (ii) density and distribution of dispersoids and (iii) dislocation substructure. The parameters, which are observed to increase tensile strength of the alloy, are also observed to increase plane strain fracture toughness ( $K_{IC}$ ). In the case of dynamic fracture toughness ( $K_{Id}$ ), however, the dispersoids are also observed to play a vital role.

From the present investigation it is established that through appropriate thermomechanical ageing it is possible to produce a desired microstructure, which may not only result in improved tensile properties, but also improved fracture toughness and fatigue properties in the 2014 Al alloy. It is observed that, among all the TMA treatments, the TMA IIb treatment provides maximum improvement in all the measured properties except fatigue. The endurance limit observed in TMA IIb treated alloy is only slightly lower than that observed after TMA Ib, which is observed to

The effect of thermomechanical ageing treatment on various mechanical properties observed in the present investigation is discussed on the basis of various structural parameters in Chapter 5.

Conclusions and suggestions for further work in this field of study are given in Chapter 6.

tangles.

Best fatigue properties are observed in TMA Ib treated sample, as this treatment results in the finest distribution of  $\theta'$  and minimum density of dispersoids. The  $\theta'$  particles restrict the growth of fatigue crack fronts. The failure due to dispersoid-matrix decohesion is also greatly reduced after this treatment due to a very low density and a fine size of dispersoids.

The various structural parameters, which are observed to affect fracture toughness, are (i)  $\theta'$ ; (ii) density and distribution of dispersoids and (iii) dislocation substructure. The parameters, which are observed to increase tensile strength of the alloy, are also observed to increase plane strain fracture toughness ( $K_{IC}$ ). In the case of dynamic fracture toughness ( $K_{Id}$ ), however, the dispersoids are also observed to play a vital role.

From the present investigation it is established that through appropriate thermomechanical ageing it is possible to produce a desired microstructure, which may not only result in improved tensile properties, but also improved fracture toughness and fatigue properties in the 2014 Al alloy. It is observed that, among all the TMA treatments, the TMA I Ib treatment provides maximum improvement in all the measured properties except fatigue. The endurance limit observed in TMA I Ib treated alloy is only slightly lower than that observed after TMA Ib, which is observed to

be next best treatment for general improvement of mechanical properties.

The entire work reported in this thesis has been spread over six chapters.

Chapter 1 deals with the critical review of the available literature on thermomechanical processing of Al-alloys. Various concepts concerning morphology, size and distribution of precipitates and dispersoids and their interaction with dislocations have been critically examined in the light of present date theories. Influence of sequences employed during thermomechanical processing on various mechanical properties viz. tensile, fatigue- and fracture toughness properties has been reviewed.

In Chapter 2 the problem of the present investigation has been formulated and posed on the basis of the perspective of present investigation.

Chapter 3 describes details of experimental set-up; alloy and sample preparation; method and machines used for measuring the various properties and corresponding microstructural changes.

The results of various microstructural characteristics, mechanical properties, namely hardness, tensile properties, fatigue and fracture toughness of TMA treated alloy samples have been presented in different sections of Chapter 4.

The effect of thermomechanical ageing treatment on various mechanical properties observed in the present investigation is discussed on the basis of various structural parameters in Chapter 5.

Conclusions and suggestions for further work in this field of study are given in Chapter 6.

## C O N T E N T S

Chapter	Page
ACKNOWLEDGEMENTS	... i
ABSTRACT	... iii
LIST OF FIGURES	...xiii
LIST OF TABLES	...xvii
1 LITERATURE REVIEW	... 1
1.1 Introduction	... 1
1.2 The Phenomenon of Precipitation	... 4
1.2.1 Historical review	... 4
1.2.2 Clustering	... 12
1.2.3 Zone formation and their growth	... 13
1.2.4 Intermediate precipitates	... 14
1.2.5 Equilibrium precipitate	... 15
1.2.6 General conclusions on precipitation phenomenon	... 16
1.3 Precipitation Behaviour of 2014 Al-Alloy	... 20
1.4 Effect of TMA Treatments on Ageing Characteristics of Al-Alloys	... 23
1.5 Effect of TMA Treatments on Various Properties of Al-Alloys	... 27
1.5.1 Tensile properties	... 27
1.5.2 Fatigue properties	... 29
1.5.3 Fracture toughness	... 33
2 FORMULATION OF PROBLEM	... 46
3 EXPERIMENTAL PROCEDURE	... 50
3.1 Alloy Preparation	... 50
3.2 Ageing and Thermomechanical Ageing Treatment	... 51
3.2.1 Peak ageing treatment	... 51
3.2.2 Preageing treatment	... 54
3.2.3 Mechanical working and final ageing	... 54

Chapter	Page
3.3 Hardness Measurements	... 55
3.4 Tensile Properties	... 55
3.5 Fatigue Properties	... 55
3.6 Fracture Toughness Measurements	... 58
3.7 Metallographic Studies	... 61
4 RESULTS AND ANALYSIS	... 62
4.1 Effect of Ageing on Mechanical Properties	... 62
4.2 Effect of Thermomechanical Ageing (TMA) on Various Mechanical Properties	... 67
4.3 Transmission Electron Microscopic (TEM) Studies	... 91
4.4 Scanning Electron Microscopic (SEM) Studies of Fatigue Failure	... 97
4.5 Optical Microscopic Studies	... 114
5 DISCUSSION	... 125
5.1 Effect of Thermomechanical Ageing (TMA) on Structural Characteristics	... 126
5.2 Effect of Thermomechanical Ageing (TMA) on Strengthening Behaviour	... 135
5.3 Effect on Fatigue Properties	... 145
5.4 Effect on Fracture Toughness	... 152
5.5 Choice of Thermomechanical Ageing Treatment	... 161
6 CONCLUSIONS AND SUGGESTIONS FOR FUTURE WORK	... 164
6.1 Conclusions	... 164
6.2 Suggestions for Future Work	... 166
REFERENCES	... 168
APPENDIX: Tables of Experimental Results	... 185



## List of Figures

Fig.No.	Caption	Page
1.1	The basic modes of crack surface displacements	... 34
3.1	Specimen for tensile test	... 56
3.2	Specimen for fatigue test	... 57
3.3	Double edge-notched (EN) specimen for plane strain fracture toughness test (ASTM E24)	... 59
3.4	Charpy V-notch specimen for dynamic fracture toughness test (ASTM E23)	... 60
4.1	Effect of ageing on hardness	... 63
4.2	Effect of ageing on tensile properties	... 65
4.3	Effect of ageing on fatigue properties	... 66
4.4	Ageing curves for thermomechanically processed 2014 Al-alloy at 160°C	... 69
4.5	Ageing curves for thermomechanically processed 2014 Al-alloy at 160°C	... 70
4.6	Effect of preageing on peak hardness	... 72
4.7	Effect of thermomechanical ageing on tensile properties	... 74
4.8	Peak UTS values after different thermomechanical treatments and after 100 hour exposure at different temperatures	... 75
4.9	Peak YS values after different thermomechanical treatments and after 100 hour exposure at different temperatures	... 76
4.10	Peak values of pct. elongation after different thermomechanical treatments and after 100 hour exposure at different temperatures	... 77
4.11	Effect of thermomechanical ageing on fatigue properties	... 79
4.12	Effect of thermomechanical ageing and applied stress on fatigue life	... 81

Fig. No.	Caption	Page
4.13	The relationship between $K_{IC}$ and YS	... 84
4.14	The relationship between $K_{Id}$ and YS	... 85
4.15	Effect of thermomechanical ageing on $K_{IC}$	... 86
4.16	Effect of thermomechanical ageing on $K_{Id}$	... 87
4.17	Relationship between dynamic fracture toughness parameter ( $K_{Id}^2/E$ ) and energy absorbed per unit area (CVN/A)	... 90
4.18	Transmission electron micrographs showing the existence of $\theta''$ , $\theta'$ and dispersoids in peak aged condition (a and b different locations)	... 92
4.19	Transmission electron micrographs showing the existence of predominantly $\theta''$ platelets together with small amount of $\theta'$ in peak aged condition (a and b different locations)	... 93
4.20	Comparison of transmission electron micrographs (a) peak aged (b) TMA Ib and (c) TMA IIb treated specimens	... 95
4.21	Transmission electron micrographs of (a) TMA IIa and (b) TMA IIb treated specimens	... 96
4.22	Transmission electron micrographs of TMA IIb treated specimen showing thick dislocation-precipitate tangles (a and b different locations)	... 98
4.23	Transmission electron micrographs of TMA Ib treated specimen showing dislocation-precipitate tangles (a and b different locations)	... 99
4.24	Transmission electron micrographs of TMA Ia treated specimen showing dislocation-precipitate tangles (a and b different locations)	... 100
4.25	Transmission electron micrographs of TMA IIa treated specimen showing dislocation-precipitate tangles (a and b different locations)	... 101

Fig.No.	Caption	Page
4.26	Low magnification SEM fractographs of fatigue tested samples (a) as quenched (b) peak aged (c) TMA Ib and (d) TMA Iib	... 102
4.27	Straight, parallel and regularly spaced striations in fatigue tested as quenched sample	... 104
4.28	Wavy striations in fatigue tested as quenched sample	... 104
4.29	Dimple network in fatigue tested as quenched specimen showing crack along the striations (a and b different locations)	... 105
4.30	Nearly straight striations in fatigue tested peak aged sample (a and b different locations)	... 106
4.31	Ill defined primary dimples surrounded by high density of irregular and broken up striations in peak aged sample (a and b different locations)	... 107
4.32	Network of close loop striations in fatigue tested specimens (a) TMA Ia (b) TMA Ib	... 109
4.33	Close loop striations in fatigue tested specimens (a) TMA IIA (b) TMA IIB	... 110
4.34	Fine network of secondary dimples on walls of primary dimples (a) TMA Ia (b) TMA IIA	... 112
4.35	Formation of fatigue cracks along tangles of striations in TMA Ib treated sample (a and b different locations)	... 113
4.36	Formation of void due to growth of cracks from different fronts in TMA Ia treated sample	... 115
4.37	Coalescence of microvoids leading to failure (a) as quenched (b) peak aged (c) TMA Ib and (d) TMA Iib	... 116
4.38	Dispersoids observed on the fracture surface (a) as quenched (b) peak aged	... 117
4.39	Formation of cracks along particle-matrix interfaces (a) as quenched (b) TMA Ia	... 118
4.40	Line scan of various elements in dispersoids (a) $Al_{12}(Fe, Mn)_3Si$ (b) $Al_4CuMg_5Si_4$	... 120
4.41	Optical micrographs showing (i) light etching $Al_4CuMg_5Si_4$ and (ii) dark etching $Al_{12}(Fe, Mn)_3Si$ dispersoids (a) as quenched (b) Peak aged	... 121

Fig.No.	Captions	Page
4.42	Optical micrographs showing dispersoids (a) TMA Ia (b) TMA Ib	... 123
4.43	Optical micrographs showing dispersoids (a) TMA IIa (b) TMA IIb	... 124
5.1	Schematic representation of free energy versus composition curves for various phases during ageing	... 129
5.2	Change in peak UTS values after 100 hour exposure at different temperatures	... 142
5.3	Change in peak YS values after 100 hour exposure at different temperatures	... 143
5.4	Change in peak values of elongation after 100 hour exposure at different temperatures	... 144
5.5	Relationship between fatigue ratio and fatigue life	... 153
5.6	$K_{Ic}$ as a function of center to center spacing $\lambda$ of dispersoids	... 158
5.7	Effect of space-to-size ratio $\lambda/d$ of dis- persoids on $K_{Id}$	... 160
5.8	Percent increase in various properties from peak age value after different TMA treatments	... 163

## List of Tables

Table No	Title	Page
1.1	Chemical composition limits of 2014 Al-alloy	... 5
1.2	Properties of 2014 Al-alloy	... 6
1.3	Common precipitation hardenable alloys	... 17
1.4	Correction factors for a double edge-notched strip	... 37
1.5	Effect of TMA treatments on properties of various Al-alloys	... 41
3.1	Nominal and actual compositions of 2014 Al-alloy	... 52
3.2	Detail of treatments employed in the present investigation	... 53
APPENDIX		
1	Hardness and tensile properties during ageing at 160°C	... 185
2.	Hardness and tensile properties during TMA Ia treatment	... 186
3.	Hardness and tensile properties during TMA Ib treatment	... 187
4.	Hardness and tensile properties during TMA IIa treatment	... 188
5.	Hardness and tensile properties during TMA IIb treatment	... 189
6.	Hardness values during ageing at 160°C after 75 pct. preageing and 10 pct. deformation	... 190
7.	Hardness values during ageing at 160°C after 75 pct. preageing and 20 pct. deformation	... 191

Table No.	Title	Page
8.	Hardness values on subsequent ageing after peak ageing and 10 pct. deformation ...	192
9.	Hardness values on subsequent ageing after peak ageing and 20 pct. deformation ...	192
10.	Peak age values of hardness and tensile properties after different treatments ...	193
11.	Room temperature tensile properties of peak aged alloy after 100 hour exposure at various temperatures ...	193
12.	Room temperature tensile properties of TMA Ia treated alloy after 100 hour exposure at various temperatures ...	194
13.	Room temperature tensile properties of TMA Ib treated alloy after 100 hour exposure at various temperatures ...	194
14.	Room temperature tensile properties of TMA IIa treated alloy after 100 hour exposure at various temperatures ...	195
15.	Room temperature tensile properties of TMA IIb treated alloy after 100 hour exposure at various temperatures ...	195
16.	Fatigue properties of as quenched alloy at various stress levels ...	196
17.	Fatigue properties of peak aged alloy at various stress levels ...	196
18.	Fatigue properties of TMA Ia treated alloy at various stress levels ...	197
19.	Fatigue properties of TMA Ib treated alloy at various stress levels ...	197
20.	Fatigue properties of TMA IIa treated alloy at various stress levels ...	198
21.	Fatigue properties of TMA IIb treated alloy at various stress levels ...	198
22.	Fatigue life at various endurance limits (derived from Fig.4.11) ...	199
23.	Plane strain fracture toughness data ...	200

Table No.	Title		Page
24.	Dynamic fracture toughness data	...	201
25.	Space-to-size ratio ( $\lambda/d$ ) of dispersoids after various treatments	...	202
26.	Increase in various properties from peak age value after different TMA treatments	...	203

\*\*\*\*\*

CHAPTER 1

LITERATURE REVIEW

\*\*\*\*\*



## CHAPTER-1

### LITERATURE REVIEW

#### 1.1 INTRODUCTION

Aluminium and its alloys are selected as materials of construction in many fields because of their low weight to volume ratio, ability to resist corrosion and capability of undergoing precipitation hardening treatment. These alloys can be safely used at low temperatures, but they start losing their strength when exposed to higher temperatures, primarily due to coarsening of the second phase precipitated particles which are responsible for strengthening at lower temperatures. However, as has been reported by several workers in different series of Al-alloys, it should be possible to introduce a dislocation substructure which can withstand the effect of elevated temperatures without much loss in hardness and strength [1-6]. Thus, such a substructure should be a source of strength at elevated temperatures and responsible for controlling the coarsening of precipitate particles even at elevated temperatures.

Both wrought and casting Al-alloys may be divided into two groups, (i) those which require heat treatment \*

to develop their full properties and (ii) those which do not respond to heat treatment.

The alloys which are not heat treatable depend for their properties on the normal solution in Al of the alloying elements. These alloys are not as strong as some of the heat treatable ones, but in general they may be appreciably strengthened by cold working and by other strengthening techniques. Heat treatable Al-alloys are given solution treatments at temperatures between  $450^{\circ}\text{C}$  and  $550^{\circ}\text{C}$ , as a result of which the solubility of certain alloying elements, which are only slightly soluble at room temperature, is increased appreciably. In order to retain the dissolved elements in solution the alloys are quenched, thus becoming supersaturated with respect to these elements. This produces a metastable state, and on ageing or thermomechanical processing, a certain amount of controlled precipitation occurs and as a result, an improvement in mechanical properties and fatigue strength is observed.

The greater number of Al-alloys are available for use in the form of castings than in the form of wrought products. Limitations involved in shaping the metal into various wrought products causes restriction in the use of many of the alloys in the wrought forms.

The superiority in fatigue strength of the

wrought Al-alloy products over cast alloys is what would be expected. Wrought metal products usually originate from cast ingots. Depending upon the quality of such ingots, the various metal working processes involved in producing wrought products may have beneficial effects of the fatigue properties in the final products. Most of the undesirable conditions obtained in the ingots can be modified or corrected, so that the ultimate fabricated products yield improved fatigue properties.

A comparative study shows that the ratios of fatigue strength to ultimate tensile strength for non heat treatable alloys generally lie between 0.45 and 0.6 (and are comparable with the corresponding ratios for mild steel); whereas the ratios for heat treated materials are relatively much lower, ranging from .2 to .35.

In the 2000 series of Al-alloys Cu is one of the most important alloying ingredients, because of its appreciable solubility and its strengthening effect. Many commercial alloys contain Cu, either as the major addition or among the principal alloying elements, in concentrations of 1 to 10 pct. It imparts substantial precipitation hardening characteristics to many of these alloys. Mg is used in combination with Cu, to accelerate and increase age hardening at room temperature.

Al-Cu-Mg alloys were introduced over seventy years ago. The first alloy, modified and now designated 2017 was discovered by Wilm [7] and is still in limited use, chiefly for rivets. The development of 2014 alloy utilized the effect of Si to make an Al-Cu-Mg alloy that is more susceptible to artificial ageing than 2017. This response to artificial ageing provides a desirable high level of strength unobtainable in naturally aged 2017 or 2014 alloy. Although 2014 Al-alloy was used initially as a high-strength forging alloy, it is now available in a range of wrought products and is widely used in structural applications, heavy duty forgings, truck frames, power shovel bails and aircraft fittings. The nominal composition and properties of 2014 Al-alloy are given in Table 1.1 and 1.2 respectively.

## 1.2 THE PHENOMENON OF PRECIPITATION

### 1.2.1 Historical Review

The phenomenon of age hardening was discovered by Alfred Wilm [7,8] in the years 1903-1911. It was observed that Al-Cu Alloys, when quenched from elevated temperatures, harden with time at room temperature. Hence the name age hardening was given to the phenomenon. The term precipitation hardening is also used to denote this phenomenon, because hardening takes place due to the

Table 1.1

Chemical Composition Limits of 2014 Al-alloy

Elements	Nominal Range (wt.pct.)
Copper	3.9-5.0
Silicon	0.5-1.2
Manganese	0.4-1.2
Magnesium	0.2-0.8
Aluminium	Balance

Table 1.2

## Properties of 2014 Al-Alloy

1. Density	: $2.80 \times 10^3$ Kgm/m <sup>3</sup> at 20°C
2. Liquidus Temperature	: 635°C
3. Solidus Temperature	: 510°C
4. Thermal Expansion	: (20 to 100°C) 23 $\mu\text{m}/\text{m}/^\circ\text{C}$
5. Specific heat	: 0.23 KCal/Kgm at 100°C
6. Thermal conductivity	: 144 KCal/hr-m-°C
7. Electrical volume conductivity	: 50 pct. IACS
8. Electrical resistivity	: 44 n ohm-m at 20°C
9. Hot working Temperature Range	: 260 to 480°C
10. Directional Properties	: In sheet, tensile strength and elongation are approximately equal in longitudinal and transverse directions. In forgings transverse tensile strength is same as longitudinal; transverse elongation is approximately 70 pct. of longitudinal

Table continued

Table 1.2 continued

11. Mechanical Properties:					
Temper	UTS (N/mm <sup>2</sup> )	YS (N/mm <sup>2</sup> )	Elongation (Pct.)	Hardness (BHN)	Fatigue Limit* (N/mm <sup>2</sup> )
O	186	98	18	45	90
T4	433	293	20	105	140
T6	489	419	13	135	125

\* Fatigue limit based on 500,000,000 cycles using R.R.Moore type rotating beam machine.

12. Heat treatment :			
Purpose		Temperature	Time
Complete Annealing	(O)	415 $\pm$ 5 <sup>o</sup> C	2 to 3 hrs, then furnace cooled
Solution Heat Treatment	(W)	500 $\pm$ 5 <sup>o</sup> C	1.50 hrs for small section, then water quench
Precipitation Hardening (Artificial)	(T6)	160 $\pm$ 5 <sup>o</sup> C	8 to 12 hrs.

process of precipitation from a supersaturated solid solution. This fact was brought home by Merica et al [9] in 1921 by carrying out a detailed study of the process.

From a metallurgical view point, it is nucleation and growth type of transformation in which atomic rearrangement is involved mainly by the phenomenon of diffusion, resulting in the breakdown of supersaturated solid solution. These changes in the structure and constitution of the alloy during ageing, result in changes in physical and mechanical properties of the alloy.

To start with, it was assumed that the phase precipitating out from the supersaturated solid solution is the equilibrium phase and that hardening was associated with the formation of submicroscopic particles of equilibrium phase. However, resistometric studies of the phase changes taking place during precipitation, revealed an anomalous behaviour [10, 11]. It was observed that during early stages of ageing, there is an increase in resistivity and is followed by the expected decrease. This behaviour was explained by Gayler and Preston [12] on the basis of two stage precipitation process. The first stage being pre-precipitation of an intermediate or nonequilibrium phase to the equilibrium phase. Gayler and Preston [12] arrived at their conclusion on the basis of extensive study carried out on hardness, density, electrical resistance and X-ray measurements. They attributed hardening



to the internal changes in the lattice of the super-saturated alloy, due to precipitation of non-equilibrium phase. Rosenhain[13] and Tammann[14] also postulated theories of two stage precipitation. However, there was little agreement between these workers on the nature of the intermediate precipitate.

Merica [15] in 1932 suggested that the first step towards precipitation is segregation of solute atoms on certain sites within the solid solution. The segregated regions were referred as 'Knots'. He further suggested that a strain field is developed around the knots due to size difference (misfit) between the solute and solvent atoms. As a result, the process of slip is rendered difficult and this leads to hardening. Experimental work of Jenkins and Bucknall[16] lent support to Merica's suggestions and the existence of clusters [17,18] was established at a much later date.

The discovery of zones by Guinier [19] and Preston[20] was a major breakthrough in the study of the age hardening process. Their findings were based on the observations of diffraction effects produced in X-ray line pattern of single crystals. A more thorough study of zones has been made possible by application of small angle scattering[21-23] and it is now established [24-26] that difference between cluster and zones is only of nomenclature. The hardening mechanism associated with zones [27] has undergone considerable change from the one suggested by Merica [15]. Modified

mechanisms have been proposed to explain hardening that takes place in spherical zones. Spherical zones are formed when size difference between the solvent and solute atoms is only marginal. Hence, they are not associated with strain fields.

With identification of non-equilibrium transition phases (e.g.  $\theta'$  in Al-Cu alloys) in precipitation sequence, the concept of coherency came into existence. A precipitate may be coherent, partially coherent or noncoherent depending on the nature of the interface between the precipitate and the matrix. An interface is said to be coherent when continuity of lattice is maintained across it. If all the interfaces are coherent the precipitate is said to be fully coherent with respect to matrix. If some of the interfaces are coherent and others are non-coherent, then the precipitate is said to be partially coherent. If all the interfaces are noncoherent then the precipitate is said to be noncoherent. The matrix and precipitate have different lattice constants. Hence to maintain coherency across the interface, the lattices will have to be matched by a process which requires lattice distortion. Hence, whenever there is coherent precipitation, coherency strains are developed and thus result in hardening. When these precipitated particles grow up, the associated elastic strain energy [28,29] increases, till a critical size is attained and coherency is lost, resulting in lowering of hardness. The credit of

explaining the process of precipitation hardening including overageing goes to Mott and Nabarro [30] on the basis of coherency strains.

With this background the structural changes during ageing can be stated as follows:

Supersaturated Solid Solution  $\longrightarrow$  clustering  $\longrightarrow$   
 formation of zones and their growth  $\longrightarrow$  Precipitation of nonequilibrium transitional phase  $\longrightarrow$   
 Transformation of nonequilibrium phase into equilibrium phase.

Actual number of steps involved varies from system to system, and depends on various factors, like the degree of supersaturation which in turn depends on solute concentration. Also as ageing occurs by diffusional process involving solute atoms and quench-in-vacancies, the homogenization temperature and the ageing temperature are most important factors governing the kinetics of ageing process. Nature of interface between the matrix and the second phase is the most important parameter in controlling the structural properties of age-hardenable alloys.

The chemical free energy change, which is the driving force for precipitation, depends on the degree of supersaturation and decreases as precipitation proceeds. Precipitation follows the path of minimum activation energy. As the primary mode of precipitation is by diffusion phenomenon which amounts to simple interchange of atoms and excess

quench-in-vacancies, the factors such as the homogenization temperature, quenching rate, ageing temperature, solute concentration etc. govern the structure and sequence of precipitation. In general, the precipitation sequence can be classified into following steps, in increasing order of the activation energy:

- |   |   |                   |
|---|---|-------------------|
| i) Clustering                                     | } | pre-precipitation |
| ii) Zone formation                                |   |                   |
| iii) Formation of intermediate transitional phase |   |                   |
| iv) Formation of noncoherent, equilibrium phase.  |   |                   |

### 1.2.2 Clustering

The first stage in the process of precipitation invariably consists of the collection of solute atoms along certain preferential planes of the matrix, and as this takes place by the process of diffusion of solute atoms, the first aggregates of solute atoms are completely coherent with the matrix. The misfit, due to difference in the atomic sizes of solute and solvent atoms, must be accommodated by elastic strains to maintain coherency. Since all the f.c.c. metals have a minimum Young's modulus along  $\langle 100 \rangle$  directions, the initial clusters in f.c.c. metal (Al) form as plates on  $\{100\}$  planes. This is also because Al has anisotropic elasticity with

$$E_{\langle 100 \rangle} = 0.99 \times 10^5 \text{ N/mm}^2$$

$$E_{\langle 111 \rangle} = 1.14 \times 10^5 \text{ N/mm}^2$$

The clusters constitute stable coherent regions having higher concentration of solute atoms. The elastic strains, due to difference in atomic sizes of solute and solvent, govern the form of these clusters. Nabarro [28] showed that elastic strain energy of the coherent cluster increases as it grows with time, and this energy can be reduced, due to anisotropy of elastic constants, thereby causing changes in the initial shape of clusters. Baker et al [31] explained that elastic strains in and around growing clusters may be relieved by aggregation of atoms and vacancies. Atoms and vacancies condense most easily on spacious and close packed planes respectively.

Activational energy for clustering is low, and is equal to the activational energy for migration of solute atoms or single vacancies. Critical size of the nucleus for clustering is of the order of one atomic diameter. With no nucleation barrier, the process consists of competitive growth of clusters. Most of the facts concerning the kinetics of clustering have been explained by Zener [32], Seitz [33], Federighi [34] and later by Herman [35] on the basis of excess vacancy theory.

### 1.2.3 Zone Formation and their growth

When the clusters attain a definite shape, they are termed as zones, and the difference between clusters and zones is only of nomenclature. Clustering, which is over in a short

time, is followed by competitive growth of zones. By X-ray studies it has been observed that the radius of zones is a function of solution temperature and alloy content. Initial rate of growth is generally very rapid but after some time zone radius reaches almost constant value and these stages correspond to fast and slow reactions. Considering the competitive growth theory, the initial rate of growth is determined by solution temperature, whilst the final zone radius is a function of the life time of vacancy [36-38]. The shape of the zones is determined by the atomic mismatch between the solute and the solvent atoms. A spherical shape is observed if the mismatch is less than 3 pct. as in Al-Ag and Al-Zn systems and disclike if it is greater than 3 pct. as in Al-Cu alloys.

#### 1.2.4 Intermediate Precipitates

Usually the decomposition of supersaturated solid solution to equilibrium phase takes place through one or more intermediate phases e.g.  $\gamma'$  in Al-Ag,  $\alpha'$  in Al-Zn and  $\theta''$  and  $\theta'$  in Al-Cu systems. These phases are obtained by partial loss of coherency of usually larger zones with the matrix during ageing. Friedel [39] and Brooks [40] discovered condition for an initial coherent precipitate to become partially coherent and finally noncoherent as it grows and according to them the precipitates become

noncoherent when they are so large that the elastic strain energy due to difference in atomic volumes of matrix and precipitate becomes greater than the surface energy ( $\gamma$ ). This criterion then predicts that a precipitate larger in radius than  $4\gamma/\delta^2 G$  will be noncoherent where  $\delta$  represents degree of misfit between precipitate and lattice parameter, and  $G$  represents modulus of rigidity of matrix. Friedel [39] took  $\gamma = 5 \times 10^{-4}$  J/mm<sup>2</sup> which is clearly limited to completely noncoherent interfaces. If, in addition, we take  $G = 4 \times 10^4$  N/mm<sup>2</sup> and  $\delta = 10^{-2}$  corresponding to a 1 pct. mismatch in lattice parameter, this criterion predicts that precipitates larger than radius of 5000 Å will be noncoherent.

### 1.2.5 Equilibrium Precipitate

This is thermodynamically the most stable state which the structure ultimately attains after any ageing sequence. Thus the final microstructure constitutes the phases predicted by the phase diagram viz., the matrix and the second phase. The initial stages of ageing and other ageing variables, determine the morphology (size, shape and distribution) of the final structure. The appearance of intermediate phase is characterized by the peak in hardness while the appearance of equilibrium phase is characterized by a fall in hardness, thus getting the

name 'overageing', which basically corresponds to the loss of coherency.

Table 1.3 gives comprehensive information about various age hardenable alloy systems.

### 1.2.6 General conclusions on precipitation phenomenon

Following conclusions have emerged from the studies about structural changes during ageing:

- i) Alloy decomposes during or immediately after quench, and there is formation of coherent clusters with simple growth.
- ii) Clusters grow with diffusion controlled migration of solute atoms and vacancies, until they attain a size which may be called zones. The shape of zone is dependent on misfit between solute and solvent atoms. being spherical if it is low, and disc or plates if it is high.
- iii) Rate of growth of clusters and zones is determined by the motion of vacancies and solute atoms. which is governed by concentration of vacancies and ageing temperature.
- iv) As the zones grow with ageing it is not possible to maintain coherency after attaining a critical size and thus development of transitional phase having partial coherency with the matrix.



Table 1.3

Common precipitation hardenable alloys [38.59]

S.No.	Alloy	Crystal structure of matrix	Intermediate precipitate		Matrix habit plane or direction	Equilibrium precipitate		Atomic mismatch (pct.) with respect to base metal
			Nomenclature	Morphology		Nomenclature	Crystal structure	
1.	Al-Ag	FCC	GPZ Zones $\gamma'$	sphere plate	{111}	$\gamma'$ (Ag <sub>2</sub> Al)	HCP	+0.7
2.	Al-Cu	FCC	GP Zones $\theta''$ and $\theta'$	disc disc	{100}	$\theta$ (CuAl <sub>2</sub> )	Tetragonal	-11.8
3.	Al-Mg	FCC	$\beta'$ (?)	rod	$\langle 110 \rangle$	$\beta$ (Mg <sub>2</sub> Al <sub>3</sub> )	FCC	+10.8
4.	Al-Zn	FCC	GP Zones $\alpha'$	sphere disc	{111}	Zn(?)	HCP	-1.9
5.	Al-Cu-Mg	FCC	GPB Zones $S''$ and $S'$	rod or sphere sphere	-	S(CuMgAl <sub>2</sub> )	FC ortho	-1.0 (Cu:Mg=1:1) -6.5 (Cu:Mg=3:1)
6.	Al-Mg-Si	FCC	GP Zones $\alpha'$	rod rod	$\langle 100 \rangle$	$\beta$ (Mg <sub>2</sub> Si)	FCC	+2.5 (Mg:Si=2:1)
7.	Al-Zn-Mg	FCC	GP Zones $M'$	sphere sphere	-	M(MgZn <sub>2</sub> )	HCP	+2.6 (Mg:Zn=1:2)
8.	Cu-Be	FCC	GP Zones $\gamma'$	disc disc	{100}	$\gamma$ (CuBe)	-	-8.8

Table continued

Table 1.3 continued

S.No.	Alloy	Crystal structure of matrix	Intermediate precipitate			Equilibrium precipitate		Atomic mis-match (pct.) <sup>x</sup> with respect to base metal
			Nomenclature	Morphology	Matrix habit plane or direction	Nomenclature	Crystal structure	
9.	Cu-Co	FCC	G.P.zones	sphere	-	$\beta$	FCC	-2.0
10.	Cu-Ti	FCC	$\gamma'$	disc	{100}	$\gamma$	-	19.0
11.	Cu-Ni-Fe	FCC	Conjugate solid-solution	Periodic	{100}	-	FCC	0.4 <sup>xxx</sup>
12.	Cu-Ni-Co	FCC	Conjugate Solid-solution	Periodic	{100}	-	FCC	1.5 <sup>xxx</sup>
13.	Cu-Al <sub>2</sub> O <sub>3</sub>	FCC	Al <sub>2</sub> O <sub>3</sub>	Triangular disc	{111}	Al <sub>2</sub> O <sub>3</sub>	-	-
14.	Cu-BeO	FCC	BeO	Triangular disc	{111}	BeO	-	-
15.	Cu-SiO <sub>2</sub>	FCC	SiO <sub>2</sub>	Sphere	SiO <sub>2</sub> is amorphous	SiO <sub>2</sub>	Amorphous	-
16.	Fe-C	BCC	$\epsilon$ Carbide Fe <sub>3</sub> C	Disc Lath	{110} {110} <111>	Fe <sub>3</sub> C Fe <sub>3</sub> C	Orthorhombic	+70 ( $\gamma$ ) +2.0 along <111>
17.	Fe-Cu	BCC	GP Zones	Sphere	-	-	-	+4.6
18.	Fe-N	BCC	$\alpha'$ (Fe <sub>16</sub> N <sub>2</sub> )	Disc	{100}	$\gamma'$ (Fe <sub>4</sub> N)	BCT	+10.1
19.	Fe-Mo	BCC	GP Zones	Disc	{100}	-	-	+ 7.2
20.	Ni-Al	FCC	$\gamma'$	Disc	{100}	$\gamma$ (Ni <sub>3</sub> Al)	FCC	+ 5.0
21.	Ni-Si	FCC	$\gamma'$	Cube	Sides    {100}	-	-	- 2.2

Table 1.3 continued

S.No.	Alloy	Crystal structure of matrix		Intermediate Precipitate		Equilibrium precipitate		Atomic mismatch (pct.)* with respect to base metal
		Nomenclature	Morphology	Matrix habit plane or direction	Nomenclature	Crystal structure		
22.	Ni-Ti	FCC	$\gamma'$ and $\eta'$ disc	{100}	$\eta'$ (Ni <sub>3</sub> Ti)	HCP	+9.5	
23.	Ni-Cr-Ti	FCC	$\gamma'$ cube	sides// {100}	$\eta'$ (Ni <sub>3</sub> Ti)	HCP	+5.0 (Ni:Cr=4:1)	
			$\eta'$ disc	{100}				
24.	Ni-Cr-Al	FCC	$\gamma'$ cube	sides// {100}	$\gamma$ (Ni <sub>3</sub> Al)	FCC	+4.8 (Ni:Cr=4:1)	
25.	Ni-Cr-Ti-Al	FCC	$\gamma'$ cube	sides// {100}	$\gamma$ (Ni <sub>3</sub> TiAl)	FCC	-	

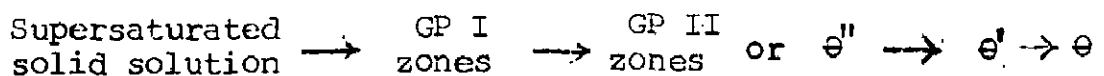
\* calculated from the change of lattice parameter with addition of solute and the figure is therefore greater than the calculated mismatch between matrix and precipitate

\*\*\* These figures denote the misfit between the two conjugate solid solutions.

- (v) Ultimately the noncoherent equilibrium phase is developed out of the transition phase.
- (vi) The matrix-precipitate interface energy is probably the single parameter of greatest importance in controlling both the microstructural and mechanical properties of the alloy.

### 1.3 PRECIPITATION BEHAVIOUR OF 2014 AL-ALLOY

The 2014 Al-alloy contains Cu, Mn, Si and Mg as alloying elements, and Fe as impurity element. It is clear from the constituents that this alloy basically belongs to Al-Cu system, on which extensive studies have been made and the following sequence of precipitation has been established [41-45]:



Addition of various elements causes change in the ageing kinetics and thus the precipitation sequence. The elements which are soluble in the matrix i.e. Cu, Mg and Si have significant effect on ageing sequence in contrast to insoluble elements like Mn and Fe, which lead to the formation of dispersoids.

Additions of Mg accelerate and intensify the effect of age hardening. The apparent acceleration of this

process by the addition of Mg may result from complex interactions between vacancies and the two types of solutes. Two types of zones are observed in Al-Cu-Mg alloys [46-48]. The first type, which is predominant in alloys of high Cu-Mg ratio (about three to one), is exactly the same as the GP zones found in binary Al-Cu alloys, although the kinetics of its formation are altered by the presence of Mg atoms [48]. The nature of second type of zones, usually denoted GPB, is less certain. They are associated with smaller lattice strains than GPI zones, and have been noted in both Al-Cu-Mg and Al-Cu-Mg-Si alloys [49,50]. The formation of GPB zones along with the GPI zones in Al-Cu-Mg-Si alloys during the initial stages of ageing has been documented recently [51-53] by hardness measurement and transmission electron microscopic observations. These zones appear in an alloy with equal amounts of Cu and Mg, but are more stable in the Cu-rich alloys. GPB zones are probably Cu-rich and Silcock [48] has suggested that they are based on the intermetallic compound  $Mg_2Al_5Cu_5$ . X-ray diffraction patterns [48] of GPB zones show very weak small angle scattering effects and diffuse planes in reciprocal space parallel to  $[100]_{Al}$  whose spacing is identical to the matrix spots. Maxima appears within the planes which do not correspond to the matrix structure and can be roughly indexed as a face centred tetragonal cell with  $a=b=5.05 \text{ \AA}$  and  $c = 4.04 \text{ \AA}$ . Silcock [48] suggests that these results can

be interpreted in terms of a needle-shaped zones of length 40-80 Å and diameter 10-20 Å, but Gerold et al [46] consider that the structure consists of small spherical zones (~16 Å diameter) containing ordered Mg and Cu planes parallel to a (100) plane. Both these interpretations appear quite feasible since needle-shaped zones are found in Al-Cu-Mg and Al-Mg-Si system and spherical zones in Al-Mg-Zn system. If the measured lattice parameters at GPB zones are correct a needle like shape would certainly be expected from strain energy considerations.

The ageing characteristics of high purity 2014 Al-alloy depend not only on the amount of soluble elements available but also on their ratio. At high ratio (Mg:Si > 1.7)  $\text{CuMgAl}_2$  produces substantial hardening by ageing at room temperature. With the Mg:Si ratio close to 1.7 by high temperature ageing i.e., by artificial ageing, the hardening effect was observed due to the formation of  $\theta'$  and to a limited extent by the formation of  $\text{Mg}_2\text{Si}$ . While at lower Mg:Si ratios ( $\leq 1$ )  $\text{Cu}_2\text{Mg}_8\text{Si}_6\text{Al}_5$  together with  $\theta'$  was formed. These constituents were mainly responsible for producing hardening by artificial ageing [54, 55]. In case of commercial purity 2014 Al-alloy the  $\theta'$  precipitates form together with dispersoids of intermetallic compounds, which are identified as  $\text{Al}_{12}(\text{Fe}, \text{Mn})_3\text{Si}$  and  $\text{Al}_4\text{CuMg}_5\text{Si}_4$  [55-57].

The elements Mn, Si and Fe reduce the early stages of precipitation, and the formation of GP I is negligible. Thus the change in properties during early stages of ageing is due to the formation of GP II zones [54]. High temperature ageing also reduces the early stages of precipitation [58, 59].

be interpreted in terms of a needle-shaped zones of length 40-80 Å and diameter 10-20 Å, but Gerold et al [46] consider that the structure consists of small spherical zones (~16 Å diameter) containing ordered Mg and Cu planes parallel to a (100) plane. Both these interpretations appear quite feasible since needle-shaped zones are found in Al-Cu-Mg and Al-Mg-Si system and spherical zones in Al-Mg-Zn system. If the measured lattice parameters at GPB zones are correct a needle like shape would certainly be expected from strain energy considerations.

The ageing characteristics of high purity 2014 Al-alloy depend not only on the amount of soluble elements available but also on their ratio. At high ratio (Mg:Si > 1.7)  $\text{CuMgAl}_2$  produces substantial hardening by ageing at room temperature. With the Mg:Si ratio close to 1.7 by high temperature ageing i.e., by artificial ageing, the hardening effect was observed due to the formation of  $\theta'$  and to a limited extent by the formation of  $\text{Mg}_2\text{Si}$ . While at lower Mg:Si ratios ( $\leq 1$ )  $\text{Cu}_2\text{Mg}_8\text{Si}_6\text{Al}_5$  together with  $\theta'$  was formed. These constituents were mainly responsible for producing hardening by artificial ageing [54,55]. In case of commercial purity 2014 Al-alloy the  $\theta'$  precipitates form together with dispersoids of intermetallic compounds, which are identified as  $\text{Al}_{12}(\text{Fe},\text{Mn})_3\text{Si}$  and  $\text{Al}_4\text{CuMg}_5\text{Si}_4$  [55-57].

The elements Mn, Si and Fe reduce the early stages of precipitation, and the formation of GP I is negligible. Thus the change in properties during early stages of ageing is due to the formation of GP II zones [54]. High temperature ageing also reduces the early stages of precipitation [58,59].

due to which the contribution of GP I and GP II( $\theta''$ ) decreases and that of  $\theta'$  increases.

In the 2014 Al-alloy, it has been observed [51-53] that the peak hardness at a temperature of 160°C or more (upto 190°C) is associated with coherent  $\theta'$  precipitate particles with a diameter of  $\sim 850 \text{ \AA}$  and the subsequent limited overageing at these temperatures is controlled by the slow growth of  $\theta'$  particles. Measurements of  $\theta'$  particle coarsening at 220°C suggest that the process occurs by Ostwald ripening [51]. In contrast, ageing at room temperature and 130°C gives a series of hardness time plateaus, which are ascribed to the sequential precipitation of zones,  $\theta''$  and  $\theta'$  precipitates.

#### 1.4 EFFECT OF TMA TREATMENTS ON AGEING CHARACTERISTICS OF Al-ALLOYS:

The term 'thermomechanical treatment' has been limited primarily to Fe base alloys, which involve deformation prior to or during an allotropic change so as to obtain an improvement in mechanical properties [60]. In addition, metallurgical processes which involve plastic deformation and heating but no allotropic changes are termed as 'mechanical-thermal treatments' [61]. But in Al-alloys both these terms are not suitable and the treatment involves plastic deformation and precipitation phenomena without any change in the phase. Hence, the structural changes



involved in these treatments cannot be considered a simple rearrangements of dislocations because the interaction between the lattice defects and the decomposition of the solid solution is characterised by complex synergistic effects. Hence, in case of Al-alloys, it should preferably be termed as 'thermomechanical ageing (TMA) treatment' [62]. According to Rack and Krenzer [63] it can also be defined as 'the effects of combined deformation and ageing on the subsequent mechanical response of age hardenable alloys'.

Precipitation phenomena are often affected by plastic deformation prior to ageing. Plastic deformation usually causes an increase in the maximum hardness of an alloy, although the increment of hardness during ageing may be less than that in case of the unworked alloy. The effect of plastic deformation on the kinetics of ageing is complex, generally the rate of hardening is increased, although Berghezan [64] has found the opposite effect in high purity binary Al-alloys. In some cases contradictory results have been obtained with the same alloy, e.g. in Al-Cu alloy Graf [65] found an increased rate of zone formation after about 30 pct. deformation, but Murakami et al [66] found a decreased rate of zone formation and an increased rate of precipitation of  $\theta'$ .

Plastic deformation has no effect on the initial rate of ageing of a rapidly quenched specimen but the

rate of decay of vacancies is increased and hence the final degree of decomposition of the resulting phase is less [17,18]. The negligible effect on the initial rate of decomposition is expected since the concentration of vacancies introduced by severe plastic deformation is much less ( $\sim 10^{-5} - 10^{-6}$ ) than the concentration introduced by quenching ( $\sim 10^{-4}$ ) [38]. During ageing the dislocations introduced by plastic deformation will act as additional sinks for the migrating vacancies and hence the rate of decay of vacancies will increase, leading to a delay in the zone formation. On the other hand these dislocations act as nucleation sites for the intermediate precipitates.

Many workers [67-74] have found that deformation prior to ageing increases the rate of nucleation of an intermediate precipitate. In an alloy which is hardened by zone formation and softened by the formation of the intermediate precipitate, e.g. Al-Zn, cold work prior to ageing will cause rapid softening. On the other hand an alloy which can be hardened by the precipitation of a fine dispersion of the intermediate phase, e.g. Al-Cu-Mg, will show rapid and increased hardening when deformed before ageing.

The influence of plastic deformation on the ageing process may usually be of two kinds [75-81]: (i) in the case of as quenched material, plastic deformation will

remove some vacancies and then retard the formation of GP zones in some regions by vacancies sinking to boundaries etc. and (ii) after certain preageing plastic deformation may provide preferential sites for the nucleation of intermediate precipitate. In 2000 series Al-alloys increased number of nucleation sites, for intermediate precipitate, due to plastic deformation during ageing treatment, leads to a fine distribution of  $\theta'$ . On subsequent ageing after plastic deformation, the  $\theta'$  preferentially nucleates on the edge character of dislocation and simultaneously either partial or complete dissolution of  $\theta''$  also takes place. Similar effect has been observed in the other alloy systems as well [82, 83].

In the peak hardened condition 2000, 6000 and 7000 series Al-alloys, without TMA treatment, normally exhibit pronounced precipitate free zones (PFZ) along grain boundaries leading to intergranular fracture [84-93]. The formation of PFZ and this type of fracture could be avoided by proper TMA treatments [94-99].

By TMA treatment it is possible to develop such dislocation substructure which can avoid the formation of PFZ and can control the coarsening of second phase precipitate particles even after long exposures at elevated temperatures. Presence of such dislocation arrangement is responsible for improvement in overall properties of Al-alloys [1-6, 63, 79, 100, 101].

## 1.5 EFFECT OF TMA TREATMENTS ON VARIOUS PROPERTIES OF Al-ALLOYS

In general, it has been observed that TMA treatments significantly affect the various mechanical properties of Al-alloys. The effect of TMA treatments on tensile-, fatigue-, and fracture toughness properties is discussed here under.

### 1.5.1 Tensile properties

There is a marked difference in deformation behaviour of Al-alloys containing coherent GP zones and those containing partially coherent or noncoherent precipitates [102-105]. Alloys containing only GP zones have a high yield stress but their subsequent deformation is similar to that of unaged specimens. The rate of work hardening is low and slip lines are fine and straight. On the other hand, specimens containing semicoherent or incoherent precipitates have a lower yield stress, but a very high initial rate of work hardening which increases as the size and spacing of the particles decrease. The high work hardening rate is no doubt due to the high density of dislocation loops left at precipitate particles and the operation of several slip systems.

Effect of TMA treatment on tensile properties has been studied by several workers [4-6, 63, 79, 100, 106-124] on Al-alloys. Although different cycles of TMA have been employed by different workers, the results obtained on

tensile properties are positive. Thermomechanical ageing after solution heat treating and quenching gives an extra degree of freedom in alloy selection, since strength can be achieved by many combinations of working and ageing. The TMA processes investigated include variations in pre-age (underaged or overaged), working to different extents and at various temperatures (cold or warm rolling), and an appropriate final ageing.

The tensile strength higher than the peak aged value has been obtained by different cycles of TMA treatments. Pattanaik et al [6] and Thompson et al [106,123,124] employed cold rolling after overageing as thermomechanical cycles for developing higher tensile strength. The final step of TMA treatment suggested by several investigators [63,107-110, 112-114, 116] is always an ageing process. The suggested cycle consists of the following sequence :

Solution heat treat → quench → preage → work  
harden → final age

The reasons suggested for improvement in tensile properties are (i) introduction of a particular type of dislocation substructure [4-6,100,117], (ii) optimisation of grain size and shape [113,114] and (iii) production of a homogeneous distribution of dislocations and precipitated particles [112].

### 1.5.2 Fatigue Properties

The effects of TMA treatment on fatigue properties of Al-alloys have been studied by several workers [106, 107, 111, 117, 125-139]. The results reported, however, are not consistent. Some workers [106, 111, 126, 130, 132, 135, 137, 138] report an appreciable improvement in fatigue properties after TMA treatment whereas some other [129, 139] report either no effect or detrimental effect on fatigue properties.

Thompson et al [106], Levy et al [130], Malakondaiah et al [132] and Broek et al [138] successfully stabilized the precipitate structure in 2000 series Al-alloys by suitable TMA treatments and claimed a 25 pct. improvement in the fatigue values. Ostermann [126] and Harendranath et al [135] claimed almost same amount of improvement in fatigue properties of 7000 series Al-alloys through TMA treatment. Reimann and Brisbane [128], using the same material as Ostermann [126], found no effect of TMA using notched fatigue specimens. Di Russo et al [129] showed that TMA produced lower fatigue strength than that obtained by conventional ageing treatment. Sommer et al [107] strongly advocated for a warm working as a necessary processing step during TMA in achieving a desirable balance of fatigue properties.

Thompson et al [123, 124] claimed an appreciable improvement in fatigue strength of 2000 and 7000 series Al-alloys through TMA treatment. In their work they

suggested an optimised thermomechanical processing practice of the form:

solution heat treatment → quench → preage →  
warm roll → final age

Apart from fatigue strength, other specific goals achieved through above treatment for 2000 series alloys were yield strength, plane stress fracture toughness and corrosion resistance. In 7000 series alloys, the best combination of toughness, strength and corrosion resistance was achieved by using an overaged preage and warm rolling.

Thomson et al [106] in their work on special processing of Al-Cu-Mg aircraft alloys concluded that a better combination of strength, toughness and fatigue properties can be obtained with a T3 temper i.e., solution heat treatment, cold working, and natural ageing to a substantially stable condition. The corrosion resistance of the above material was found poor. With the help of this treatment a dislocation structure was introduced prior to ageing which acted as nucleation sites for precipitates. These precipitates were much finer than those that would be formed in the absence of dislocations. The fine precipitates were observed to be responsible for the improvement in fatigue and other properties.

Harendranath and Mallik [135] observed an appreciable improvement in fatigue properties of Al-Zn-Mg alloys by the use of optimised thermomechanical processing

practice of the form: (a) TMT I: solution treatment, water quench, age at 150°C for 400 minutes, 30 pct. cold work, further age at 150°C for 80 minutes and (b) TMT II: solution treatment, water quench, age at 70°C for 500 minutes, 30 pct. cold work, further age at 150°C for 60 minutes. They observed an improvement in fatigue life of the order of 50 to 125 pct. by the use of above mentioned TMT I and TMT II practice respectively.

Malakondaiah and Rama Rao [132] applied to RR 58 alloy a TMA practice consisting of: Solution treatment, age at room temperature for 15 hrs, 4 pct. cold work, further age at 190°C for 15 hrs. They observed a significant improvement in the fatigue life of the alloy by this treatment.

Most of the studies on Al-alloys [126, 130, 132, 137] have established that the fatigue life of Al-alloys could be increased by TMA treatments in which the final step is ageing. Sanders Jr. et al [111] concluded that the application of intermediate thermomechanical treatment had a considerable improvement in fatigue life of 7000 series alloys due to the formation of fine grained recrystallized microstructure. Such type of microstructure is responsible for increasing the resistance to fatigue crack initiation and growth.

A review was made by Ostermann et al [127] of the available information on TMA treatment of Al-alloys, especially with respect to their fatigue behaviour. On the



basis of existing literature they concluded that suitable processing offers the advantage of improving both strength and ductility. They also concluded that significant benefits were possible in fatigue properties, at least improved resistance against crack initiation and stage I propagation, by thermomechanical processing.

The factors affecting the fatigue crack initiation and growth have been studied by various investigators [140-150]. The general agreement is that improvement in the fatigue performance could be attained by appropriate control on structural parameters responsible for fatigue failure, i.e., density and distribution of dispersoids, size, shape and distribution of strengthening precipitates, density and degree of homogeneity of deformation structure. A marked reduction in the density of dispersoids due to TMA treatment causes an appreciable increase in the resistance against crack initiation. The TMA treatment with ageing as the final step leads to relatively more uniform deformation structure which causes the resistance against dynamic recovery and thus localised or planar slip could be avoided, which would otherwise facilitate crack growth. The fine distribution of coherent and semicoherent precipitates resulting from TMA treatment locks up the dislocations and makes cross slip difficult. Thus fatigue properties of Al-alloys can be significantly improved by suitably modifying the metallographic structure of these alloys

by an appropriate choice of TMA treatment.

### 1.5.3 Fracture Toughness

The inherent ability of material to resist crack propagation is termed as fracture toughness of the material and is usually designated as  $K_{IC}$ . The rapid crack propagation is controlled by a material constant which can be described in terms of a single parameter,  $K$ , the stress intensity factor, that has the units of  $N/mm^{3/2}$ . This parameter,  $K$ , is related to both the nominal stress level in the member and the size of the crack present. It has been established that fracture occurs when the value of  $K$  at the crack reaches  $K_C$ . This  $K_C$  value is different for different mode of fracture. Traditionally, three different modes of fracture are possible (Fig.1.1). Mode I (also termed as crack opening mode) refers to a tensile stress applied in the direction normal to the faces of crack. Mode II, the forward shear mode, refers to the leading edge of the crack but in the plane of the crack. Mode III, the parallel shear mode, is for shearing stresses applied parallel to the leading edge of the crack. The mode I loading is the most important situation, encountered for more often than the others, and the majority of the research studies are devoted to this type of loading; so only this mode of failure has been considered in this text. Stress intensity factor for these modes are denoted as  $K_I$ ,  $K_{II}$  and  $K_{III}$ . Under plane strain conditions, for the small crack tip plastic

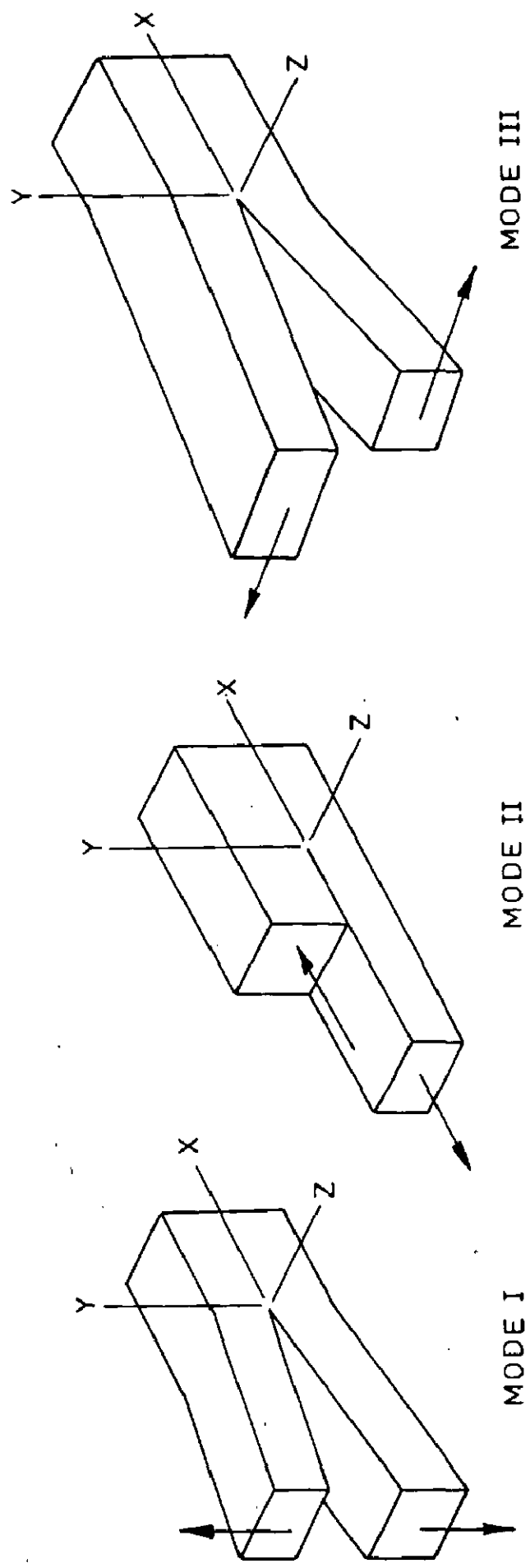


FIG.11 THE BASIC MODES OF CRACK SURFACE DISPLACEMENTS.

deformation, the critical stress intensity factor  $K_{Ic}$  for fracture instability is designated as  $K_{Ic}$  which is termed as plane strain fracture toughness for mode I, and represents the inherent ability of material to resist crack propagation [151-154]. The greater the value of  $K_{Ic}$ , the greater the stress required to produce rapid propagation and greater the resistance of the material to brittle fracture [155].

Fracture toughness values at high strain rate under dynamic conditions are denoted by  $K_{Id}$  [156] and termed as dynamic fracture toughness. At room temperature the values of dynamic fracture toughness,  $K_{Id}$ , are higher than the static fracture toughness,  $K_{Ic}$  [157].

The simplified relation of stress intensity factor to the applied normal stress and crack size or notch size for mode I can be written as

$$K_I = \sigma \sqrt{\pi a} F\left(\frac{a}{w}\right) \quad \dots (1.1)$$

where,

$\sigma$  is stress required to cause fracture,

$2a$  is the size of notch or crack size,

$2W$  is the width of plate,

and  $F\left(\frac{a}{w}\right)$  is a correction factor and is a function of notch size and width of the plate.

If  $K_I \ll K_{Ic}$ , crack will never initiate and failure will not occur.

Thus under limiting conditions the minimum possible value of fracture toughness,  $K_{Ic}$ , should be equal to  $K_I$ . Therefore,

$$K_{Ic} = \sigma \sqrt{\pi a} F\left(\frac{a}{W}\right) \quad \dots (1.2)$$

The correction factor  $F\left(\frac{a}{W}\right)$  for a double edge-notched strip is given in table 1.4. The relation of plane strain fracture toughness to the critical crack opening displacement has been developed [158] as

$$K_{Ic} = \sqrt{2E\sigma_Y \delta^*} \quad \dots (1.3)$$

where  $E$  is Young's modulus,  $\sigma_Y$  is yield strength and  $\delta^*$  is the crack opening displacement. Rice [159] suggests that crack propagation occurs by link up of void nuclei when the crack opening displacement is comparable to the spacing between void nuclei, e.g.

$$\delta^* = \lambda \quad \dots (1.4)$$

where  $\lambda$  is the spacing between void nuclei resulting from cracking of hard particles or interfacial separations at the precipitate-matrix boundary. From eqn. 1.3 and 1.4

$$K_{Ic} = \sqrt{2E\sigma_Y \lambda} \quad \dots (1.5)$$

This equation predicts that toughness increases both with yield strength and spacing of void nuclei under mode I fracture conditions. Since in most cases fracture toughness actually decreases with increasing strength level, it may

Table 1.4  
Correction factors for a double edge  
notched strip

$(a/w)$	$F(\frac{a}{w})$ for $\frac{L}{w} > 3$
0.1	1.12
0.2	1.12
0.3	1.13
0.4	1.14
0.5	1.15
0.6	1.22
0.7	1.34
0.8	1.57
0.9	2.09

be implied that void nucleating particles are the dominating microstructural feature and their spacing also has an important bearing on the fracture toughness values. Thus any change in the density and distribution of void nucleating particles lead to an appreciable change in the fracture toughness.

The effect of TMA treatment on fracture toughness has been studied by various workers [63, 79, 106, 110, 123, 124, 130, 160]. It is observed that an appreciable improvement in the fracture toughness could be obtained by different age-work-age cycles. Thompson et al. [106, 123, 124] concluded that toughness is not necessarily as sensitive to yield strength as has been generally believed. It depends more on how yield strength is caused to change. For 2000 series Al-alloys it is reported [106, 123, 124] that increased strengthening by precipitation at an elevated temperature leads to very severe drops in plane strain fracture toughness ( $K_{IC}$ ), while strengthening by work hardening can lead to only very small decrease in toughness. It is also observed [123, 124] that an overaged preage preage is superior to underaged practice, and warm rolling is superior to cold rolling at an equivalent yield strength level.

Thompson et al. [106] in their work on Al-Cu-Mg aircraft alloys concluded that fracture toughness and strength must be considered together since an increase in one

is usually at the expense of the other. A good combination of strength, fatigue and toughness was achieved by them in Al-Cu-Mg alloys through T3E9 temper where elevated temperature ageing is avoided. For maximum corrosion resistance or for higher service temperatures they recommended that the alloy must be used in T8 temper.

An appreciable amount of increase in the tensile strength and fracture toughness was observed by Rack et al [63] through optimum TMA treatment, involving the selection of a deformation temperature and strain which resulted in a uniformly tangled dislocation array. Subsequent ageing then resulted in dislocation assisted nucleation and growth of a needle-shaped transition phase. The increase in the strength and toughness was attributed to the formation of this type of substructure.

Through various thermomechanical practices Thompson et al [79] observed that the fracture toughness of the initially overaged material always exceeded the toughness of the comparable initially underaged material at an equivalent yield strength level. Thus a good combination of fracture toughness and strength could be obtained by applying overaged preage and warm rolling processing.

The investigations carried out by Santner [110], revealed that the fracture toughness is mainly affected by amount, size and distribution of dispersoids and precipitate particles. It is also concluded that fine



dispersoids and hardening particles give higher fracture toughness. Since thermomechanical processings control the amount, size and distribution of these particles, they can be utilized as useful means for increasing fracture toughness of engineering materials.

Table 1.5 gives an uptodate summary of various investigations on the effect of TMA treatments on mechanical properties of Al-alloy systems. These investigations reveal that changes in mechanical properties are directly linked to the modification in metallographic structure of these alloys resulting from such treatments.

Table 1.5

Effect of TMA treatments on properties of various Al-alloys  
 [↑(improvement), ↓(deterioration) and ↔ (no change in properties) ]

S.No.	Alloy System	Type of TMA treatment Employed	Effect on various properties with respect to peak age value					Remarks	Reference	
			Tensile Prop.		Fatigue strength	Fracture Toughness	Resistance against stress corrosion cracking			
			Room Temp	High Temp						
1	2	3	4	5	6	7	8	9	10	
1	Al-4 pct.Cu	Age-work-age cycle	↑	-	↑	-	-	-	Details not available	137
2	2024 Al-Cu-Mg deformed	Overaged-cold	↑	↑	-	-	-	-	Other comparable TMT employed is 8 rolling/recovering cycle after overageing	6
3		Solution treatment-cold working - ageing	↑	-	↑	-	-	-	Find ageing may be natural ageing or artificial ageing	137
4		Age-work-age cycle	↑	-	↔	-	-	-	Details not available	139
5		Aged at 100°C for 1 to 120 min.-cold rolled 10 to 70 pct.	↑	-	-	-	-	-	40 pct. deformation has been found as a critical deformation	120

Table 1.5 continued

1	2	3	4	5	6	7	8	9	10
6	2024 2124 and 2048 Al-Cu-Mg	T3E7: Room temp. ageing with large amount of cold deformation	↑	-	↑	↑	↑	(i) For very thin gauges When alloy has been overaged in order to produce acceptable exfol- iation resistance at all gauges, toughness no longer met the goals	123, 124
7	2048 Al-Cu-Mg	T3E9: Room temp. ageing with large amount of cold deformation	↑	-	↑	↑	↔	If good corrosion resistance is required, alloy must be used in T8 temper, in which case toughness and fatigue would be of secondary considerations	106
8	2048 Al-Cu-Mg	Age-work-age cycle	↑	-	↑	↑	↑	Resistance against stress corrosion cracking requires further confirmat- ion	130
9	RR 58 Al-Cu-Mg- Fe-Ni	T-NH4A: RT/15h 4 pct. reduction in thickness at RT- 463 K/15 h	↑	-	↑	-	-	Other TMT's empl- oyed are T-NH25A and T-AH4A, but T-NH4A yields best result	132

Table 1.5 continued

Table 1.5 continued

1	2	3	4	5	6	7	8	9	10
10	Al-Mg	Solution treated-cold worked-finally artificially aged	↑	-	-	-	↑		116
11	Al-Mg-Si	T10: preaged 200°C-cold worked-finally aged at 200°C	↑	-	↔	-	-	Other TMT employed is T8: cold worked and aged at 200°C, but shows poor properties than T10.	117
12	6061 Al-Mg-Si-Cu	Four step age-deform cycle, with a total ageing time of 4h at 448K and a total reduction of 50 pct.	↑	-	-	↑	-	Preageing treatment at low temp. (373K), do not appear to be as effective as those at higher temp. (448K)	63
13		Aged for 2h (448K)-deformed 25 pct. (373K)-aged for 2h (448K)-finally deformed 25 pct. (373K)	↑	↓	-	-	-	i) Deformation is given unidirectional rolling. ii) Solution treated and aged alloy provides higher thermal stability than TMT alloy	109
14	Al-Zn-Mg	Aged (70°C) for 500 min-30 pct. cold worked-Aged (150 to 180°C) for 10 to 60 min.	-	-	↑	-	-	TMT with higher final ageing temperature resulted into superior fatigue properties than TMT with same temp. during preageing and final ageing step.	135

Table 1.5 continued

1	2	3	4	5	6	7	8	9	10
15	7050 Al-Zn-Mg-Cu	ITMT: (Intermedialte thermomechanical treatment-Special ingot processing Technique)	↑	-	↑	↑	-	The results have been compared with FTMT also, and concluded that ITMT yield better resistance against Fatigue Crack Initiation	111
16	7075 Al-Zn-Mg-Cu	Aged (121°C) for 4h-aged (163°C) for 20 min-25 pct. deformed by warm rolling (150°C)-1.5 pct. stretch- finally aged (143°C) 2h	↑	-	-	↑	-	TMT alloy yield better results than T651 temper	110
17		Preaged (100°C)- cold deformed - finally aged (120°C)	↑	-	↑	-	-	TMT with ageing as final step yields homogeneous deformation structure, responsible for high fatigue resistance	126
18	7075 and 7039 AlZnMg(-Cu)	Preageing-cold rolling-final ageing	↑	-	↑	↔	↔	i) Preageing and final ageing both were carried out at same temperature in the artificial ageing temperature range	129
		Preageing-warm rolling-final ageing	↑	-	↑	↑	↔	ii) Warm rolling yields Superior Fracture toughness than cold rolling	129

Table continued

Table 1.5 continued

1	2	3	4	5	6	7	8	9	10
19.	7075, 7175, and 7475 AlZnMgCu	Overaged preage and warm rolling	↑	-	↑	↑	↑	An overaged preage was superior to an underaged preage practice. Also, warm rolling was superior to cold rolling	123, 124
20	7475 AlZnMgCu	Overaged preage and warm rolling	↑	-	-	↑	↑	i) Maximum toughness and strength were obtained with either a low Cu or low Mg  ii) Adequate strength was not obtained when both Cu and Mg were low.  iii) Overage was preferred against underage preage and warm working was preferred against cold working	79

\*\*\*\*\*

CHAPTER 2

FORMULATION OF PROBLEM

\*\*\*\*\*

## CHAPTER-2

### FORMULATION OF PROBLEM

The extensive use of age hardenable 2000 Al-alloys at high strength, high hardness levels has been hampered by poor secondary properties of fatigue and fracture toughness, as well as the strength at high temperatures. The importance of these materials in aircraft fittings, heavy duty forgings, airframe construction [55,161] and army armament items [111] has stimulated recent attempts to improve these properties. Some secondary property improvements have been obtained by employing slight changes in alloy chemistry [162,163], or removal of the impurity elements Fe and Si [56,57,164,165]. Such research has led to the development of alloys [164,165] with improved mechanical properties and fracture toughness. However, significant improvement in fatigue resistance has not been realised as yet. At present, there seems to exist no well defined approach to improve the fatigue resistance by compositional changes [127]. Another approach to the problem of fatigue improvement is the use of thermomechanical treatment [127]. In regard to thermo mechanical processing conflicting results have been reported on attempts to modify high cycle fatigue strength of several Al-alloys. While Krause and Laird [137] (Al-4%Cu), Broek and Bowles [138] (2024), Ostermann [126] (7075) found a favourable influence, Lyst [139] (2024) reported no effect and Russo et al [129]



(7075 and 7039) a detrimental effect of thermomechanical treatments on high cycle fatigue resistance. It is well known that the fatigue strengths of high strength, age-hardened aluminium alloys are inherently poor in relation to their static strengths. Unfortunately, however, the relationship between the fatigue processes and the microstructure in these alloys is not clearly understood owing to the complexity of the metallurgical structure and the fineness of the precipitates. Besides the conflicting observations, there is a general opinion that in the commercial purity Al-alloys, if the effects of inclusions can be minimised, significant benefits are possible in fatigue, at least in stage I crack resistance, by thermomechanical processing.

From literature it is well known that the fracture toughness of high strength Al-alloys is mainly influenced by alloy content, degree of purity and heat treatment [56,57]. The results of Low et al [56] and Tanaka et al [57] show that the fracture process is dominated by fracture of the large ( $1\mu$  to  $10\mu$ ) second phase particles which contain Fe or Si or both, tentatively identified as  $Al_{12}(Fe,Mn)_3Si$  and a combination of excess Cu with either Al, Si or Mg i.e.  $Al_4CuMg_5Si_4$ . From their size, volume fraction, and distribution, it is unlikely that these large inclusions contribute to the strength

of the alloys and presumably, greatly decrease their fracture toughness. Although some studies have been made on the 2014 (Al-Cu-Mg-Mn-Si) alloy system, which is of utmost importance in the aircraft industry, specially for aircraft fittings and general structural purposes where high hardness and high strength are required; even then systematic information regarding fatigue strength and fracture toughness is scarce. Therefore, the present investigation is concentrated on a systematic study of the thermomechanical ageing (TMA) of 2014 Al-alloy. An attempt has been made to modify or control microstructure of 2014 alloy by appropriate treatment so as to eliminate or minimise the number/density of dispersoids/inclusions to bring about an improvement in the overall mechanical properties. Microstructure control through modification of conventional primary processing methods has been examined as a way of upgrading the properties of the alloy. The effect of various parameters on tensile properties, fatigue, fracture toughness and microstructural changes has been studied on 2014 Al-alloy of commercial purity. The main parameters investigated are degree of preageing and amount of deformation prior to final ageing. Different thermomechanical treatments have been developed on the basis of the above parameters. The resultant mechanical properties are correlated with the microstructural features of precipitate, dislocation density and particle/dispersoid

distribution using optical and transmission electron microscopic (TEM) techniques. Scanning electron microscopic (SEM) studies have been made on the fracture surfaces of fatigue tested samples to reveal the effect of microstructural features on the crack initiation. These observations are expected to throw light on the mechanisms of fatigue failure after various thermo-mechanical ageing treatments.

The present investigation is, therefore, expected to indicate the response of various thermomechanical ageing treatments towards production of a microstructure which may not only result in improved tensile properties, but also improved fracture toughness and fatigue properties. The results obtained in this investigation may also be applicable to other alloy systems under similar situations.

\*\*\*\*\*  
CHAPTER 3

EXPERIMENTAL PROCEDURE  
\*\*\*\*\*

## CHAPTER -3

### EXPERIMENTAL PROCEDURE

#### 3.1 ALLOY PREPARATION

The alloy used in this investigation was prepared from Al of 99.70 pct. purity and Cu, Si, Mn and Mg of 99.90 pct. purity. Melting was carried out in electrical resistance furnace provided with temperature controls of  $\pm 5^{\circ}\text{C}$  accuracy.

Before preparing the final alloy, a master alloy of Al-33 pct. Cu was prepared by melting Cu and adding Al to raise the composition to the eutectic point. Stirring of the melt was maintained to develop homogeneous composition. Master alloy, thus prepared, was cast in previously clamped steel moulds. On analysis the master alloy was found to contain 32.8 pct. Cu.

For the preparation of the final alloy Al was melted in graphite crucible in a pit furnace and required amount of master alloy and other alloying additions were made to get the desired composition. Si and Mn were added in the form of turnings or small chips. Mg was packed in high purity Al foil and to avoid burning it was kept immersed in the melt, till it completely dissolved. For degassing hexacholorethane was added to the melt before casting. The alloy was then

cast in rectangular steel moulds of 35mm x 35mm x 300mm size. The cast alloy was chemically analysed for Cu, Mn, Si and Mg. For Cu and Mn volumetric method of analysis was employed, whereas Si and Mg were analysed by gravimetric method. The final chemical composition of the alloy is given in table 3.1.

The cast alloy was hot rolled at  $425^{\circ}\text{C}$  into rods of 20mm x 20mm cross section, for breaking the cast structure. The rods thus obtained after rolling were completely homogenised at  $500\pm 5^{\circ}\text{C}$  for 48 hours. The complete homogenisation was ensured by applying the  $2\sqrt{N}$  test on hardness values and by metallographic examinations.

### 3.2 AGEING AND THERMOMECHANICAL AGEING (TMA) TREATMENT

The various treatments given to the alloy under investigation are described and shown schematically in Table 3.2. To begin with, solution treatment was given to all the specimens by heating at  $495\pm 5^{\circ}\text{C}$  for 1.50 hr. followed by water quenching at room temperature. Solution treated and quenched specimens were immediately subjected to subsequent ageing and various TMA treatments.

#### 3.2.1 Peak Ageing Treatment

The solution treated and as quenched samples were artificially aged at  $160\pm 1^{\circ}\text{C}$  in silicon oil bath furnace and the

Table 3.1

Nominal and actual compositions  
of 2014 Al-alloy

Element	Nominal range (wt.pct.)	Actual composition of the alloy used in the present study (wt.pct.)
Copper	3.9-5.0	4.44
Silicon	0.5-1.2	0.85
Manganese	0.4-1.2	0.77
Magnesium	0.2-0.8	0.45
Aluminium	Balance	Balance

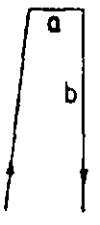
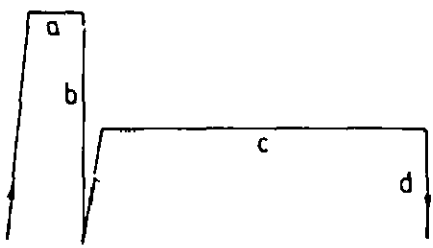
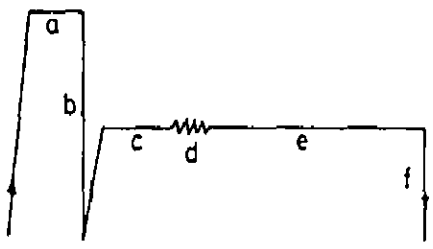
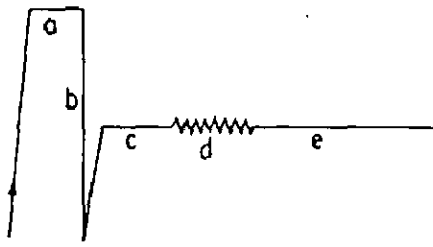
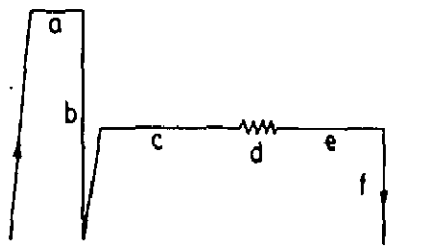
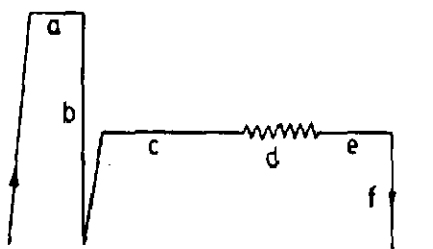
Treatment designation	Schematic Representation	Details of Treatment
As Quenched (AQ)		a Solution treatment at 500°C for 1.50 hrs b Quench in water
Peak aged (PA)		a As above b As above c Peak ageing at 160°C d Quench in water
TMA Ia		a As above b As above c 25 pct preageing at 160°C (upto 73 VHN) d 10 pct warm rolling at 160°C e Final ageing at 160°C to peak value f Quench in water
TMA Ib		a As above b As above c 25 pct preageing at 160°C d 20 pct warm rolling at 160°C e Final ageing at 160°C to peak value f Quench in water
TMA IIa		a As above b As above c 50 pct preageing at 160°C (upto 87 VHN) d 10 pct warm rolling at 160°C e Final ageing at 160°C to peak value f Quench in water
TMA IIb		a As above b As above c 50 pct preageing at 160°C d 20 pct warm rolling at 160°C e Final ageing at 160°C to peak value f Quench in water

TABLE 3.2 DETAIL OF TREATMENTS EMPLOYED IN THE PRESENT INVESTIGATION.



structural changes during ageing were followed by hardness measurements. Thus, a basic ageing curve showing variation of hardness with ageing time was plotted for undeformed specimens.

### 3.2.2 Preageing Treatments

The homogenised and as quenched alloy samples were given 25, 50 and 75 pct. preageing treatments. These preageing treatments have been worked out as under.

As quenched hardness of the alloy under investigation is 59 VHN and peak hardness on ageing at  $160^{\circ}\text{C}$  for 8.50 hrs is 114 VHN. The net increase in hardness on peak ageing (100 pct. ageing) is  $114 - 59 = 55$  VHN. Thus a 25 pct. preageing treatment will correspond to a hardness of  $59 + 14 = 73$  VHN. Similarly the 50 and 75 pct. preageing treatments will correspond to hardness values of 87 VHN and 101 VHN respectively. The timings required for 25, 50 and 75 pct. preageing treatments, as obtained from basic ageing curve, are 1.85 hrs., 4.00 hrs. and 5.80 hrs. respectively.

### 3.2.3 Mechanical Working and Final Ageing

Subsequent to preageing treatments the specimens were warm rolled at ageing temperature ( $160^{\circ}$ ) to the extent of 10 pct. and 20 pct. deformations (reduction in thickness). The deformed specimens were further aged at  $160^{\circ}\text{C}$  and the

ageing behaviour was again followed by hardness measurements. The detailed schedule of various TMA treatments employed in the present investigations are shown in table 3.2.

### 3.3 HARDNESS MEASUREMENTS

The samples of 20mm x 20mm x 25mm size were polished on emery paper upto 4/0 grade so as to obtain a fine polished surface. Hardness measurements at different locations over the entire face were taken on Vicker's hardness testing machine using a load of 5 Kg. For hardness value measurements were made on three samples at three different locations and average of nine indentations were recorded as final reading.

### 3.4 TENSILE PROPERTIES

Tensile tests were conducted on strip shaped specimens, which were filed out from 3.2 mm thick and 38 mm wide strips, to suit the specific requirements of the tensometer used (Fig.3.1). The tensile tests were carried out on Monsanto tensometer type 'W' and three specimens were tested after each treatment. The average values of UTS, YS and pct. elongation were calculated and recorded.

### 3.5 FATIGUE STUDIES

Fatigue studies on sample after various treatments were made on Wöhler type fatigue testing machine. Fatigue strength was measured, on round bar shaped specimens shown in Fig.3.2,

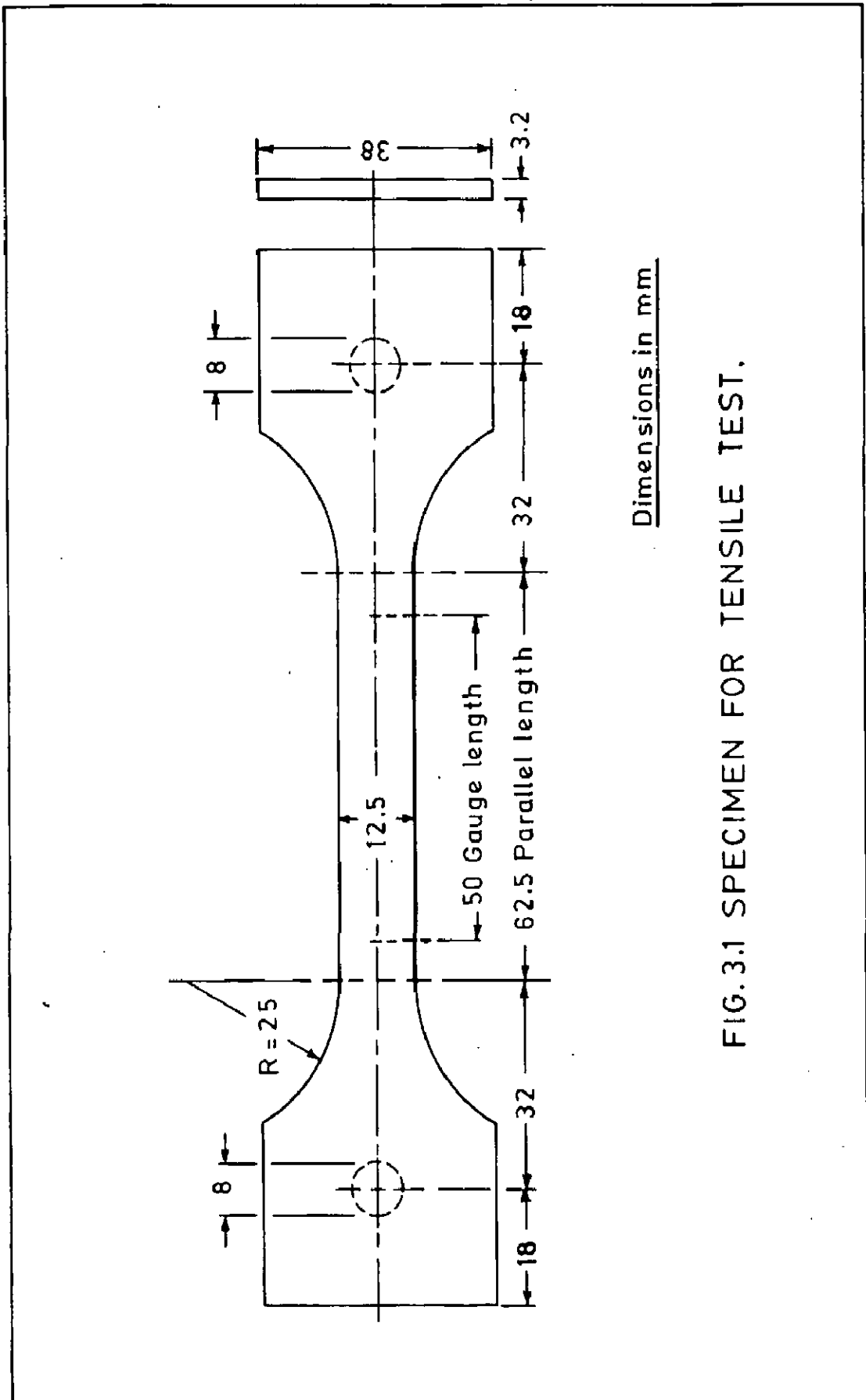
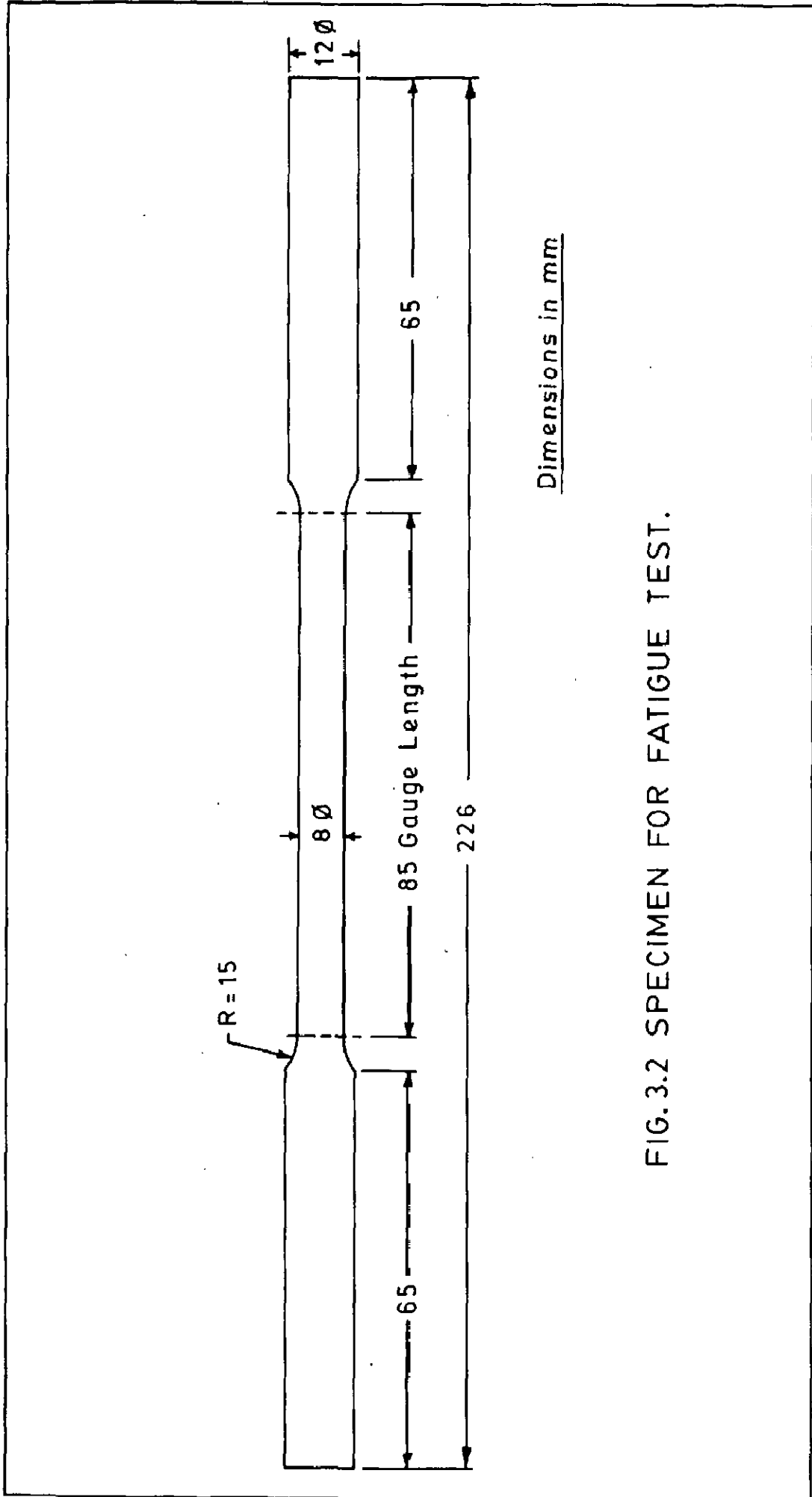


FIG. 3.1 SPECIMEN FOR TENSILE TEST.



Dimensions in mm

FIG. 3.2 SPECIMEN FOR FATIGUE TEST.

in terms of S-N curves (number of cycles to failure at a particular stress level). Tests were conducted on three samples for every point of S-N curve.

### 3.6 FRACTURE TOUGHNESS MEASUREMENTS

In the present investigation the double edge-notched (EN) test specimens were prepared as per the recommendations of ASTM Committee E-24 on fracture testing of metals (Fig.3.3). The tensile test of EN specimens were carried out on Monsanto tensometer type 'W' in the same manner as in case of unnotched specimens. Plane strain fracture toughness values were calculated on the basis of Eq.1.2. The values of correction factor  $[F(\frac{a}{w})]$  were taken from table 1.4.

The dynamic fracture toughness ( $K_{Id}$ ) measurements were conducted on standard Charpy V-notch specimens (Fig.3.4) as per the recommendations of ASTM E-23 Committee. The impact test was carried out on pendulum type impact testing machine PS-30. The  $K_{Id}$  values were computed from the energy absorbed per unit area during fracture using the relation:

$$K_{Id} = 10.05 \sqrt{\frac{E}{2(1-\nu^2)} \left(\frac{CVN}{A}\right)} \quad \dots (3.1)$$

where,

E is modulus of elasticity in  $N/mm^2$ ,

$\nu$  is Poisson's ratio,

and  $\frac{CVN}{A}$  is energy absorbed per unit area during fracture in  $J/mm^2$ .

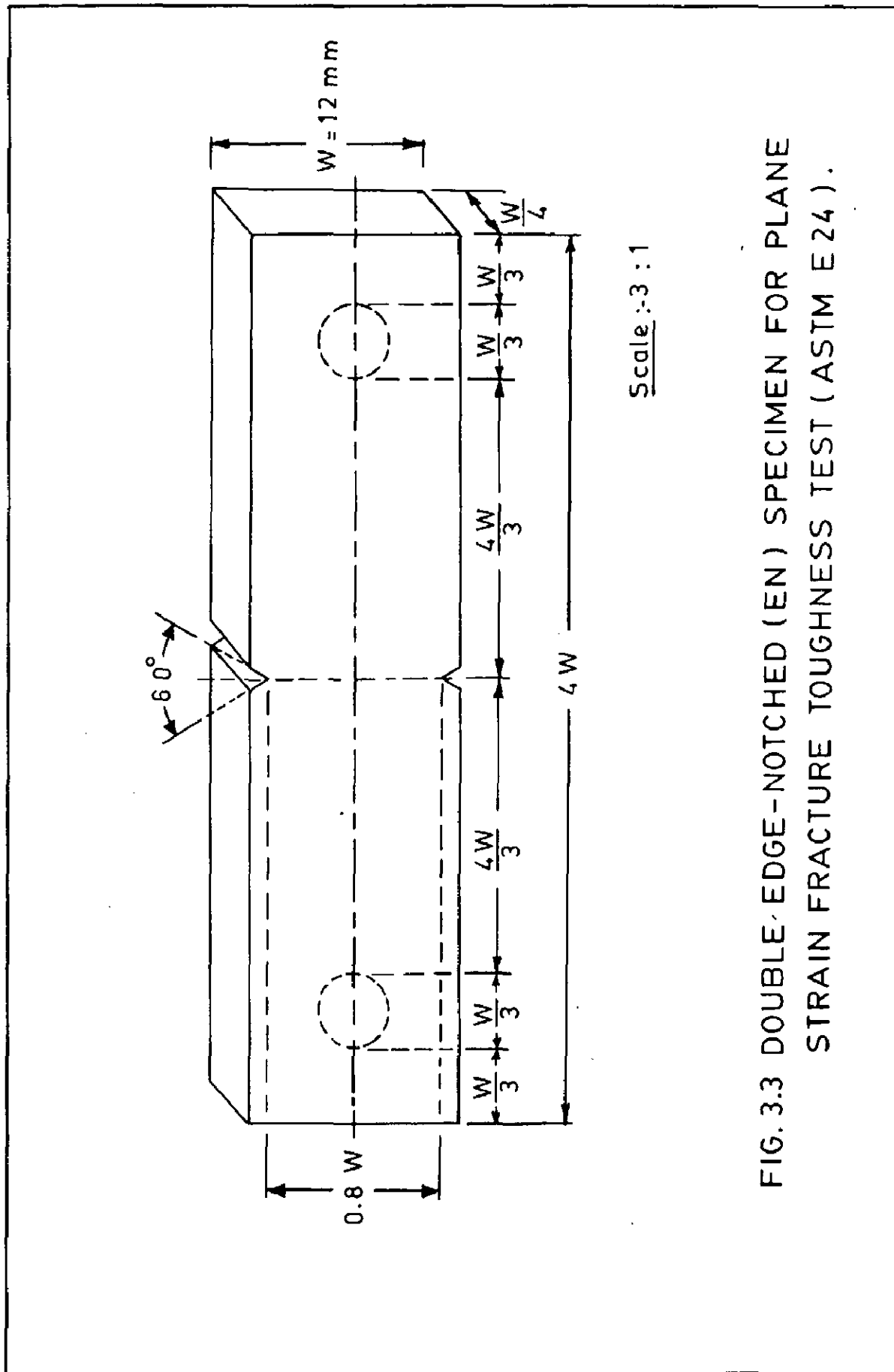


FIG. 3.3 DOUBLE-EDGE-NOTCHED (EN) SPECIMEN FOR PLANE STRAIN FRACTURE TOUGHNESS TEST (ASTM E24).

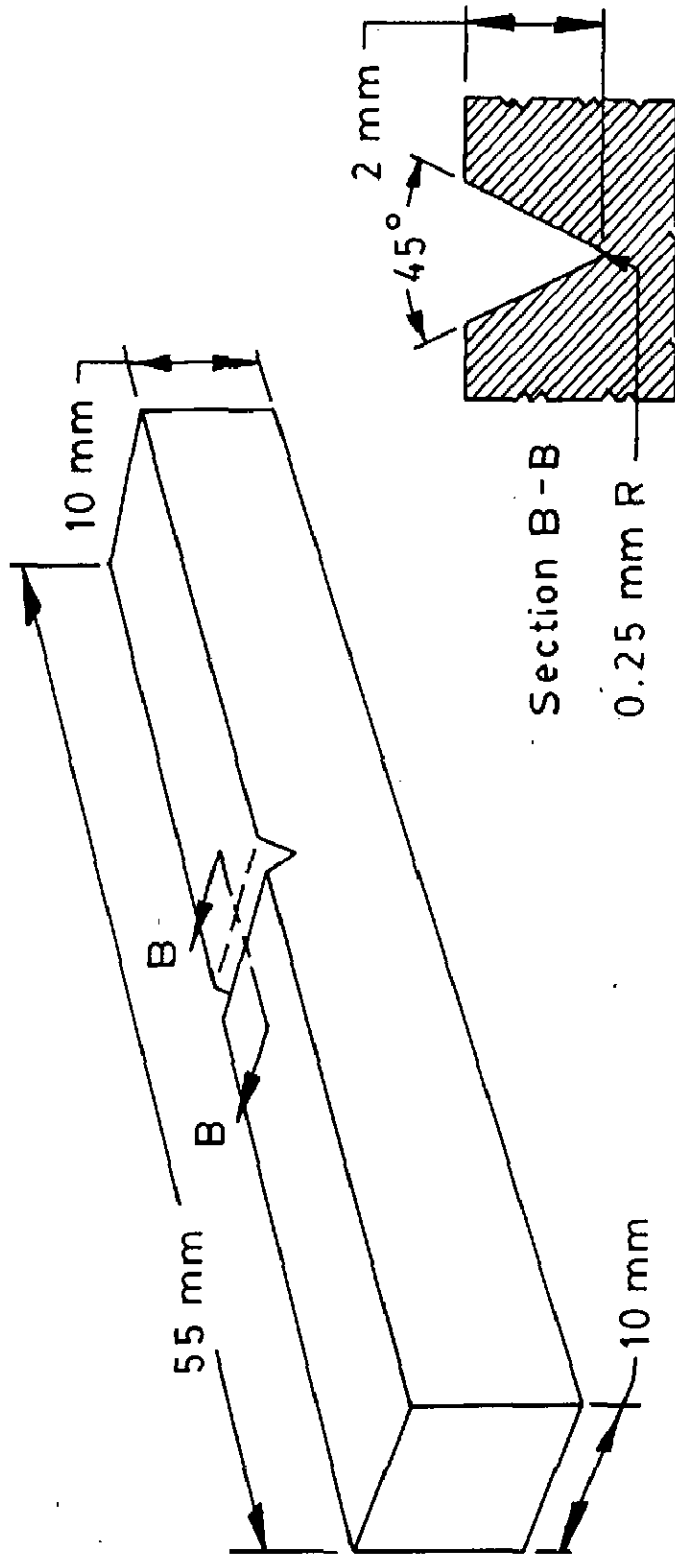


FIG. 3.4 CHARPY V-NOTCH SPECIMEN FOR DYNAMIC FRACTURE TOUGHNESS TEST (ASTM E 23).

For 2014 Al-alloy the value of modulus of elasticity is  $7.3 \times 10^4$  N/mm<sup>2</sup>, and Poisson's ratio is 0.33. By substituting these values, the Eq.3.1 can be written as,

$$K_{Id} \approx 2000 \sqrt{\frac{CVN}{A}} \quad N/mm^{3/2} \quad \dots (3.2)$$

### 3.7 METALLOGRAPHIC STUDIES

Structural changes during TMA treatments were studied with the help of metavert optical microscope and Philips EM 400 transmission electron microscope (TEM). For optical microscopic examinations the specimens prepared for hardness measurement were used. The specimens were polished by standard technique and etched with HF.

Optical microscopic technique was used to study the effect of TMA treatments on morphology, density and distribution of dispersoids. The qualitative analysis of dispersoids was carried out by electron probe microanalyser at Defence Metallurgical Research Laboratory, Hyderabad.

TEM studies were carried out at high magnifications on thin foil samples prepared by window technique. Electro-thinning was carried out at 12 volt and 70°C. The volumetric composition of the electrolyte used was:

H <sub>3</sub> PO <sub>4</sub> :	62.00 pct.,	H <sub>2</sub> O:	24.00 pct.
H <sub>2</sub> SO <sub>4</sub> :	14.00 pct.,	CrO <sub>3</sub> :	160.00 gm/litre

The mode of fracture during fatigue failure was examined by fractography on Philips SEM 501 Scanning electron microscope.



\*\*\*\*\*  
CHAPTER 4

RESULTS AND ANALYSIS  
\*\*\*\*\*

U

## CHAPTER-4

### RESULTS AND ANALYSIS

The results of this investigation have been presented in Figs.4.1 to 4.43 and Tables 1 to 26 (Appendix ) and are described in the following sections.

#### 4.1 EFFECT OF AGEING ON MECHANICAL PROPERTIES

The ageing of 2014 Al-alloy has been observed to affect significantly the hardness, tensile-, fatigue-, and fracture toughness properties.

##### Hardness:

The effect of ageing on Vickers hardness has been studied at different ageing intervals (Fig.4.1). It is seen that as the ageing proceeds the hardness of the alloy under study rises continuously from the as quenched values of 59 VHN until a peak value of 114 VHN is reached after 8.50 hrs at 160°C. On further ageing, as per the normal expectations, after peak there is a gradual fall in hardness due to overageing phenomenon. Fig.4.1 also shows that nature of curve is almost same as that available in the literature for similar type of alloys.

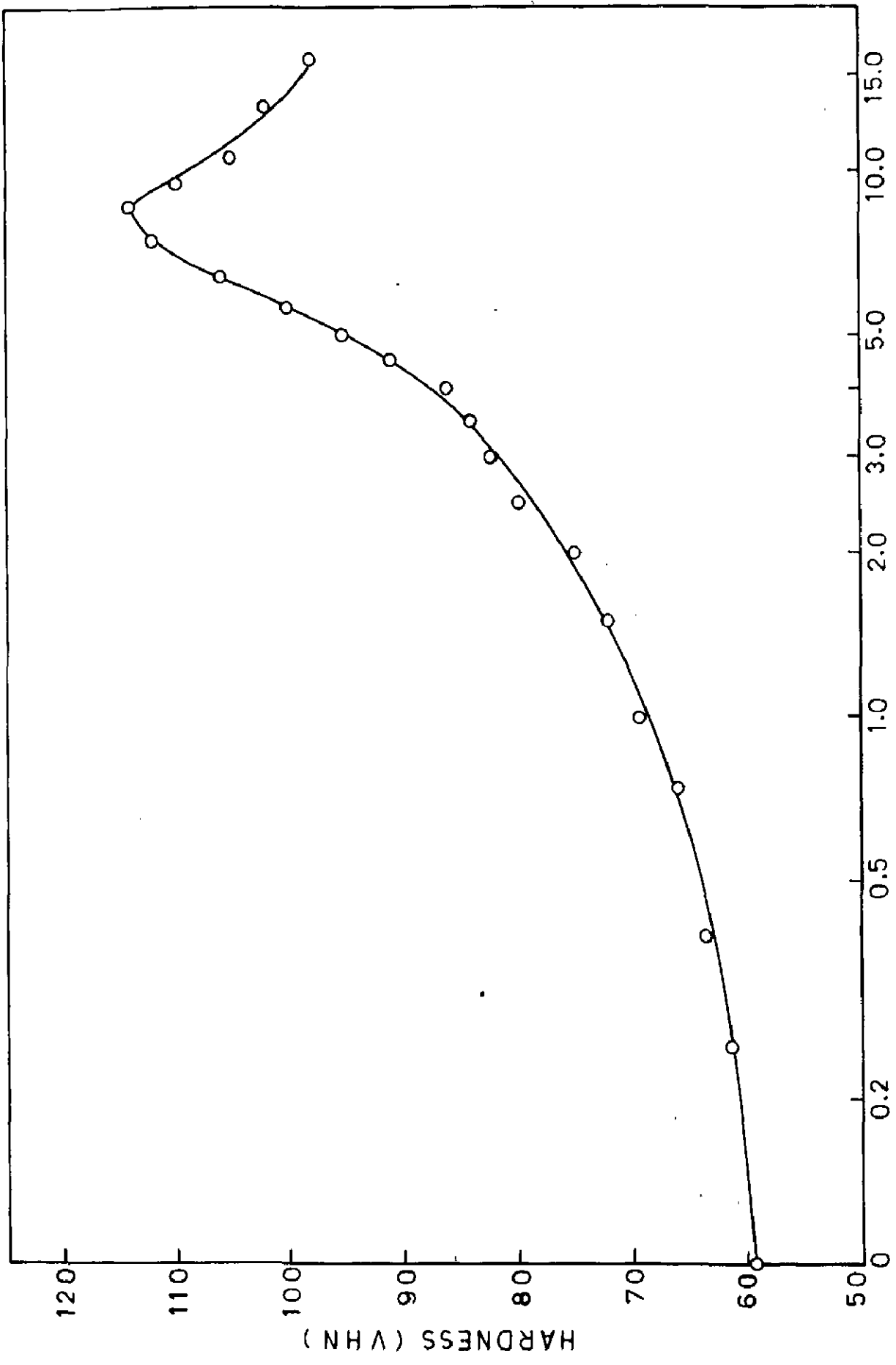


FIG. 4.1 EFFECT OF AGEING ON HARDNESS.

### Tensile Properties

Various parameters of tensile properties viz. ultimate tensile strength (UTS), yield strength (YS) and percentage elongation (% El) have been measured during ageing treatment at different ageing intervals. The results of tensile properties have been plotted against ageing time (hrs) on log scale (Fig.4.2). It is observed that as the ageing proceeds the strength of the alloy under study rises continuously from 245.18 N/mm<sup>2</sup> UTS and 198.10 N/mm<sup>2</sup> YS to a peak value of 375.12 N/mm<sup>2</sup> UTS and 313.82 N/mm<sup>2</sup> YS, after which there is a gradual fall in the tensile strength. On the other hand it is seen that the ductility (% El) decreases slowly with ageing phenomenon, reaches the lowest value corresponding to the peak in strength curve followed by an increase on further ageing due to overageing effects.

### Fatigue Properties

Fig.4.3 gives the S-N curves for the as quenched samples and the samples peak aged at 160°C. The S-N curves have been plotted for the various stress levels ranging from 98 N/mm<sup>2</sup> to 177 N/mm<sup>2</sup>. The test results on fatigue measurements indicate significant scatter in the case of as quenched samples. The S-N curves of both as quenched and peak aged alloys are more or less parallel indicating similar mechanisms of operation in both the cases. Fig.4.3 also shows that the fatigue life at any stress level is higher for as quenched samples.

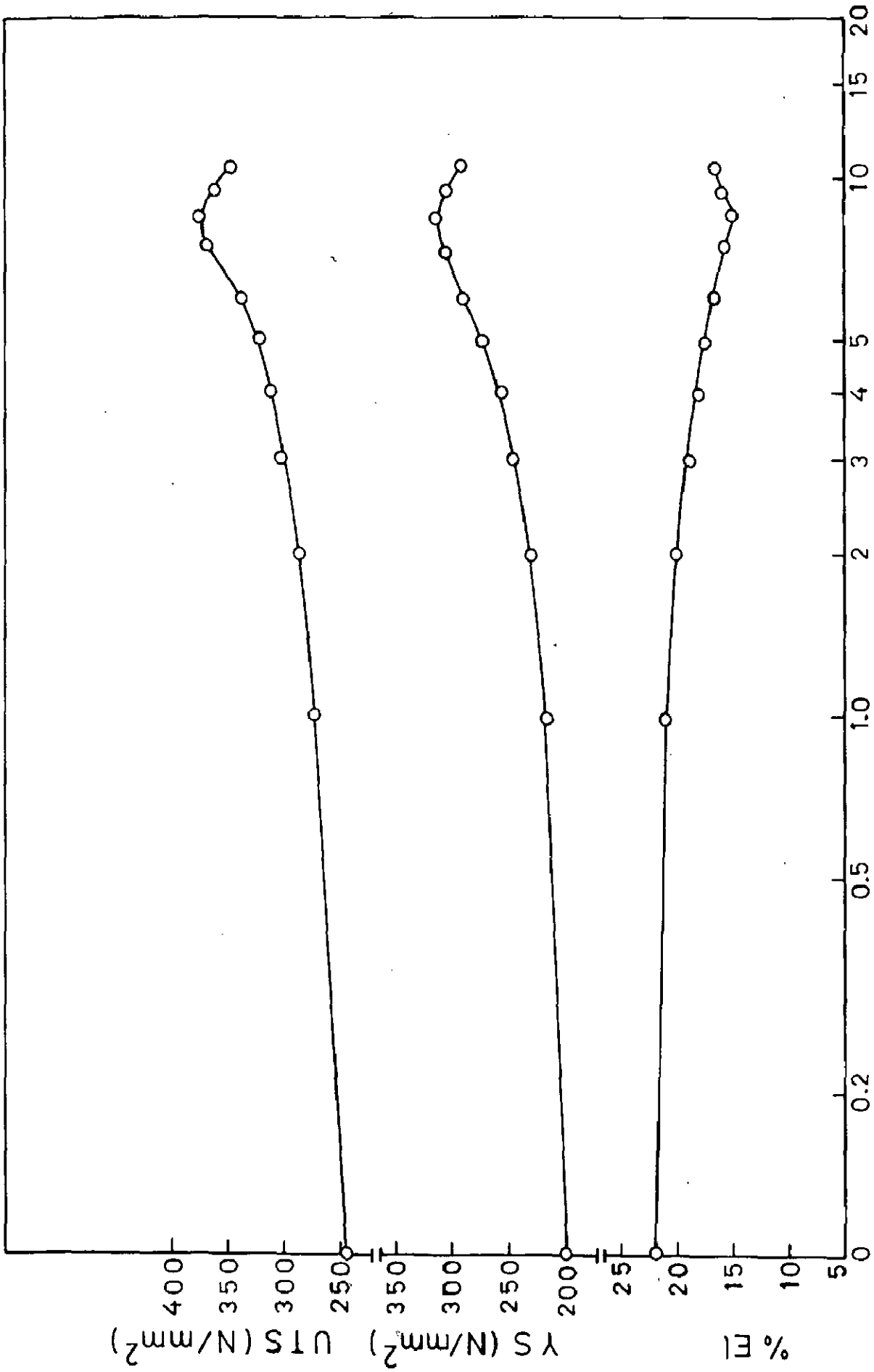


FIG. 4.2 EFFECT OF AGEING ON TENSILE PROPERTIES.

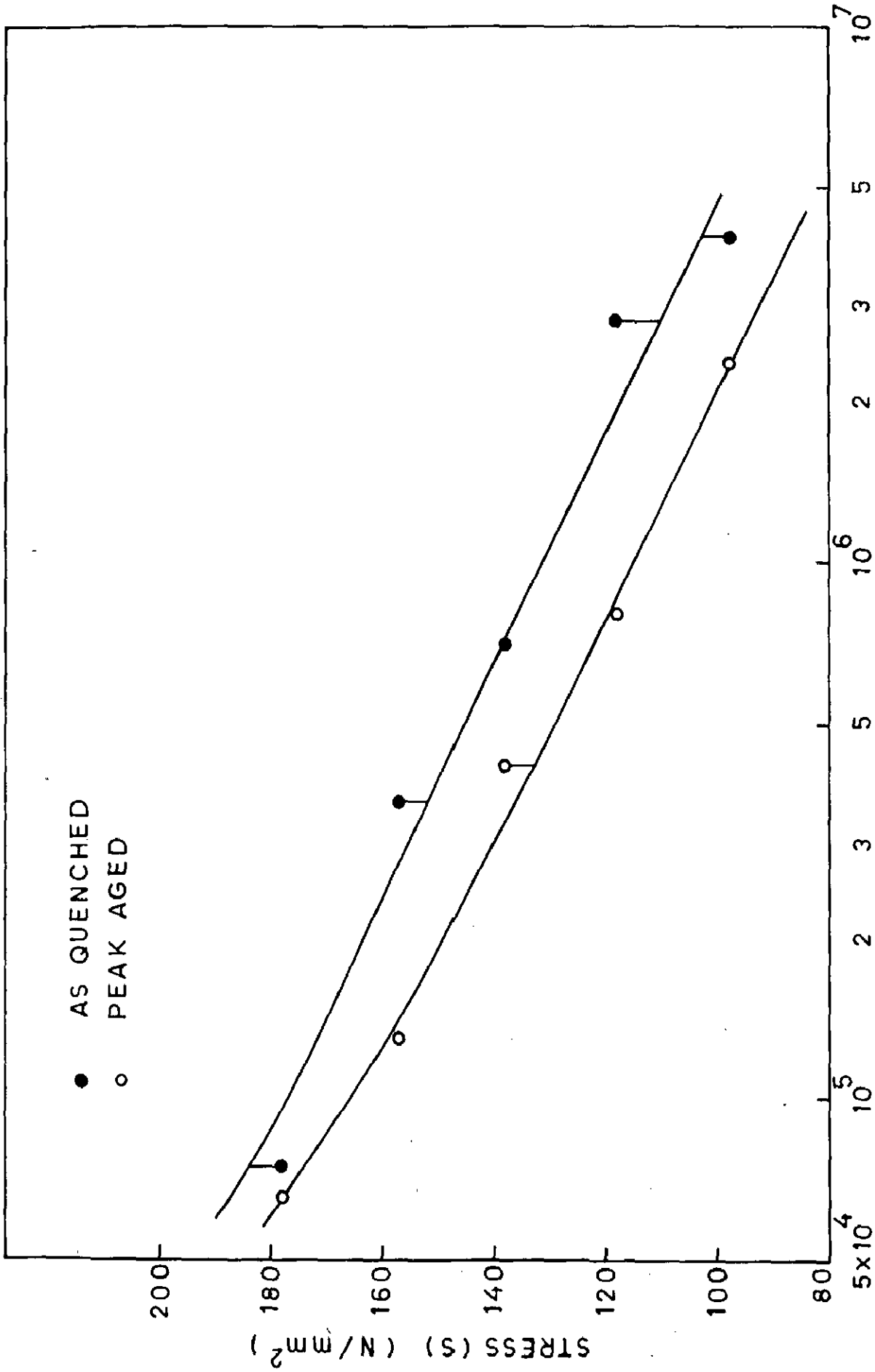


FIG.4.3 EFFECT OF AGEING ON FATIGUE PROPERTIES.

It is also seen that the relative difference between the fatigue life of as quenched and peak aged samples increases at lower stress levels i.e. in the higher cycle range. For example, it is clearly seen that at  $98 \text{ N/mm}^2$  stress level the values of fatigue life in as quenched condition is  $4.5 \times 10^6$  cycles and for peak aged samples it is  $2.7 \times 10^6$  cycles. Thus the as quenched alloy at this stress level has a fatigue life which is  $1.8 \times 10^6$  cycles higher than that in the peak aged condition. On the other hand at  $177 \text{ N/mm}^2$  stress level the as quenched sample has a fatigue life superior to peak aged one only by  $3 \times 10^4$ ,  $9.6 \times 10^4$  -  $6.6 \times 10^4$  cycles. From Fig.4.3 it is also seen that for any value of fatigue life, the corresponding fatigue stress (endurance limit) in as quenched condition is constantly higher by a marginal difference of approximately  $10 \text{ N/mm}^2$  throughout the range of investigation.

#### 4.2 EFFECT OF THERMO MECHANICAL AGEING (TMA) ON VARIOUS MECHANICAL PROPERTIES

The TMA employed in the present investigation includes preageing to various degrees, warm working and subsequent ageing at  $160^\circ\text{C}$ . It has been observed that the thermo-mechanical ageing of 2014 Al-alloy affects significantly the various mechanical properties like hardness, tensile properties, fatigue and fracture toughness. The effect of thermomechanical ageing on most of the properties has been observed as positive. The magnitude of the effect on various

mechanical properties has been given in the following sections.

#### Hardness:

In Figs.4.4 and 4.5 the hardness values after 25, 50, 75 and 100 pct. preageing and 10 and 20 pct. deformations have been plotted against ageing time (hrs.) on log scale. It is seen that the hardness rises to higher values after deformation in all the preageing conditions. The relative difference in the rise in hardness values after 10 and 20 pct. deformation is maximum for TMA II treatment, i.e. for 50 pct. preaged samples. From Figs.4.4 and 4.5 and Tables 2 to 9 (Appendix), it can be clearly seen that for 20 pct. preaged samples the hardness value rises from 73 VHN to 94.5 and to 97.9 VHN after 10 and 20 pct. deformations respectively, whereas for 50 pct. preaged samples the hardness value rises from 87 VHN to 98.6 and to 123.0 VHN after 10 and 20 pct. deformations respectively. For 75 pct. preaged samples the hardness value rises from 100.8 VHN to 116.0 and to 122.5 VHN after 10 and 20 pct. deformations respectively, whereas for 100 pct. preaged samples the hardness value rises from 114.0 VHN to 130.2 and to 137.3 VHN after 10 and 20 pct. deformations respectively.

Among all the TMA treatments the one involving 50 pct. preageing gives maximum effect on increase in peak



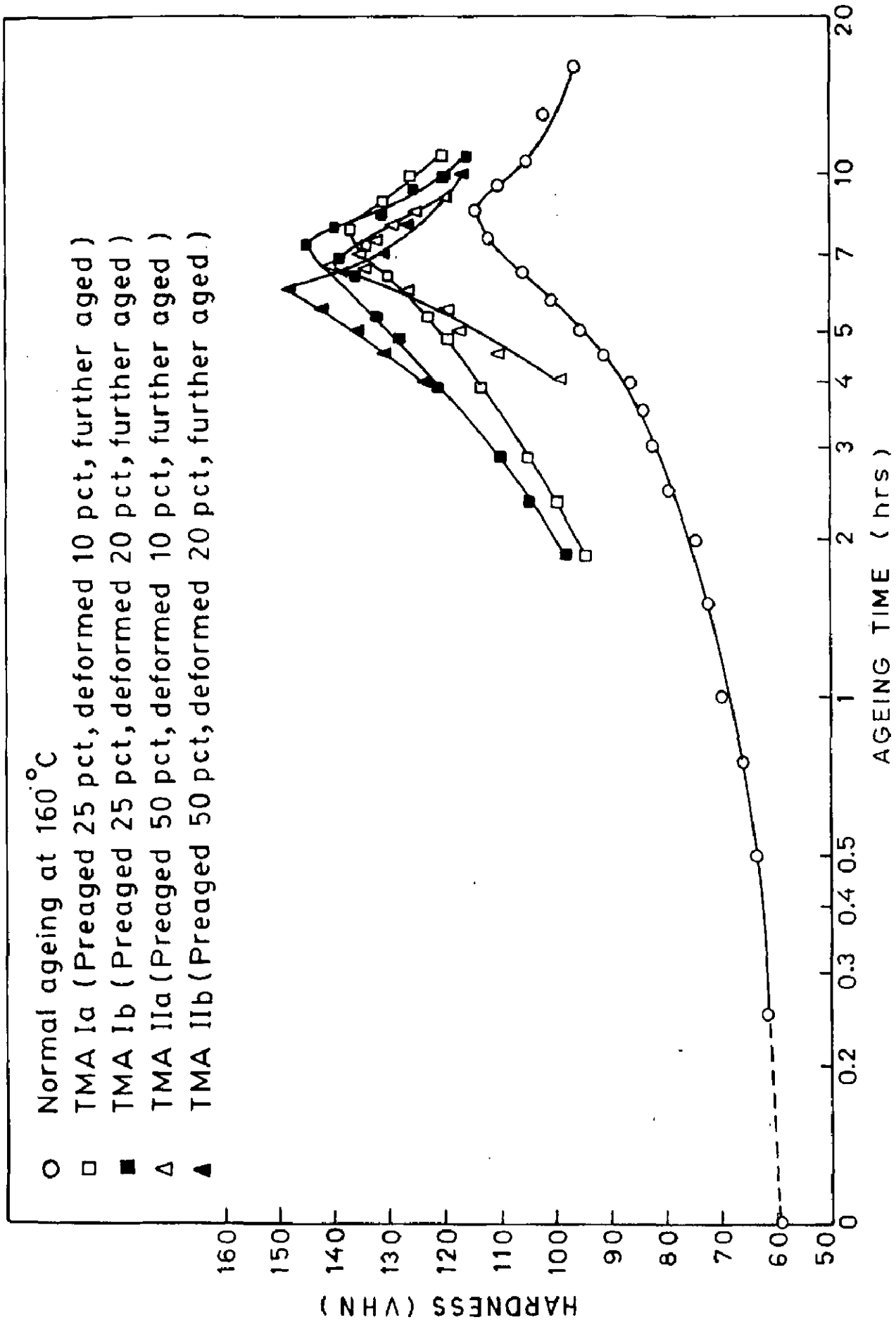


FIG. 4.4 AGEING CURVES FOR THERMOMECHANICALLY PROCESSED 2014 Al ALLOY AT 160°C.

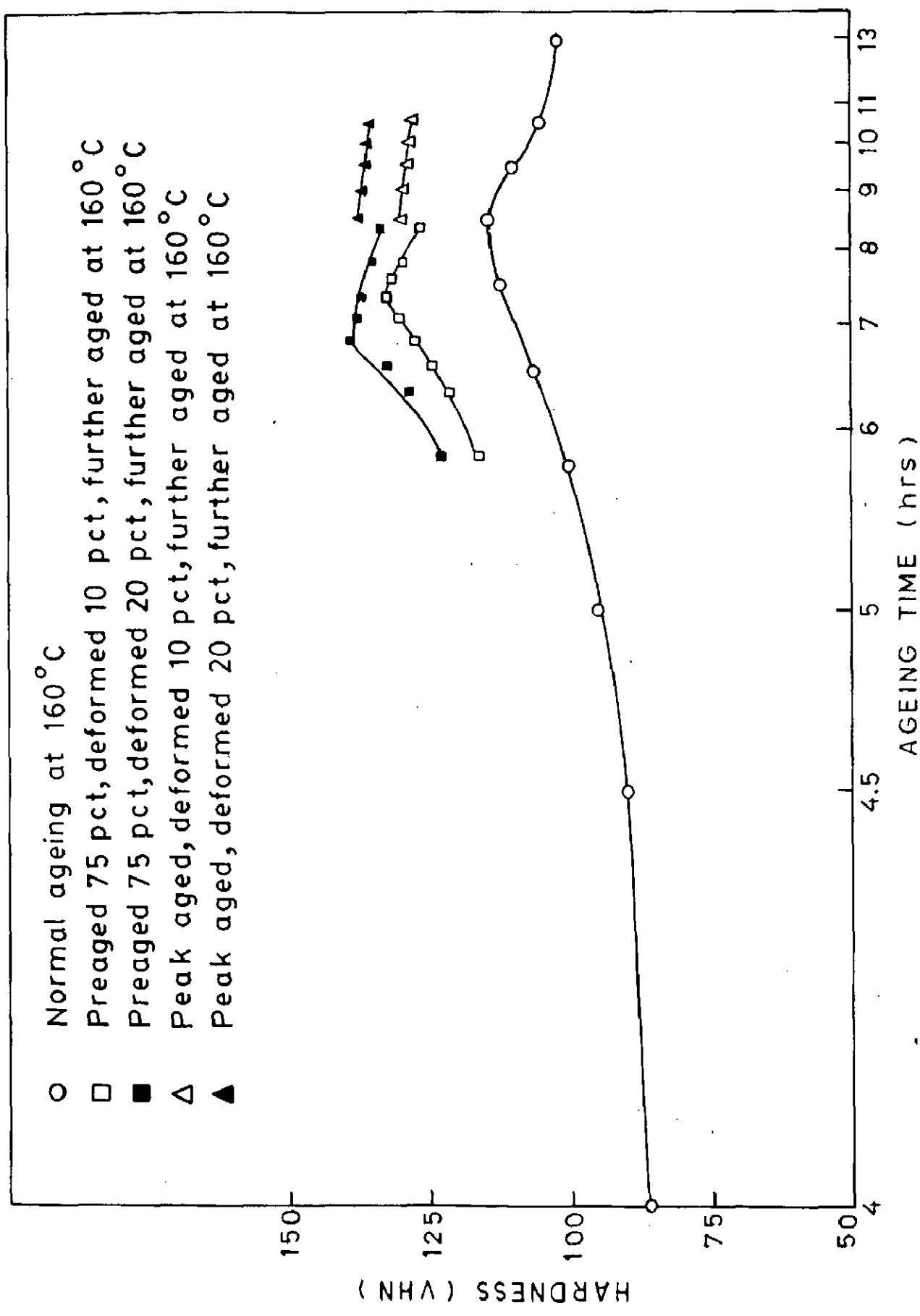


FIG. 4.5 AGEING CURVES FOR THERMOMECHANICALLY PROCESSED 2014 AL ALLOY AT 160°C.

hardness on increasing the deformation from 10 to 20 pct. It may be seen from Figs.4.4 and 4.5 that increasing the deformation from 10 to 20 pct. during thermomechanical ageing increases hardness by 24.4 VHN in 50 pct. preaged alloy whereas the hardness increase for 25 pct. preageing is only 3.4 VHN; for 75 pct. preageing the increase is 5.5 VHN and for peak aged sample it is 7.1 VHN.

It has also been observed that the TMA treatment not only enhances the peak hardness values, but also shortens the ageing periods needed for the peaks to be obtained. It can be clearly seen from Figs.4.4 and 4.5 that 20 pct. deformation is more effective in shifting the peak to lower ageing times as compared to 10 pct. deformation for all preaged samples. The maximum improvement in the hardness has been achieved through TMA IIb treatment, which is observed to raise the peak hardness from 114 VHN (achieved under normal ageing conditions) to 148 VHN and shorten the time required for the peak to be obtained by 2.50 hrs.

In Fig.4.6 the peak hardness as a function of pre-ageing treatment has been shown for both 10 and 20 pct. deformations. It is seen that the peak hardness increases with preageing, attains maximum at 50 pct. preageing, beyond which it again decreases. It is for this reason that in the present investigation the effect of thermomechanical treatment on mechanical properties viz. tensile properties, fatigue and fracture toughness has been studied

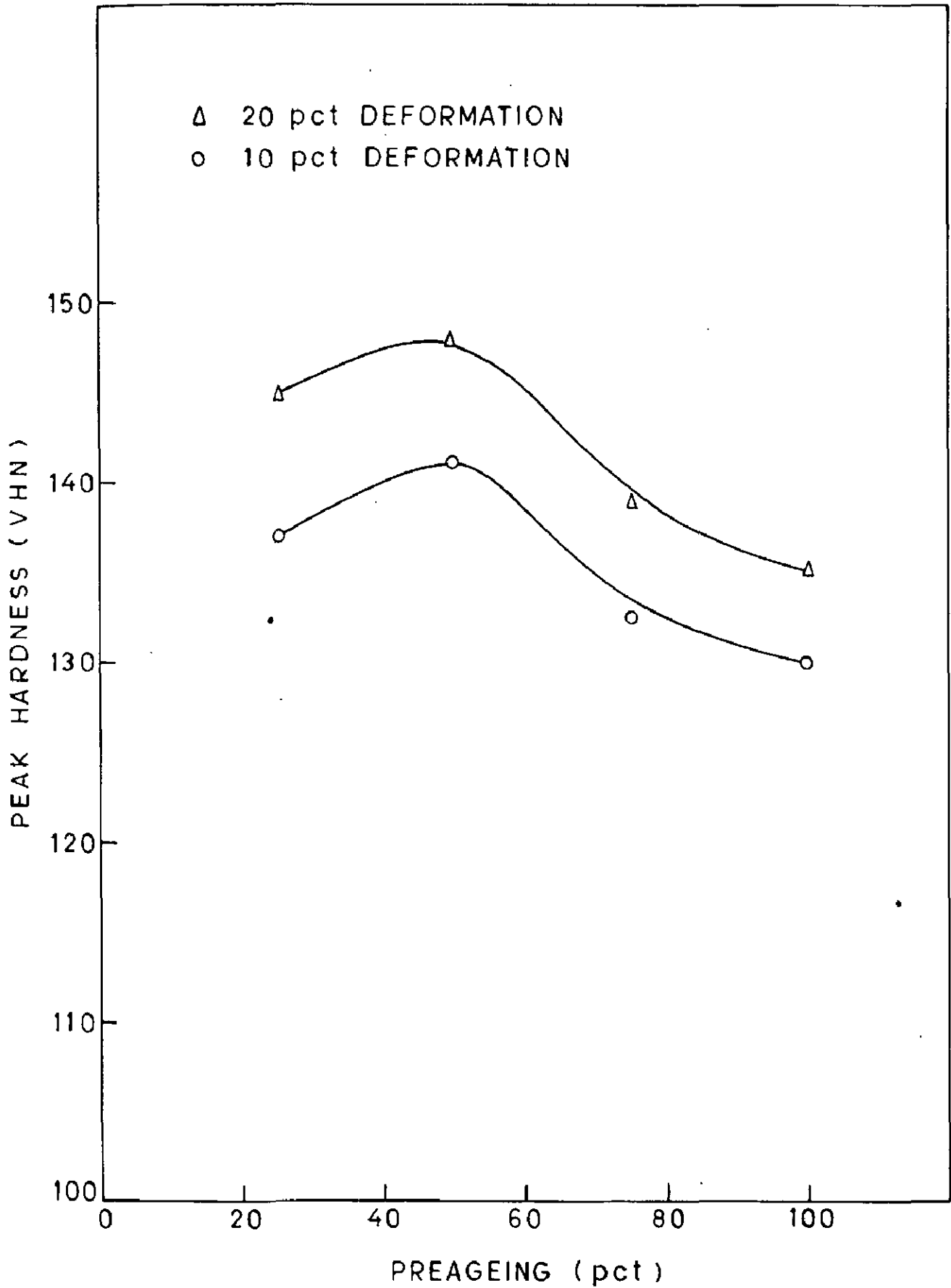


FIG. 4.6 EFFECT OF PREAGEING ON PEAK HARDNESS.

only for 25 pct. preaged (TMA Ia and TMA Ib) and 50 pct. preaged (TMA IIa and TMA IIb) conditions.

### Tensile Properties :

The effect of TMA treatment on room temperature tensile properties viz. UTS, YS and percentage elongation has been studied. Tensile properties have also been measured after various TMA treatments and after 100 hrs exposure at 100, 150, 200 and 250°C. The results are given in Figs.4.7-4.10 and Tables 2-5 and 11-15 (Appendix).

In Fig.4.7 the tensile properties resulting from TMA I and TMA II treatments are plotted against ageing time (hrs) on log scale. It is seen that the strength rises to higher values in both the TMA treatments. It is also seen that the effect of TMA II type of treatment is more than that of TMA I treatment for both 10 and 20 pct. deformations. In TMA I treatment, the UTS rises from 284.40 N/mm<sup>2</sup> to 320.68 N/mm<sup>2</sup> and to 333.44 N/mm<sup>2</sup> after 10 and 20 pct. deformations respectively, whereas in TMA II the UTS rises from 313.82 N/mm<sup>2</sup> to 341.28 N/mm<sup>2</sup> and to 370.70 N/mm<sup>2</sup> after 10 and 20 pct. deformations respectively. Thus increasing the deformation from 10 to 20 pct. causes an increase of 29.42 N/mm<sup>2</sup> in the UTS by TMA II treatment, whereas in TMA I treatment the increase is only 12.76 N/mm<sup>2</sup> in peak aged conditions.

The TMA IIb treatment raises the UTS from 375.12 N/mm<sup>2</sup> (achieved in the normal peak ageing) to a peak value of

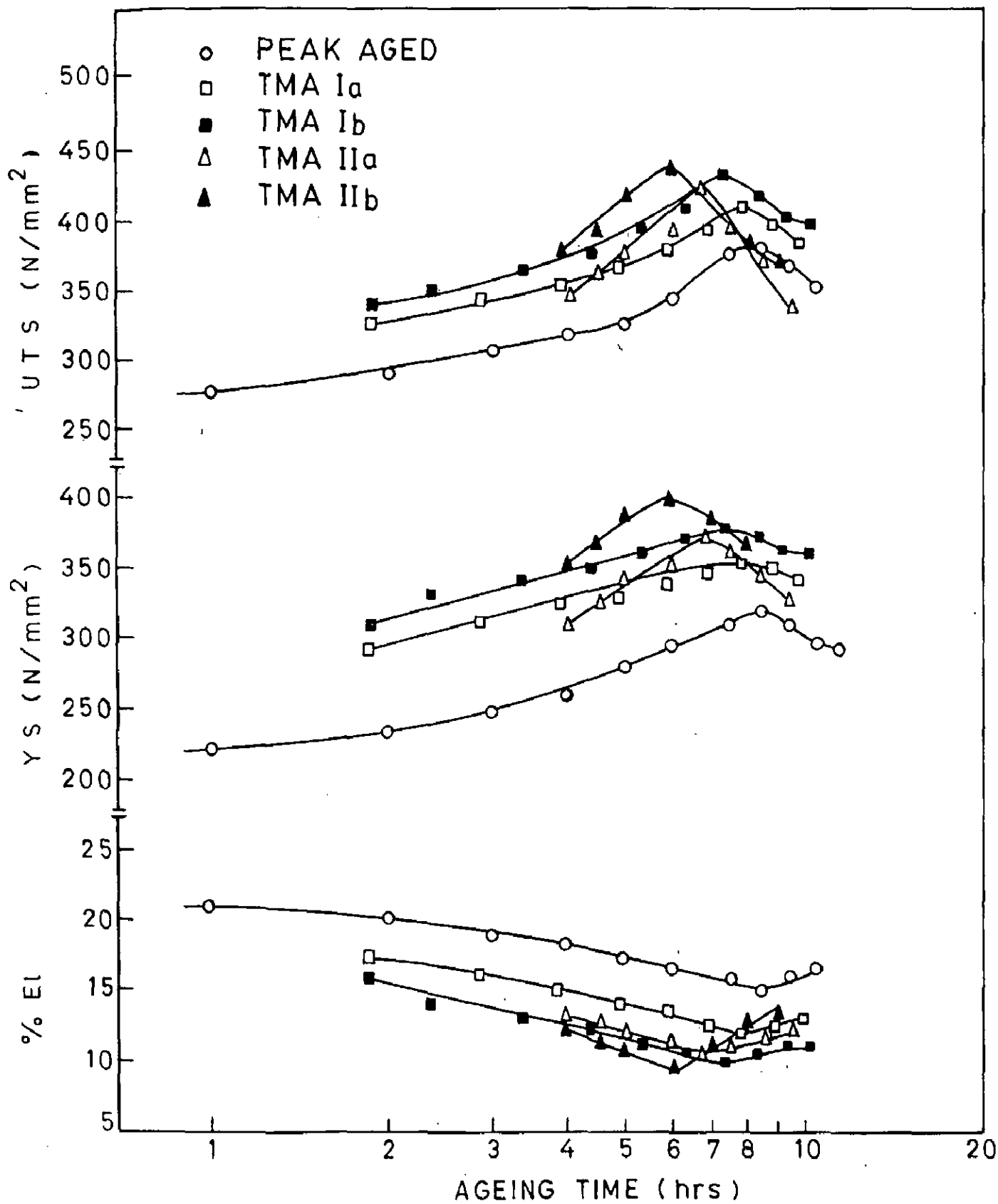


FIG. 4.7 EFFECT OF THERMOMECHANICAL AGEING ON TENSILE PROPERTIES.

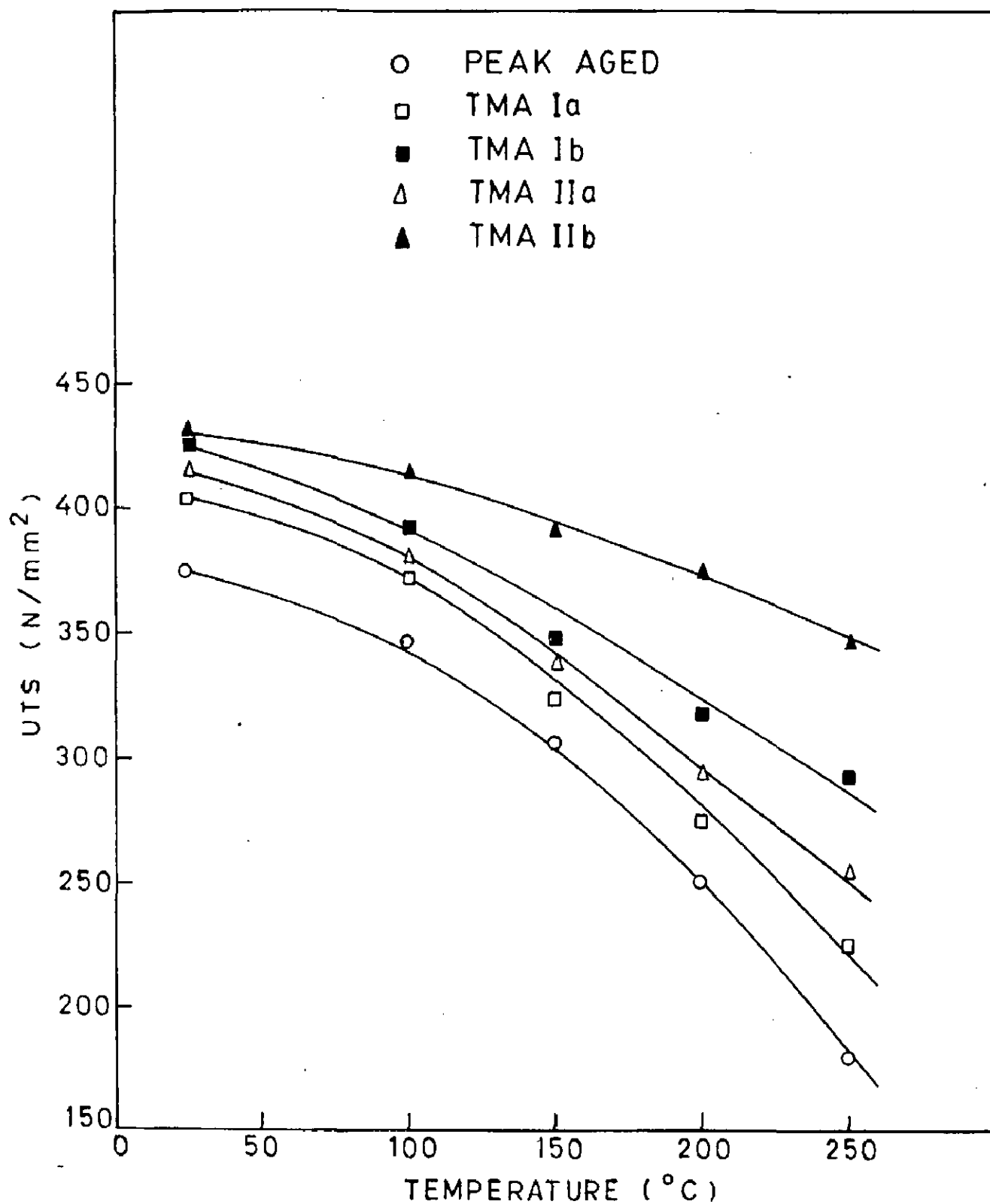


FIG. 4.8 PEAK UTS VALUES AFTER DIFFERENT THERMO-MECHANICAL TREATMENTS AND AFTER 100 HOUR EXPOSURE AT DIFFERENT TEMPERATURES.

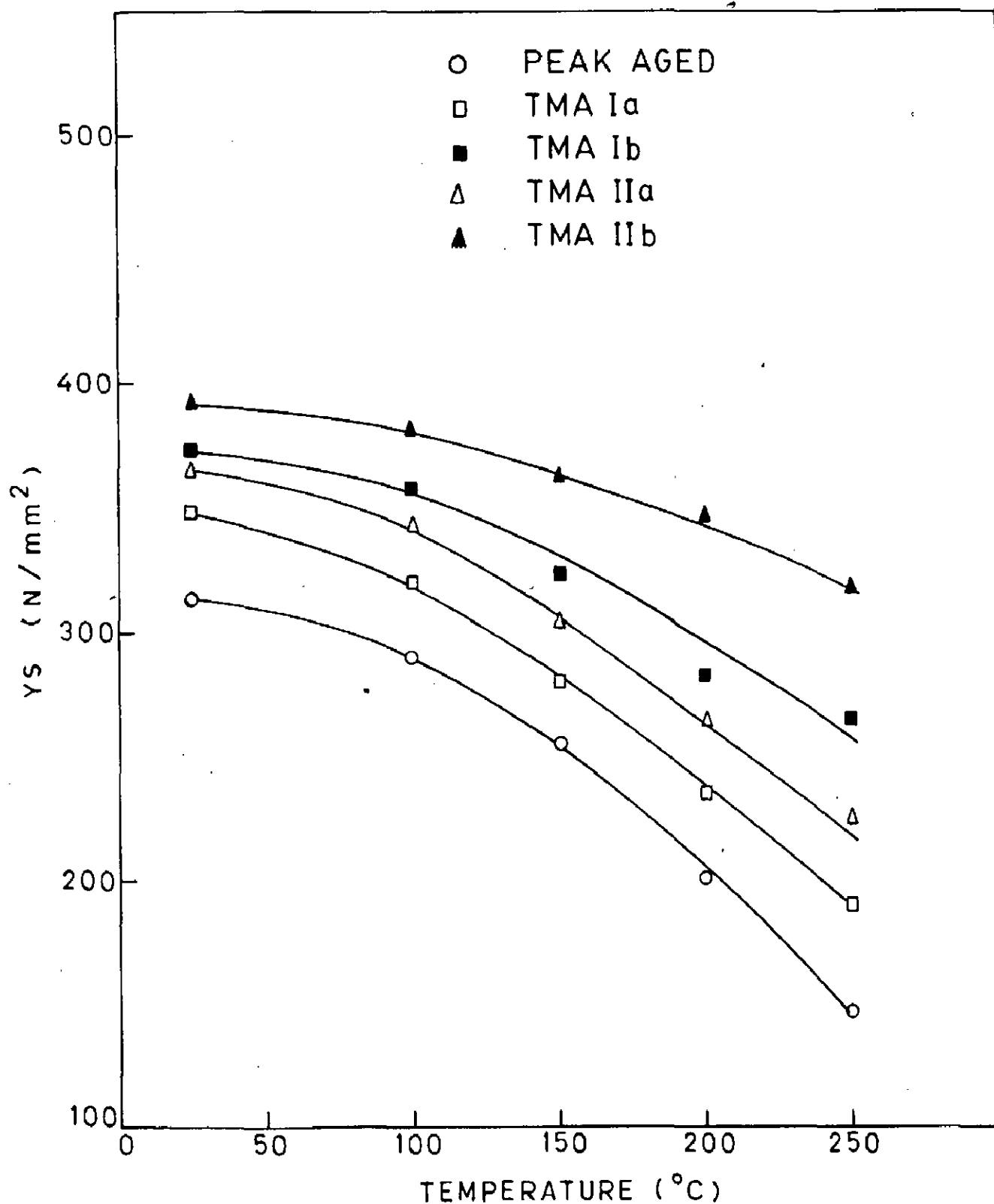


FIG. 4.9 PEAK YS VALUES AFTER DIFFERENT THERMO-MECHANICAL TREATMENTS AND AFTER 100 HOUR EXPOSURE AT DIFFERENT TEMPERATURES.



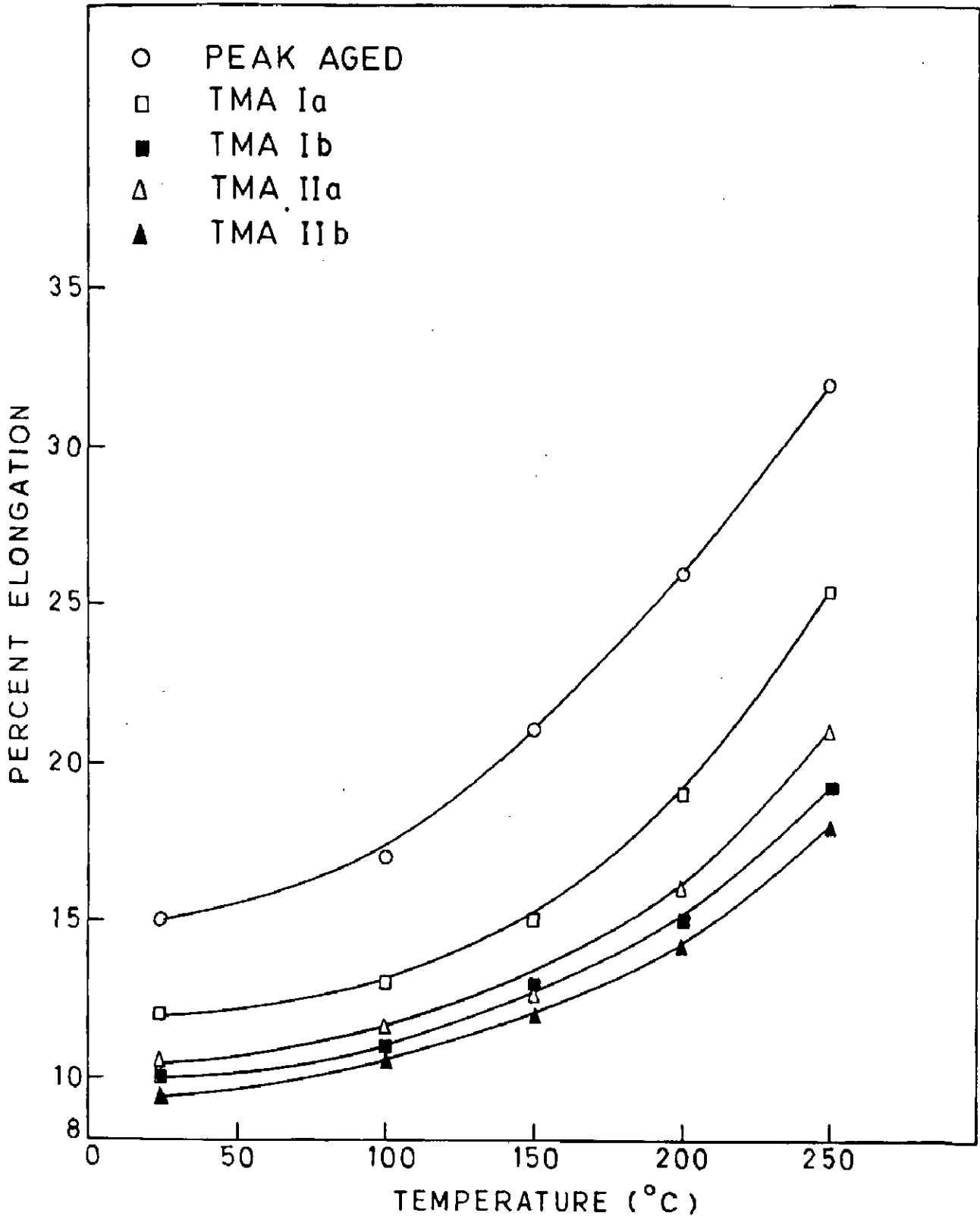


FIG. 4.10 PEAK VALUES OF PERCENT ELONGATION AFTER DIFFERENT TMTs AND AFTER 100 HOUR EXPOSURE AT DIFFERENT TEMPERATURES.

431.50 N/mm<sup>2</sup> for a loss of elongation from 15 to 9.50 pct. From fig.4.7 it is also clear that the tensile properties (UTS or YS) obtained through TMA I Ib is higher than those obtained through TMA I Ia.

The peak values of tensile properties after various TMA treatments and after 100 hrs exposure at 100°C, 150°C, 200°C and 250°C are plotted in Figs.4.8-4.10. From Fig.4.8 it can be seen that the UTS for peak aged samples decreases from 375.12 N/mm<sup>2</sup> to 178.48 N/mm<sup>2</sup> when exposed to 250°C for 100 hrs; whereas in TMA I Ib treated samples the UTS decreases from 431.50 N/mm<sup>2</sup> to 346.18 N/mm<sup>2</sup> only.

similar effect has also been observed on yield strength as may be seen in Fig.4.9. The elongation of peak samples (Fig.4.10) is observed to increase from 15 to 32 percent, whereas in the TMA I Ib treated samples the elongation increases from 9.50 to 18 percent. Thus, it is seen that the TMA I Ib treatment not only imparts maximum improvement but also provides maximum stability to tensile properties when exposed to higher working temperatures.

#### Fatigue Properties:

The results of fatigue properties have been plotted in Fig.4.11 in the form of S-N curves for as quenched, peak aged and thermomechanically aged samples. The S-N curves have been plotted for various stress levels ranging from 98 N/mm<sup>2</sup> to 177 N/mm<sup>2</sup>. The S-N curves for as quenched, peak

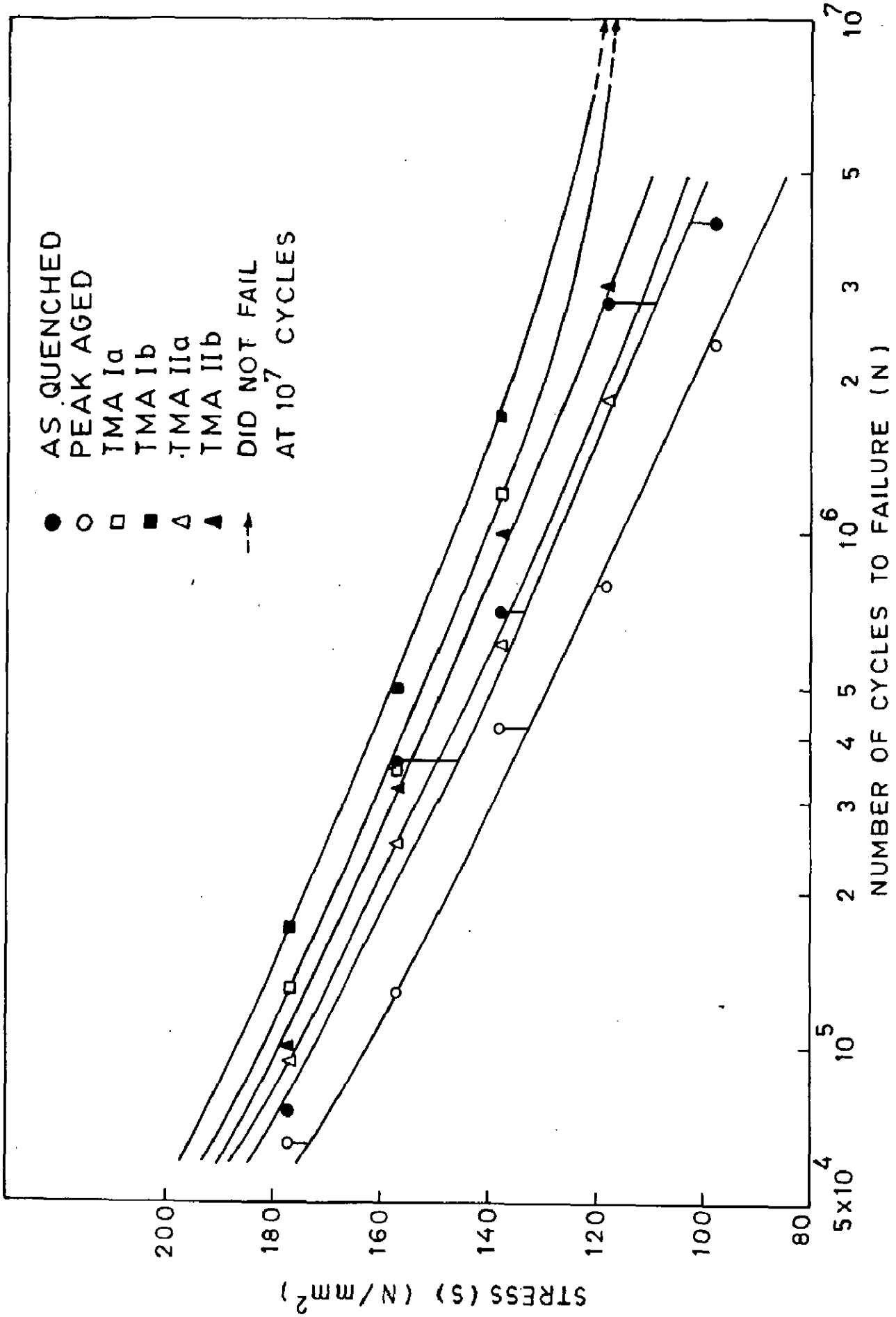


FIG. 4.11 EFFECT OF THERMOMECHANICAL AGEING ON FATIGUE PROPERTIES. 79

aged and thermo-mechanically treated samples are more or less parallel indicating similar mechanisms of operation in all the cases. It is seen from the curves that at any stress level the alloy in the peak aged condition has lower fatigue life than in the as quenched condition. Further it can also be seen from histogram (Fig.4.12) that at any stress level the fatigue life is higher for thermomechanically aged specimens as compared to as quenched and peak aged specimens. The best fatigue properties are observed in the alloy after TMA Ib treatment. In both 25 and 50 pct. preaged conditions it is seen that 20 pct. deformation is more effective in improving the fatigue properties than 10 pct. deformation. The alloy in 25 pct. preaged condition possesses better fatigue properties than in the 50 pct. preaged condition. It is seen that the fatigue life of the alloy samples given TMA Ia and TMA Ib treatments are even higher than  $10^7$  cycles at  $98 \text{ N/mm}^2$  stress level.

The S-N curves have a tendency to converge at high stress level and tend to diverge as the stress level is decreased, indicating that the relative effect of TMA treatment increases as the stress level during fatigue test is lowered, i.e. in the high cycle range, the TMA treatments are most effective in improving fatigue properties. For example, at  $118 \text{ N/mm}^2$  stress level the

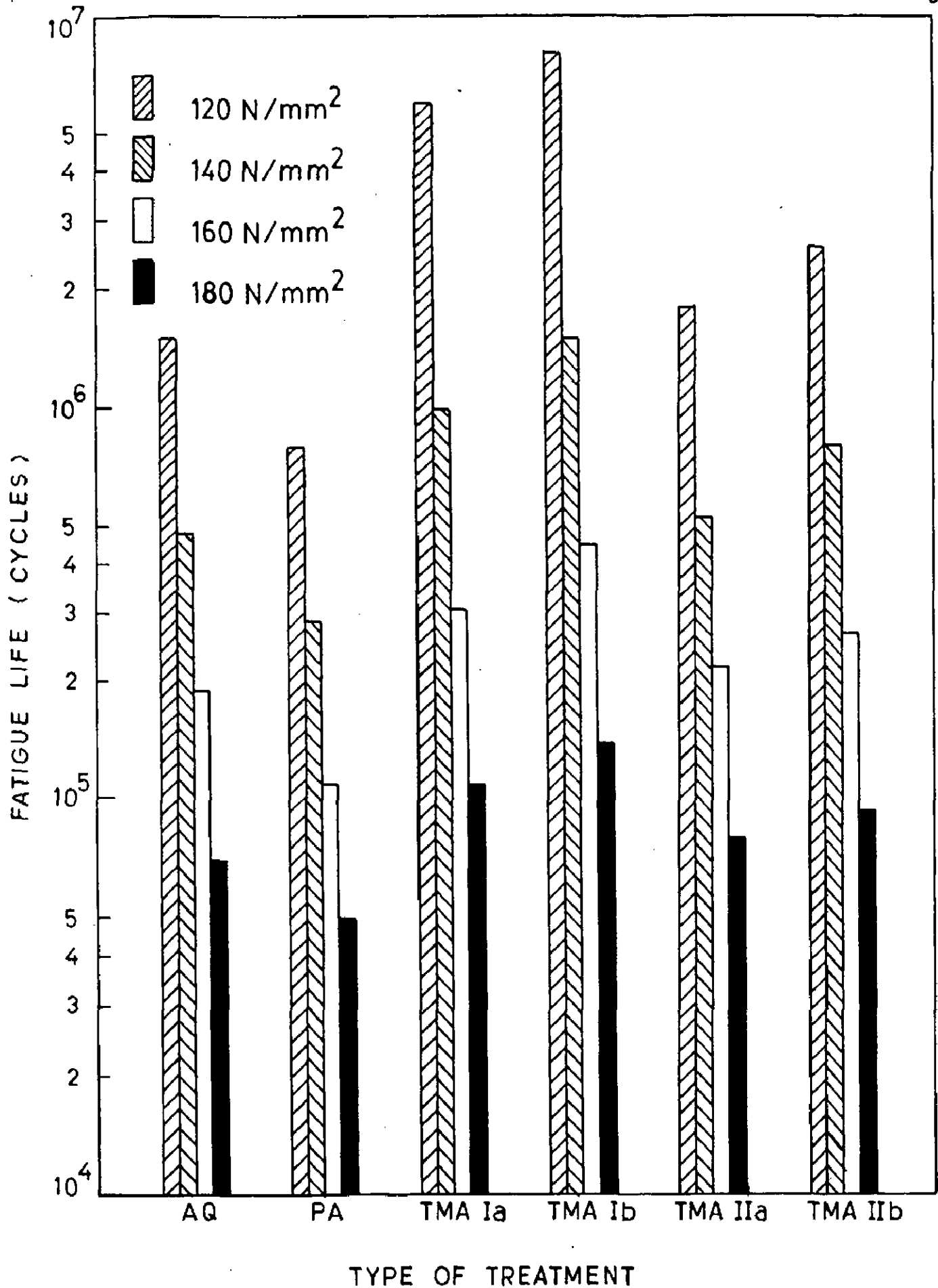


FIG. 4.12 EFFECT OF THERMOMECHANICAL AGEING AND APPLIED STRESS ON FATIGUE LIFE.

fatigue life is  $2 \times 10^6$  cycles for TMA IIa treated samples as against  $3 \times 10^6$  cycles for TMA IIb treated samples. Thus at this stress level the relative difference between the fatigue life after TMA IIb and TMA IIa treatments is  $1.0 \times 10^6 (3 \times 10^6 - 2 \times 10^6)$  cycles, whereas at  $177 \text{ N/mm}^2$  stress level this difference is only  $0.2 \times 10^5 (1.2 \times 10^5 - 1.0 \times 10^5)$  cycles. From Fig.4.11 it is also seen that for any value of fatigue life the corresponding fatigue stress (endurance limit) of the alloy after TMA Ib treatment (which gives best fatigue properties) is constantly higher by a margin of approximately 25 to 35  $\text{N/mm}^2$  from the values obtained in the peak aged condition throughout the range of investigation.

In the present study, there is considerable scatter in test results, which is typical of fatigue tests. Some variation can usually be found in repeated observations of any measureable quantity. There are, however, certain factors which are responsible for the considerable scatter in the fatigue test data. Since fatigue test is destructive, it is not possible to measure the fatigue strength of the same specimen several times. Accordingly, variation observed in test results includes effects, both of possible errors in loading and measuring and also of variability of specimen selection and preparation. Since the observed fatigue limit is sensitive to selection of samples and to details of loading, uncontrolled variations in any of the above may

introduce either systematic or random errors in test results. The machine, which has been used in the present investigation (Wöhler type), has separate drives for the load variation and the indicator. So, any slipping of chord driving the indicator may lead to error in reading the load value. However, the factor of major concern in the fatigue test is the variation of samples.

#### Fracture Toughness:

The effect of thermomechanical ageing on fracture toughness properties has been studied through notched tensile tests and charpy tests. The values of fracture toughness calculated from double edge-notched tensile testing are designated as  $K_{Ic}$  while the values obtained through V-notch charpy test are denoted as  $K_{Id}$ . Both  $K_{Ic}$  and  $K_{Id}$  are designated in terms of  $MPa\sqrt{m}$  or  $N/mm^{3/2}$  or  $KSi\sqrt{in}$ . In Figs. 4.13 and 4.14 the values of fracture toughness have been plotted against yield strength for as quenched, peak aged and thermomechanically treated samples. To see the direct effect of TMA I and TMA II treatments on fracture toughness the results have also been plotted in the form of histograms (Figs. 4.15 and 4.16). From the results obtained it is seen that the values of plane strain fracture toughness ( $K_{Ic}^*$ ) and dynamic fracture toughness ( $K_{Id}$ ) increase with increase in the yield strength of the material. Thus the thermo-mechanical treatments TMA I and TMA II enhance the fracture toughness properties of the 2014 Al-alloy.

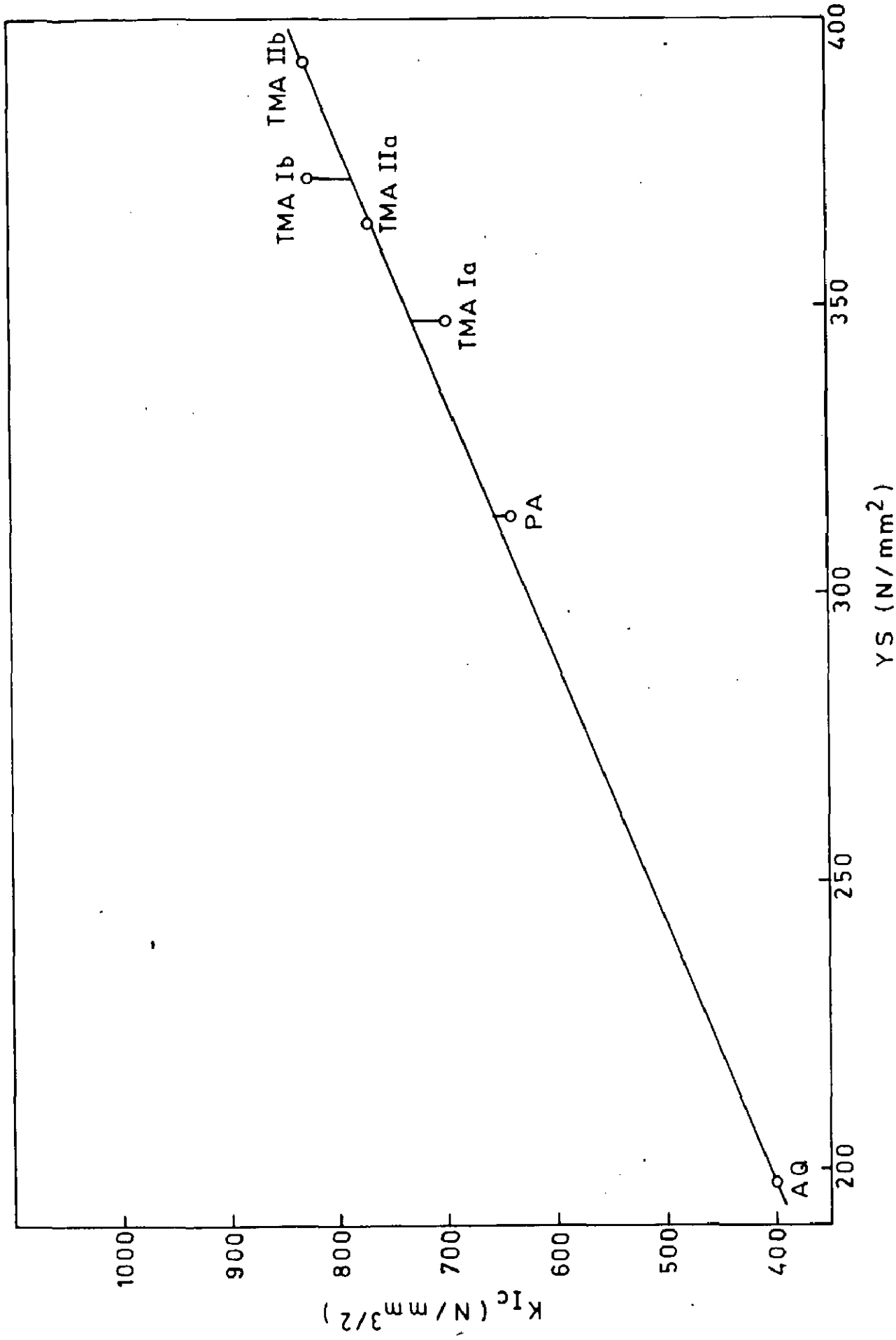


FIG. 4.13 THE RELATIONSHIP BETWEEN  $K_{Ic}$  AND  $YS$ .



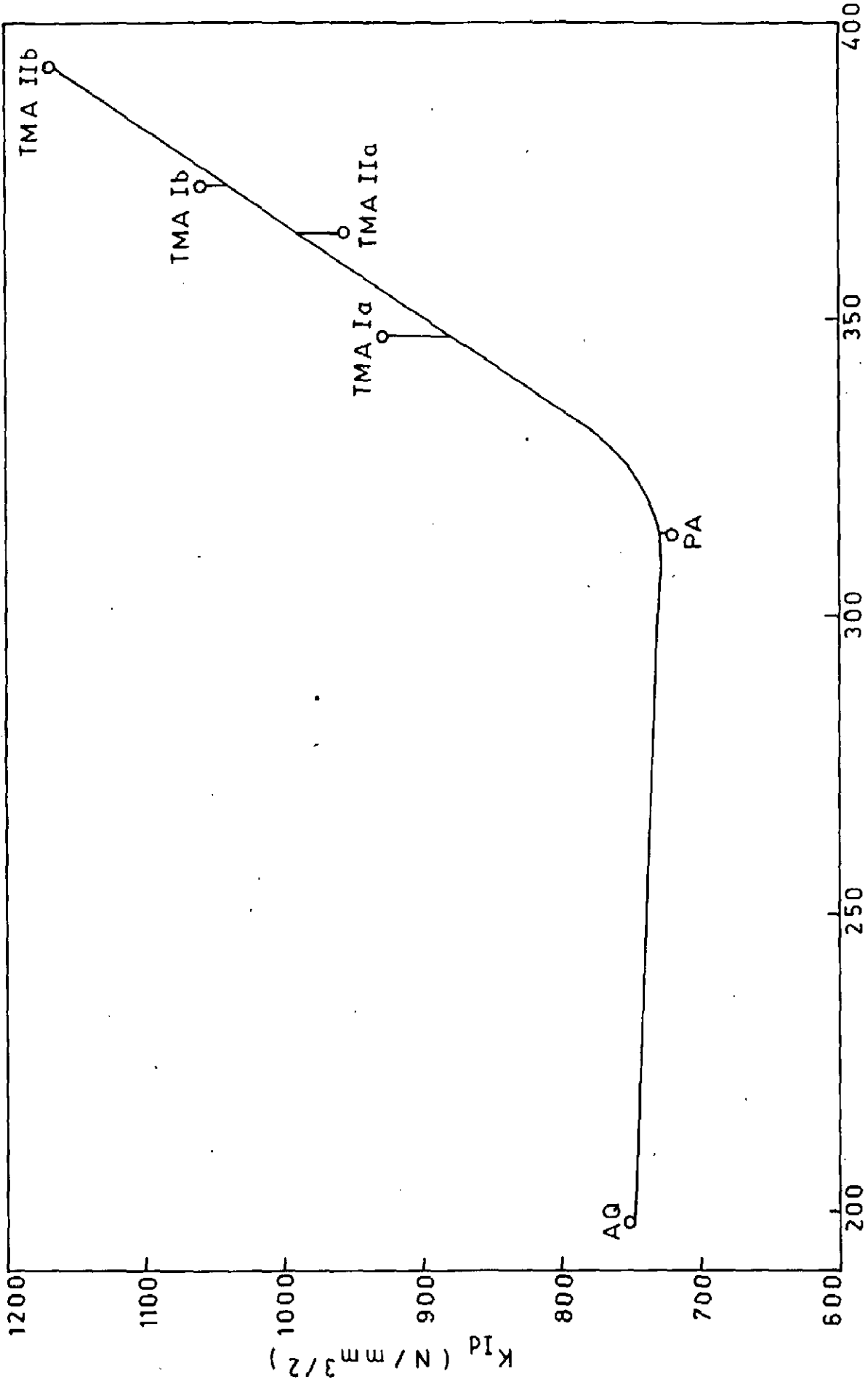


FIG. 4.14 THE RELATIONSHIP BETWEEN  $K_{ID}$  AND YS.

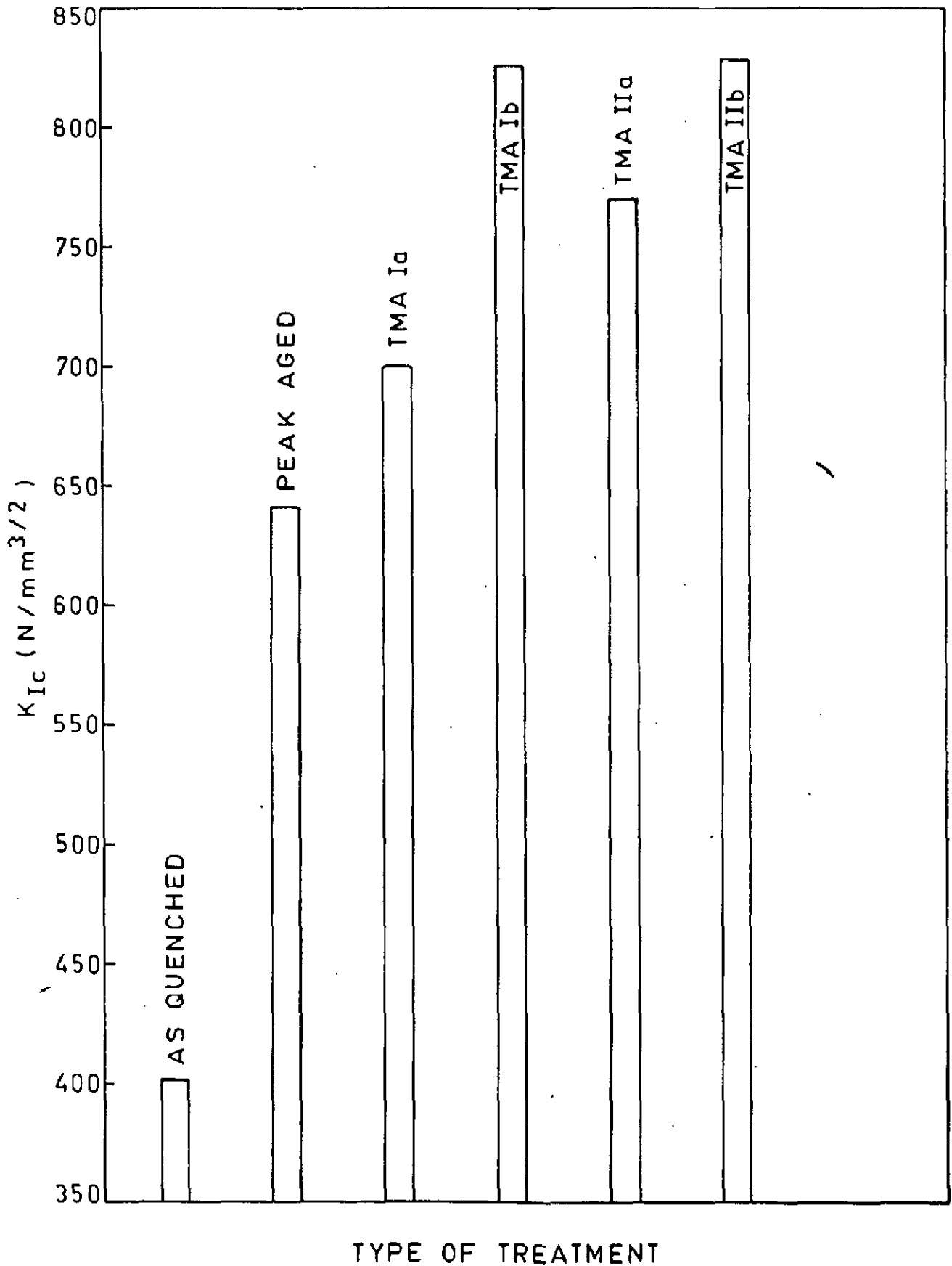


FIG.4.15 EFFECT OF THERMOMECHANICAL AGEING ON  $K_{Ic}$ .

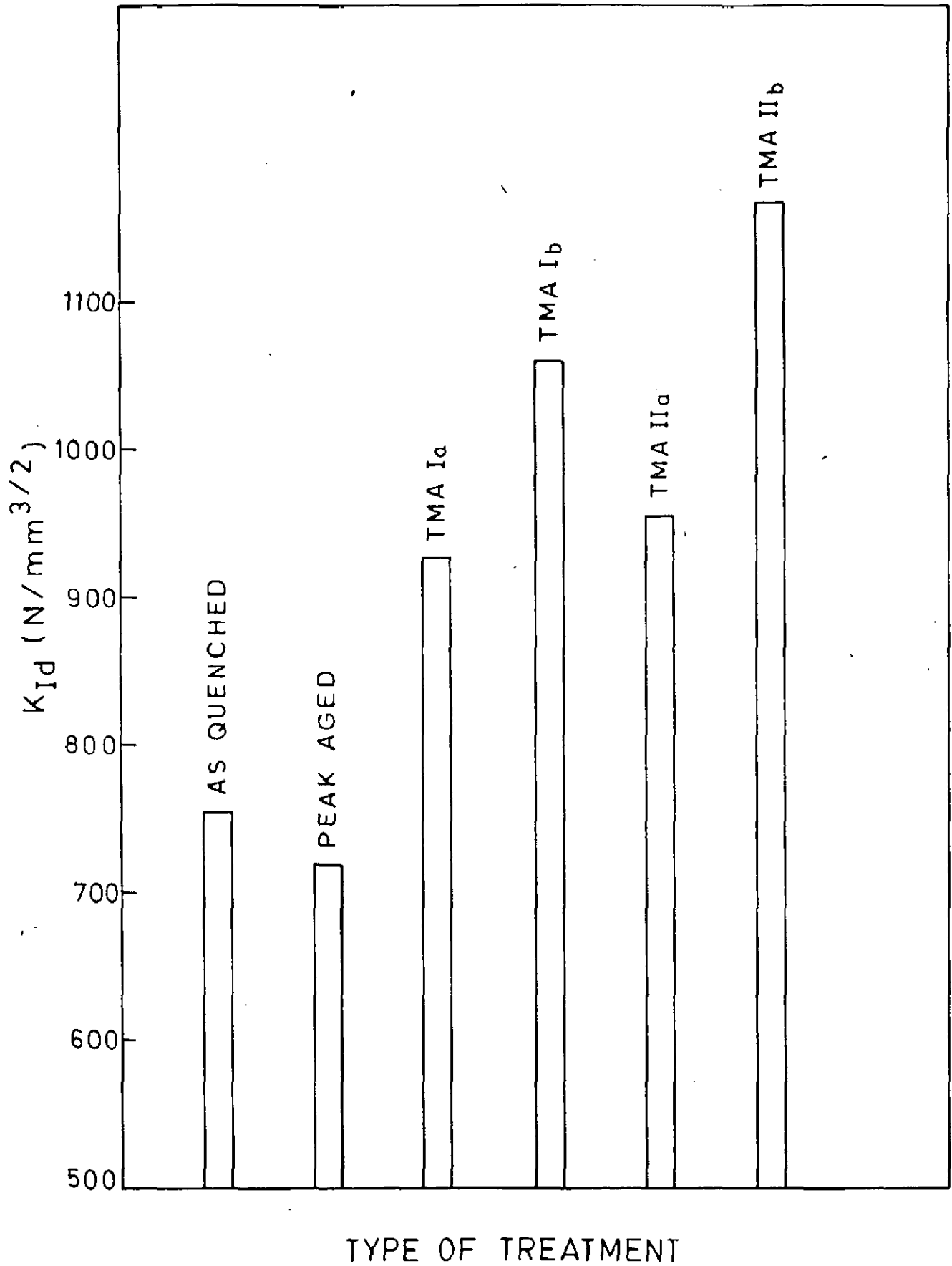


FIG. 4.16 EFFECT OF THERMOMECHANICAL AGEING ON  $K_{IId}$ .

Due to thermomechanical ageing the  $K_{IC}$  value rises from  $641.58 \text{ N/mm}^{3/2}$  in the peak aged condition to  $828.20 \text{ N/mm}^{3/2}$  after the TMA IIb treatment. From Fig.4.15 it is also clear that effects of TMA Ib and TMA IIb treatments on plane strain fracture toughness are almost same. Thus both TMA Ib and TMA IIb treatments enhance the  $K_{IC}$  value from peak aged condition by about 30 pct. From Table 23 (Appendix) and Fig.4.15 it is observed that the  $K_{IC}$  value rises to  $699.88 \text{ N/mm}^{3/2}$  and to  $826.26 \text{ N/mm}^{3/2}$  after TMA Ia and TMA Ib treatments respectively, whereas in TMA IIA and TMA IIb treatments the  $K_{IC}$  values obtained are  $770.85 \text{ N/mm}^{3/2}$  and  $828.20 \text{ N/mm}^{3/2}$  respectively. Thus the relative effect of deformation is much more in TMA I treatment as compared to TMA II treatment. It may be noted that increasing the deformation from 10 to 20 pct., in 50 pct. preaged condition, leads to a rise in  $K_{IC}$  by  $57.35 \text{ N/mm}^{3/2}$ ; whereas in 25 pct. preaged condition the rise is by  $126.38 \text{ N/mm}^{3/2}$ . The dynamic fracture toughness ( $K_{ID}$ ) values have been obtained through V-Notch Charpy tests and are plotted against yield strength in Fig.4.14 and in the form of histogram in Fig.4.16. The effect of thermomechanical processing on dynamic fracture toughness ( $K_{ID}$ ) is almost same as has been observed in case of plane strain fracture toughness ( $K_{IC}$ ). The only difference is that the value of dynamic fracture toughness ( $K_{ID}$ ) obtained for as quenched specimen is higher than that obtained in peak aged condition, presumably due to the difference in dislocation density

and difference in the density and size of dispersoids. The  $K_{Ic}$  value of as quenched specimen is  $754.00 \text{ N/mm}^{3/2}$ , whereas for peak aged specimen, it is  $720.00 \text{ N/mm}^{3/2}$ . It has been observed that TMA IIb is the most successful treatment in increasing the dynamic fracture toughness of the alloy under investigation. As described earlier the effect of TMA Ib and TMA IIb treatment is almost same on final  $K_{Ic}$  values. In case of V-notch charpy tests for dynamic fracture toughness ( $K_{Id}$ ), however, TMA IIb treatment is much more effective than TMA Ib. The effect can be clearly seen from Fig.4.16 which shows that the  $K_{Id}$  value after TMA Ib is  $1060.00 \text{ N/m}^{3/2}$ , whereas after TMA IIb treatment it is  $1168.00 \text{ N/mm}^{3/2}$ . The effect of the amount of deformation on  $K_{Ic}$  and  $K_{Id}$  values is almost same. From Figs.4.15 and 4.16 it is observed that 20 pct. deformation is more effective in raising  $K_{Ic}$  and  $K_{Id}$  values than 10 pct. deformation in both the TMA I and TMA II thermomechanical treatments.

Fig. 4.17 shows variation of dynamic fracture toughness parameter ( $K_{Ic}^2/E$ ) with total energy of fracture per unit area (CVN/A). The straight line relationship between these parameters is in agreement with the observations of Ewing and Raymond [166] and Koppenaal [167] and is indicative of the correctness of  $K_{Ic}$  measurement in the present investigation.

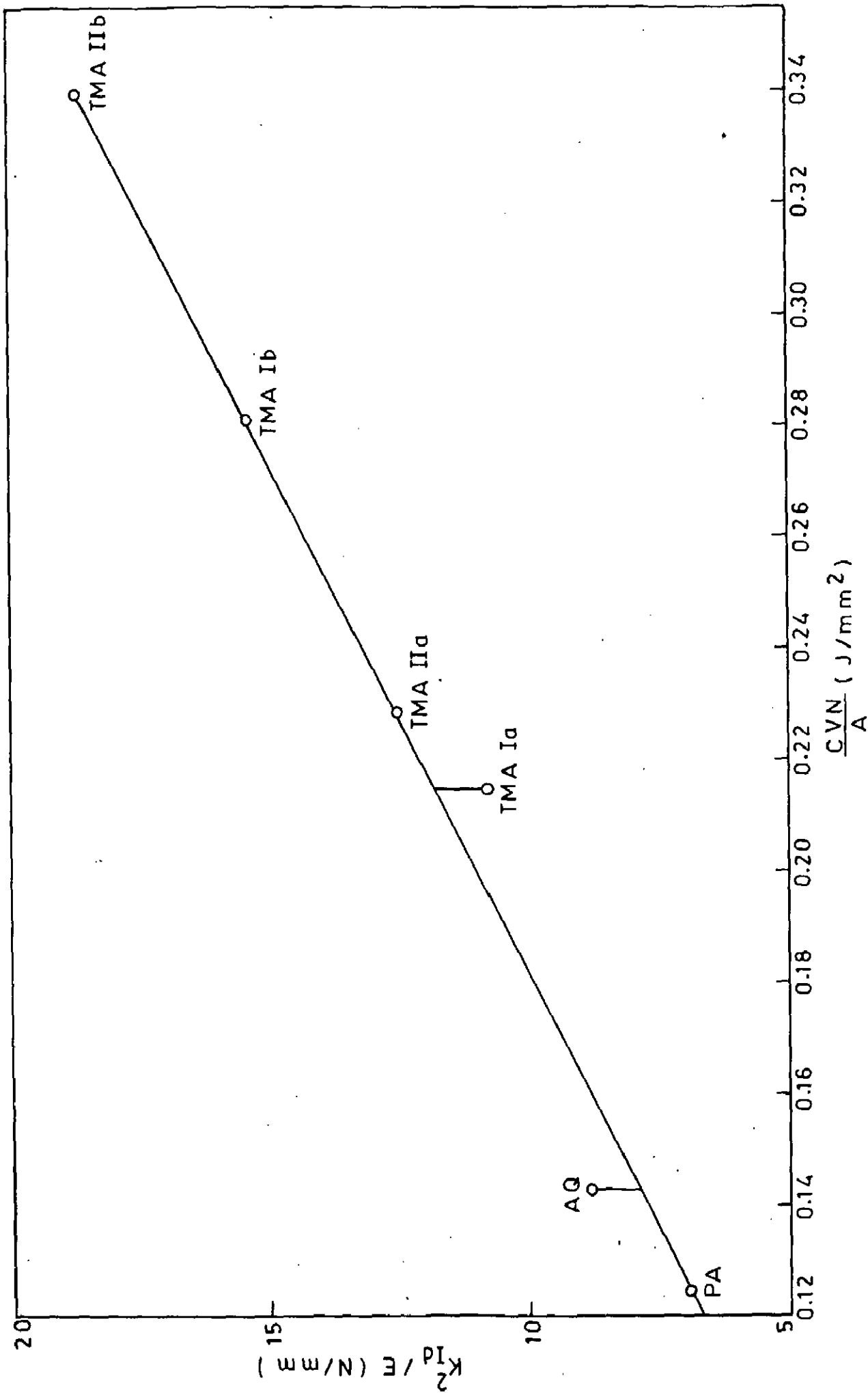


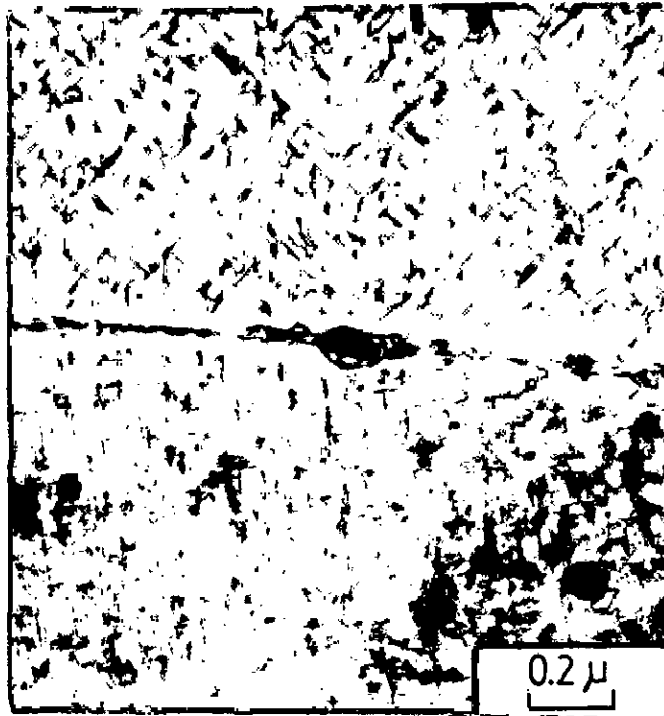
FIG. 4.17 RELATIONSHIP BETWEEN DYNAMIC FRACTURE TOUGHNESS PARAMETER ( $K_{I_d}^2/E$ ) AND ENERGY ABSORBED PER UNIT AREA ( $CVN/A$ ).

#### 4.3 TRANSMISSION ELECTRON MICROSCOPIC (TEM) STUDIES

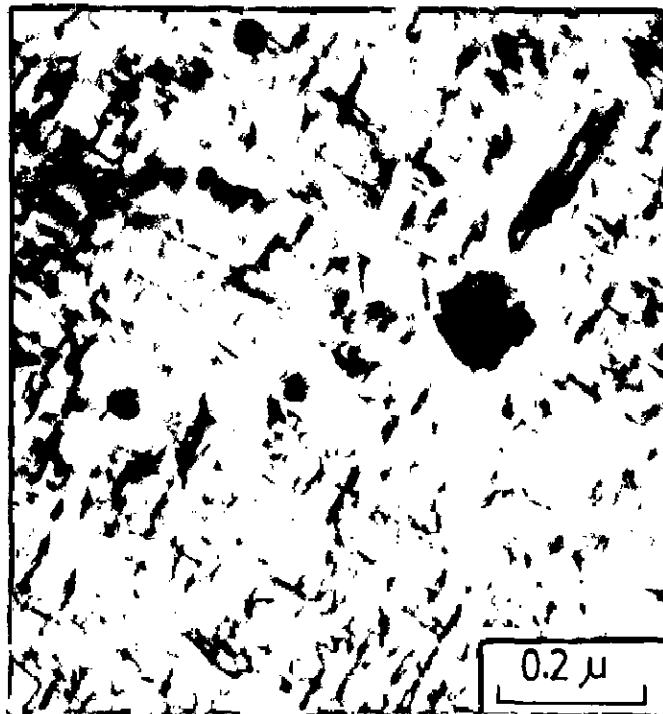
The structural changes resulting from various treatments were systematically studied using Philips EM 400 electron microscope. The results are given in Figs. 4.18 - 4.25.

In peak aged specimens we observe the formation of both  $\theta''$  and  $\theta'$  precipitates. Fig. 4.18 shows a transmission electron micrograph of a sample which has been peak aged. One also observes the existence of dispersoids at the grain boundary and in the matrix. The distribution of dispersoids is not uniform as revealed by optical microscopic studies in Section 4.5. In the peak aged condition the proportion of  $\theta''$  precipitates (GP II) is observed to be substantially higher than that of  $\theta'$  precipitates. The  $\theta'$  precipitates are characterised by their sharp needle form as compared to diffused particle-matrix interface associated with  $\theta''$  precipitates which is caused due to coherency strains. Fig. 4.19 shows the existence predominantly of  $\theta''$  platelets and a very small amount of  $\theta'$  precipitates.

The thermomechanical treatments substantially affect the ageing characteristics and the resultant microscopic structure. The degree of preageing (which affects the concentration of solutes in the matrix), the degree of deformation (which affects nucleation of  $\theta'$ ) and the final ageing treatment will affect the entire process of ageing and the resultant structures are expected to be widely



(a)



(b)

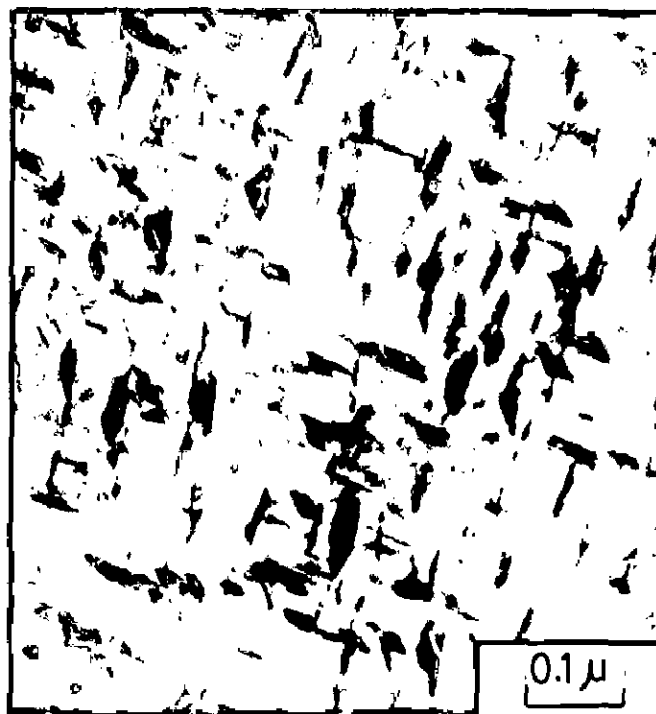
FIG. 4.18 TRANSMISSION ELECTRON MICROGRAPHS SHOWING THE EXISTENCE OF  $\theta''$ ,  $\theta'$  AND DISPERSOIDS IN PEAK AGED CONDITION.

( a and b different locations )





(a)



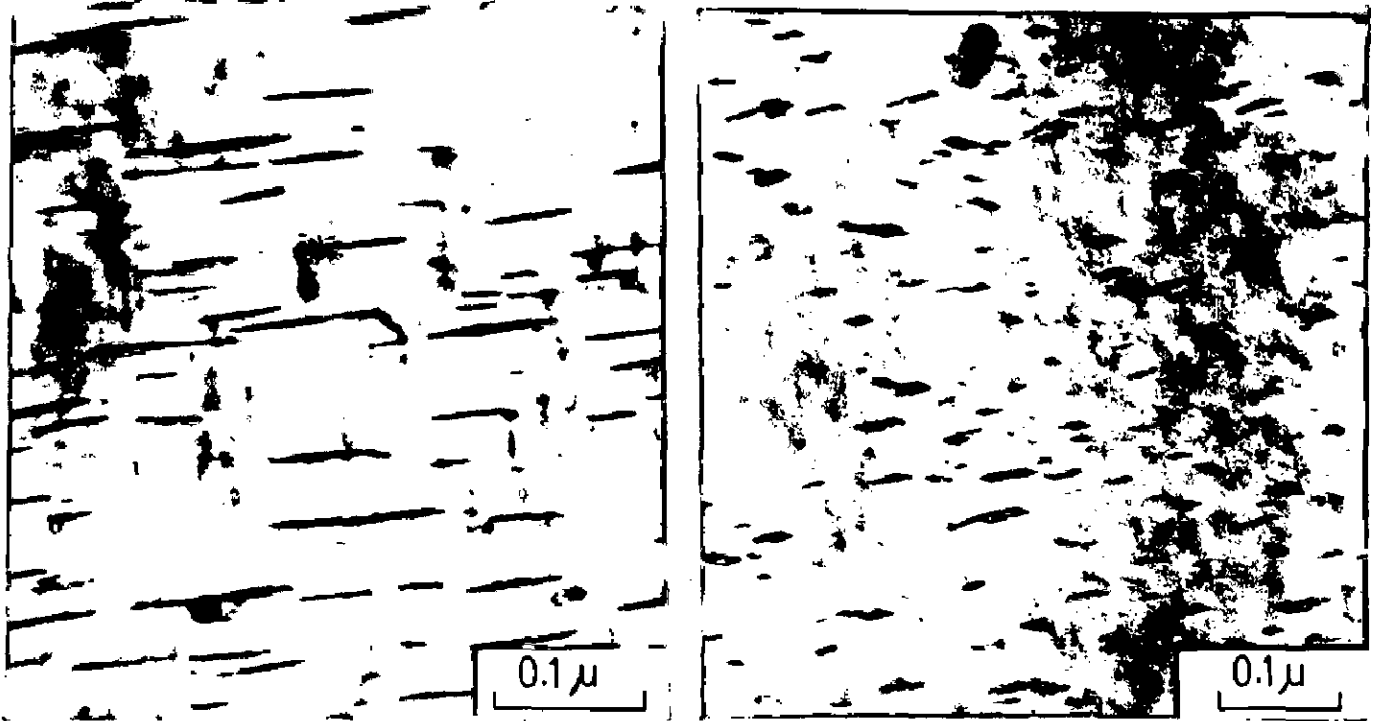
(b)

FIG.4.19 TRANSMISSION ELECTRON MICROGRAPHS SHOWING THE EXISTENCE OF PREDOMINENTLY  $\theta''$  PLATELETS TOGETHER WITH SMALL AMOUNT OF  $\theta'$  IN PEAK AGED CONDITION.

( a and b different locations )

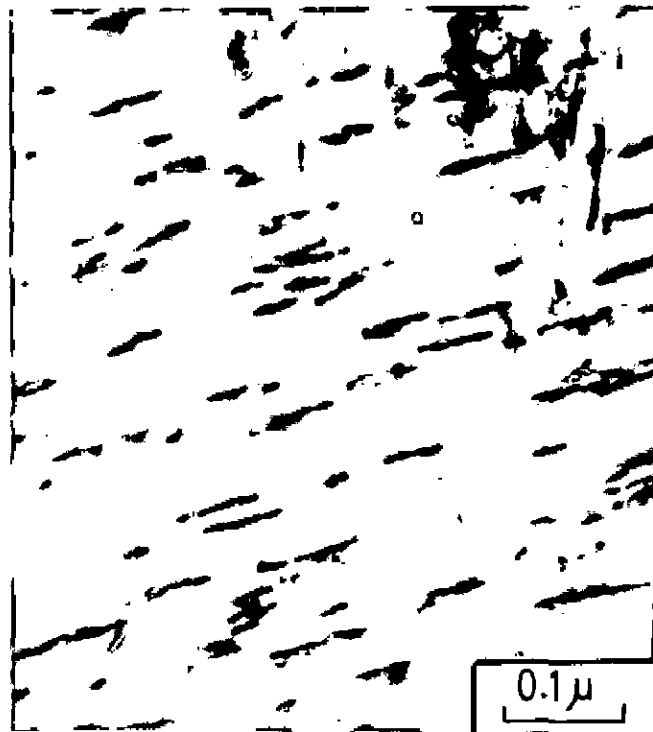
different under different conditions of thermomechanical ageing.

From the present study it is also observed that the TEM structure in all the samples varied from region to region, presumably due to inhomogeneity of deformation and the ageing sequence. Deformation causes additional nucleation centres for  $\theta'$  precipitates during the thermomechanical treatments. The maximum effect of  $\theta'$  nucleation appears to be in TMA Ib treatment. A comparison of the transmission electron micrographs obtained for peak aged, TMA Ib and TMA IIb treated specimens is given in Fig. 4.20. It is clearly observed that TMA Ib treated sample has  $\theta'$  precipitates in the finest form ( $\sim 400 \text{ \AA}$ ). Coarsest size  $\theta'$  needles ( $\sim 850 \text{ \AA}$ ) are observed in peak aged treatment; the TMA IIb treatment yield  $\theta'$  in the intermediate size ( $\sim 600 \text{ \AA}$ ). Both the TMA I and TMA II treatments suppress the formation of  $\theta''$  platelets. From the TEM studies, it is observed that intermediate deformation and ageing treatments during TMA I and TMA II cause dissolution of  $\theta''$  and /or its conversion to  $\theta'$ , as the final TEM structures hardly reveal any presence of  $\theta''$  platelets. At any degree of preageing, the amount of deformation also plays important role in the subsequent ageing kinetics. It is observed in both TMA I and TMA II treatments that 20 pct. deformation leads to finer  $\theta'$  as compared to 10 pct. deformation. Fig. 4.21 shows this effect for TMA II treatments.



(a)

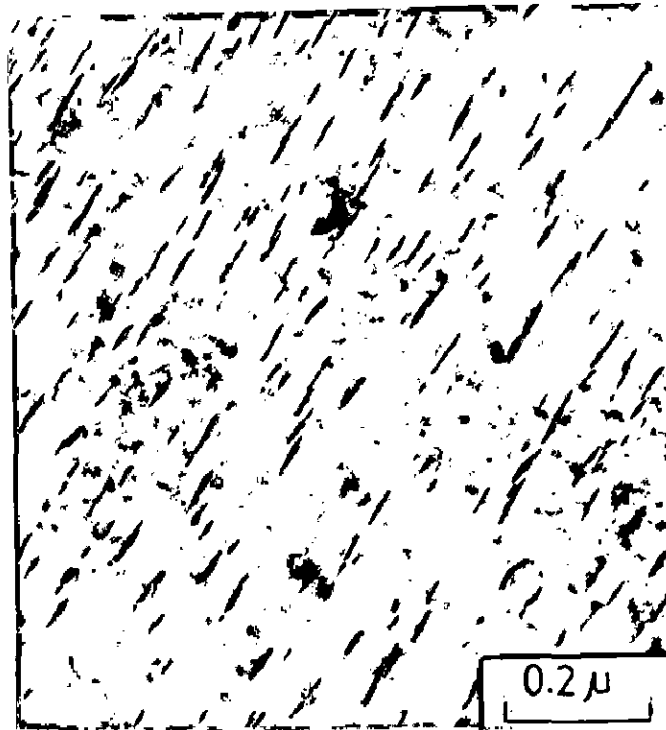
(b)



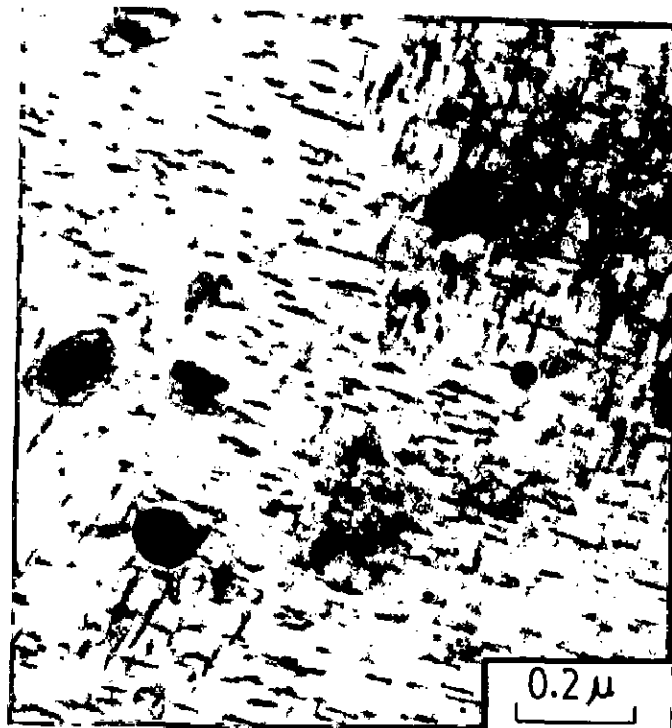
(c)

FIG. 4.20 COMPARISON OF TRANSMISSION ELECTRON MICROGRAPHS OF (a) PEAK-AGED (b) TMA Ib AND (c) TMA IIb TREATED SPECIMENS.

[ TMA Ib GIVES THE FINEST DISTRIBUTION OF  $\theta'$  ]



(a)



(b)

FIG. 4.21 TRANSMISSION ELECTRON MICROGRAPHS OF  
(a) TMA II $\alpha$  AND (b) TMA II $\beta$  TREATED SPECIMENS.  
TMA II $\beta$  SHOWS FINER  $\theta'$  PRECIPITATES. THE  
LARGE PARTICLES ARE DISPERSOIDS.

The TMA I and TMA II treatments, besides affecting the ageing kinetics, also lead to precipitates-dislocation tangles of different magnitudes, which affect the resultant mechanical properties of the alloy. Dislocations generated during warm rolling tend to rearrange and interact with precipitate particles during subsequent final ageing operations. In the present study it is observed that TMA IIb treatment results in thickest dislocation-particle tangles among all the thermomechanical treatments (Fig.4.22).

The dislocation- $\theta'$  interaction is observed to be slightly weaker in TMA Ib treated alloy (Fig.4.23). The treatments involving 10 pct. deformation (TMA Ia and TMA IIa) yield microstructures depicting poor dislocation- $\theta'$  interactions (Figs.4.24 and 4.25).

#### 4.4 SCANNING ELECTRON MICROSCOPIC (SEM) STUDIES OF FATIGUE FAILURE

A systematic study of the fatigue fracture surfaces was carried out by examination under the Philips SEM 501 scanning electron microscope. The results of the SEM study have been shown in the representative fractomicrographs in Figs.4.26-4.39.

At low magnifications all the fractures appear more or less similar and are smooth surfaces as shown in low magnification SEM photographs (Fig. 4.26). Detailed observations at high magnifications have shown all fractures to be



(a)



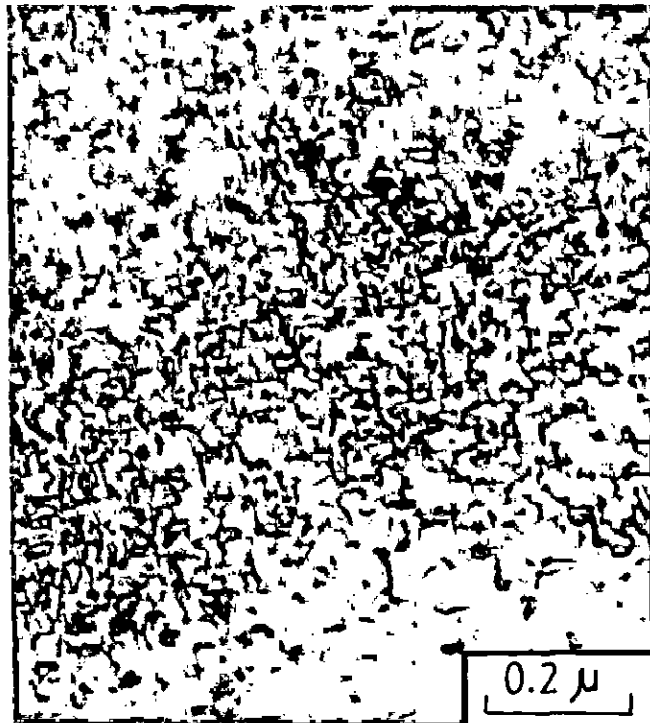
(b)

FIG. 4.22 TRANSMISSION ELECTRON MICROGRAPHS OF TMA IIb TREATED SPECIMEN SHOWING THICK DISLOCATION-PRECIPITATE TANGLES.

( a and b different locations )



(a)



(b)

FIG. 4.23 TRANSMISSION ELECTRON MICROGRAPHS OF TMA 1b TREATED SPECIMEN SHOWING DISLOCATION - PRECIPITATE TANGLES.

( a and b different locations )



(a)

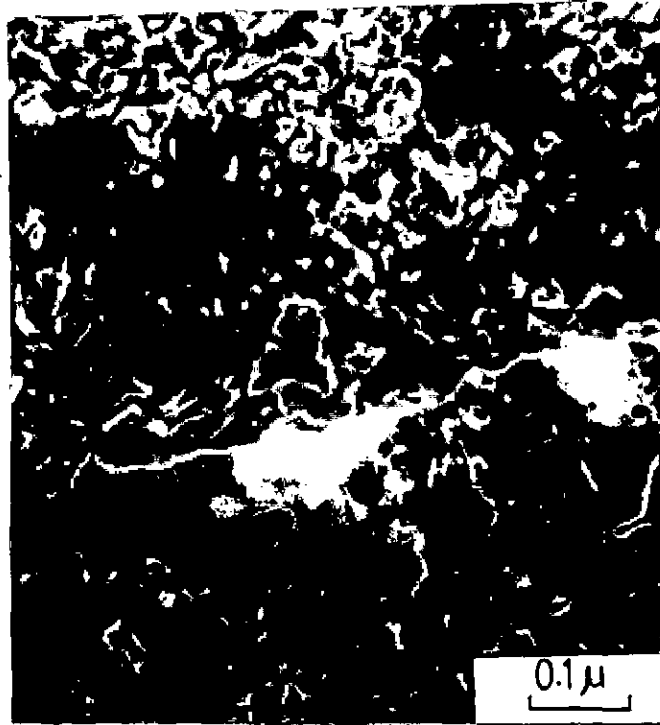


(b)

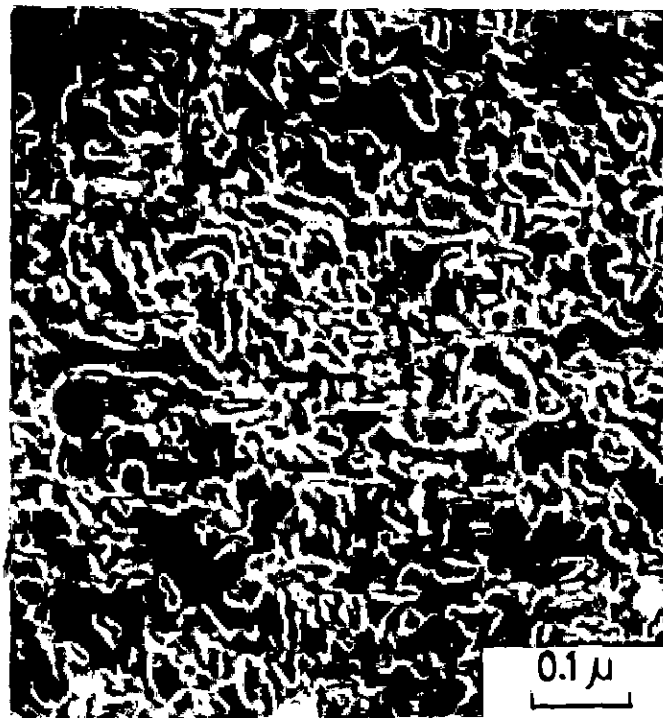
FIG. 4.24 TRANSMISSION ELECTRON MICROGRAPHS OF TMA Ia TREATED SPECIMEN SHOWING DISLOCATION-PRECIPIRATE TANGLES.

(a and b different locations)





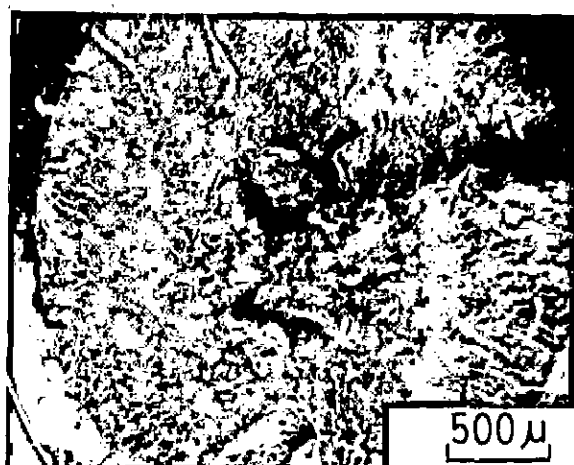
(a)



(b)

FIG. 4.25 TRANSMISSION ELECTRON MICROGRAPHS OF TMA IIa TREATED SPECIMEN SHOWING DISLOCATION-  
PRECIPITATE TANGLES.

( a and b different locations )



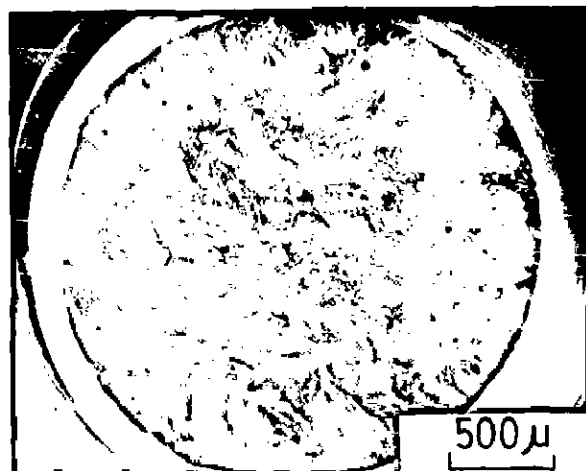
(a)



(b)



(c)



(d)

FIG. 4.26 LOW MAGNIFICATION SEM FRACTOGRAPHS OF FATIGUE TESTED SAMPLES.

(a) AS QUENCHED

(b) PEAK AGED

(c) TMA Ib

(d) TMA IIb

apparently transcrystalline and there is no instance of intergranular failure in all the fatigue tested specimens.

The present investigation reveals that at high cycle fatigue the failure may be basically by (i) formation and interaction of striations and (ii) dispersoid/matrix decohesion. The characteristic appearance of striations is observed to vary widely from region to region in all the samples and it was therefore necessary to study the fracture surfaces under scanning electron microscope at various locations.

In the as quenched samples the striations in several regions are observed to be more or less straight and parallel (Fig.4.27). These do correspond to cycle to cycle crack growth, with each striation indicating successive positions of the crack front. Each striation consists of a light and dark band of about the same width. The smooth, well defined and regularly spaced striations are seen only in as quenched samples and there is no trace of such striations in peak aged and thermomechanically treated samples. In some regions the fracture surface also shows the formation of irregular and wavy form striations (Fig.4.28) as well as a well defined dimple network (Fig.4.29). From Fig.4.29 it is also seen that the fatigue cracks are developed by interaction of striations.

In the peak aged samples the striations are in general irregular, ill defined and broken (Figs. 4.30 and 4.31)



FIG. 4.27 STRAIGHT PARALLEL AND REGULARLY SPACED STRIATIONS IN FATIGUE TESTED AS QUENCHED SAMPLE.

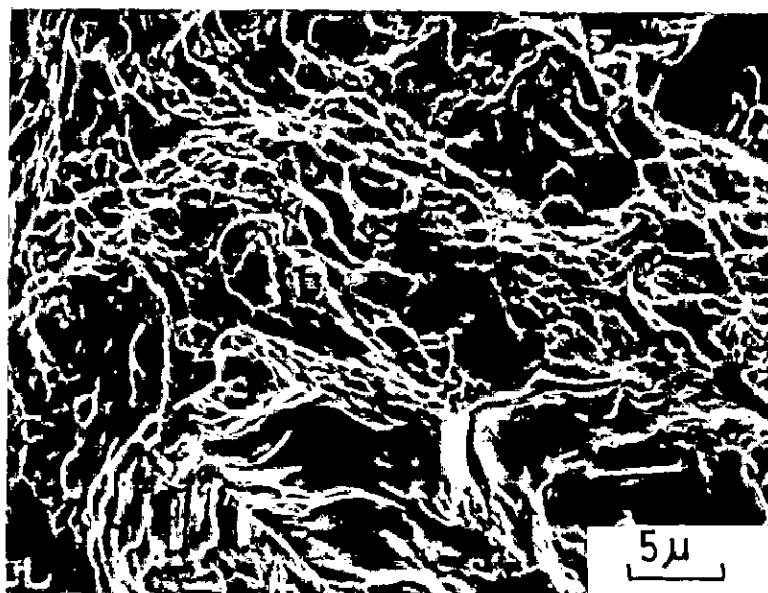
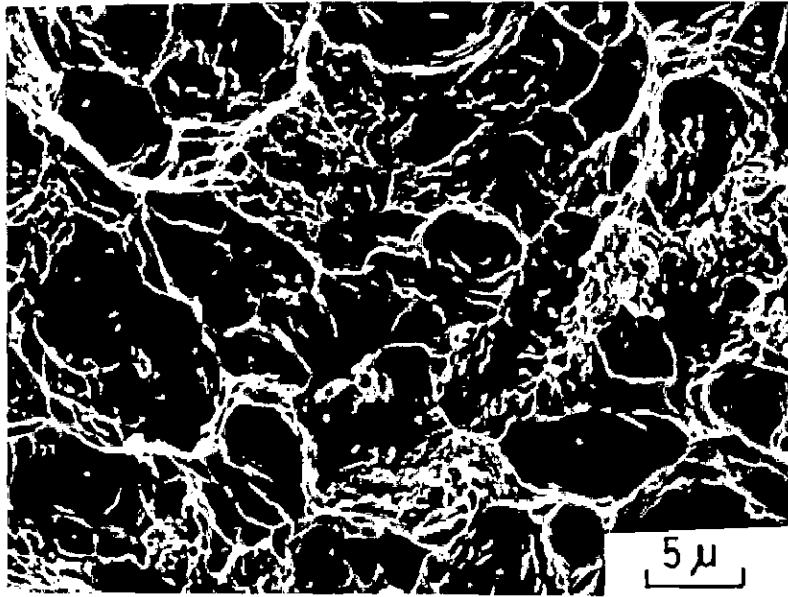
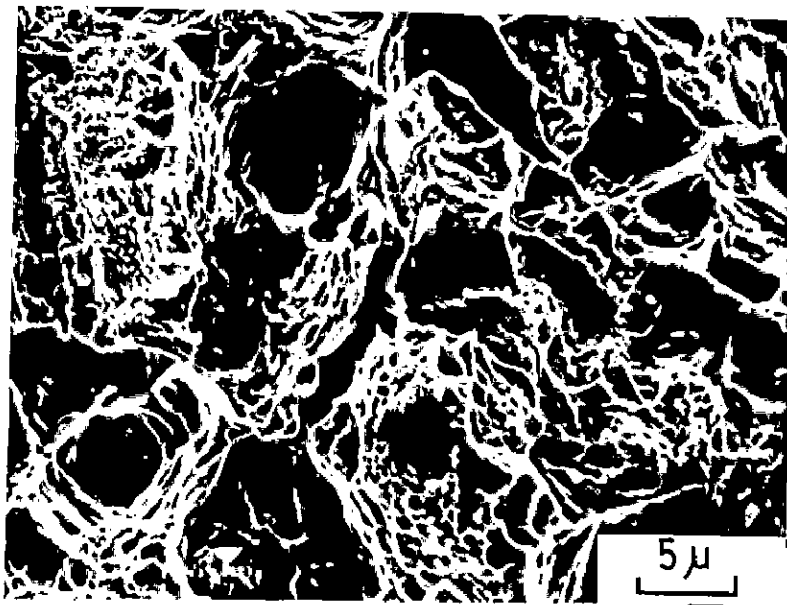


FIG. 4.28 WAVY STRIATIONS IN FATIGUE TESTED AS QUENCHED SAMPLE.

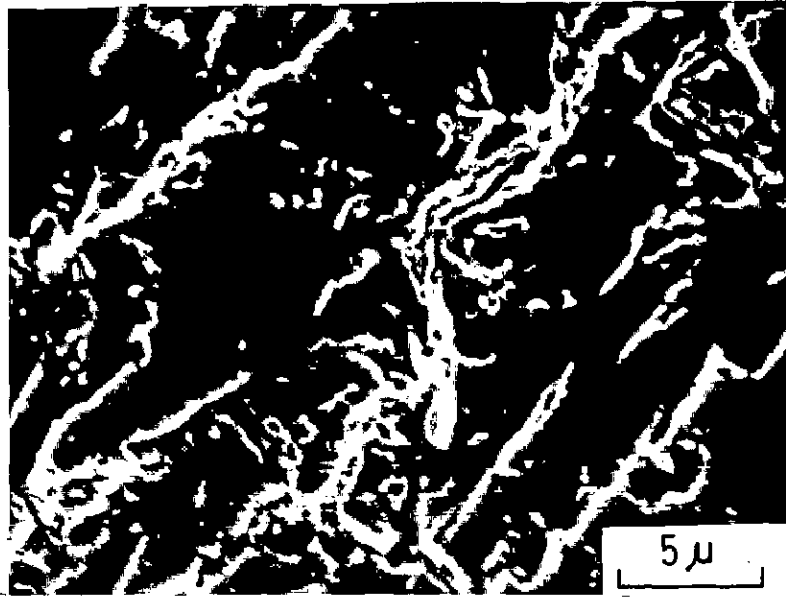


(a)

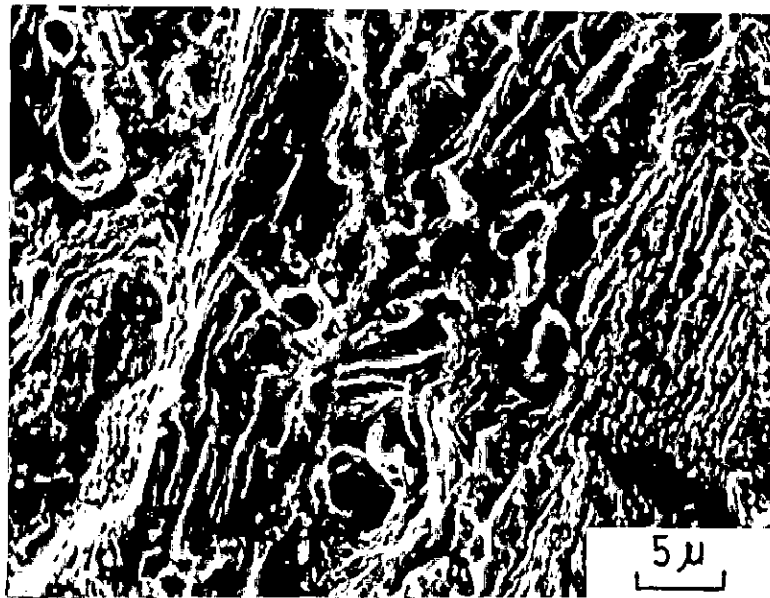


(b)

FIG. 4.29 DIMPLE NETWORK IN FATIGUE TESTED AS QUENCHED SPECIMEN SHOWING CRACK ALONG THE STRIATIONS.  
( a and b different locations )



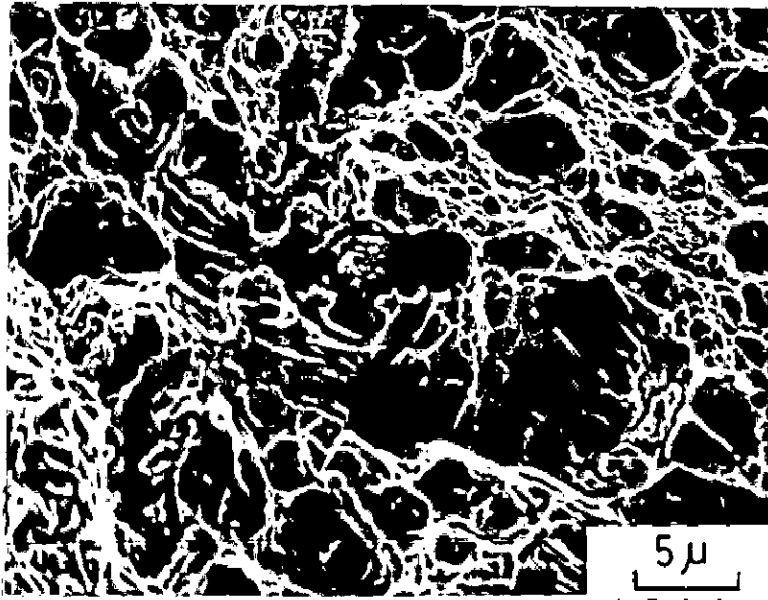
(a)



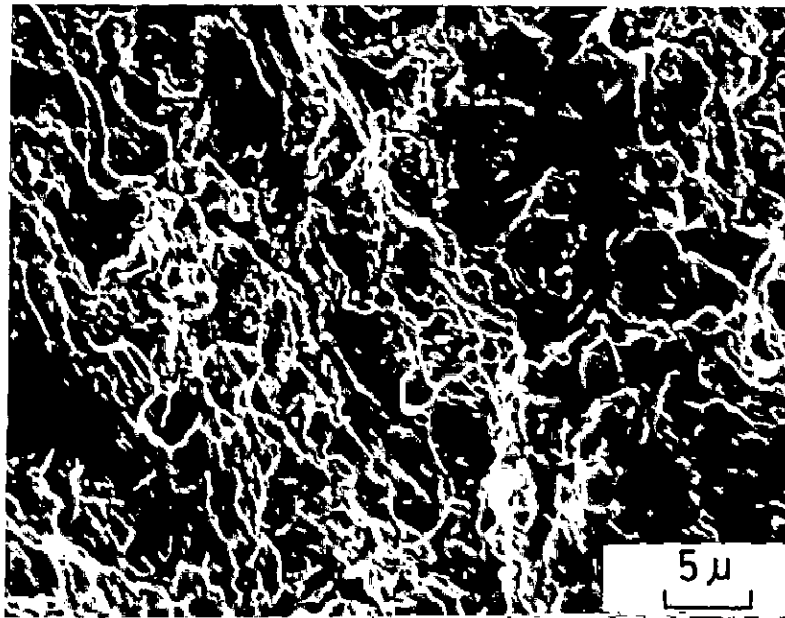
(b)

FIG. 4.30 NEARLY STRAIGHT STRIATIONS IN FATIGUE TESTED PEAK-AGED SAMPLE. FATIGUE CRACK CAN BE SEEN ALONG THE STRIATIONS.

( a and b different locations )



( a )



( b )

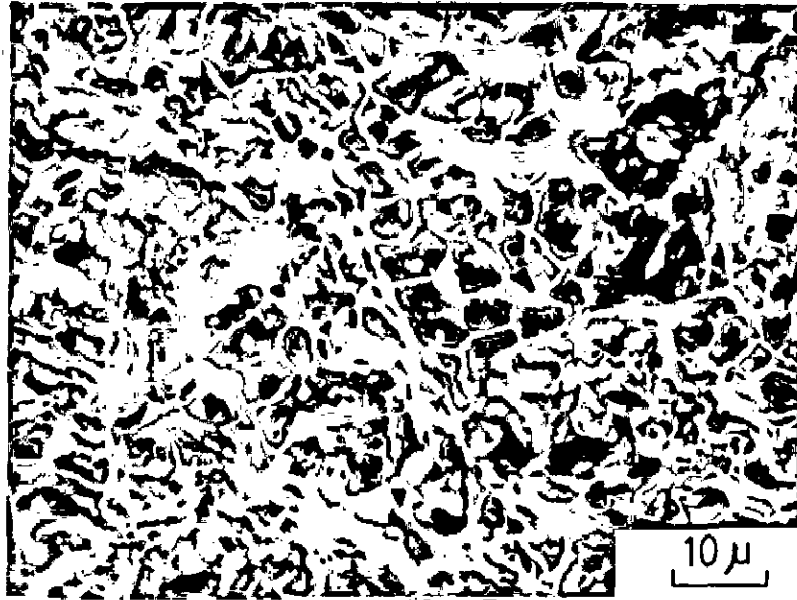
FIG.4.31 ILL DEFINED PRIMARY DIMPLES SURROUNDED BY HIGH DENSITY OF IRREGULAR AND BROKEN UP STRIATIONS IN PEAK-AGED SAMPLE.  
( a and b different locations )

and are indicative of quasi-cleavage or brittle type of crack growth and the proportion of smooth, regular and well defined striations is much smaller as compared to the as quenched specimens.

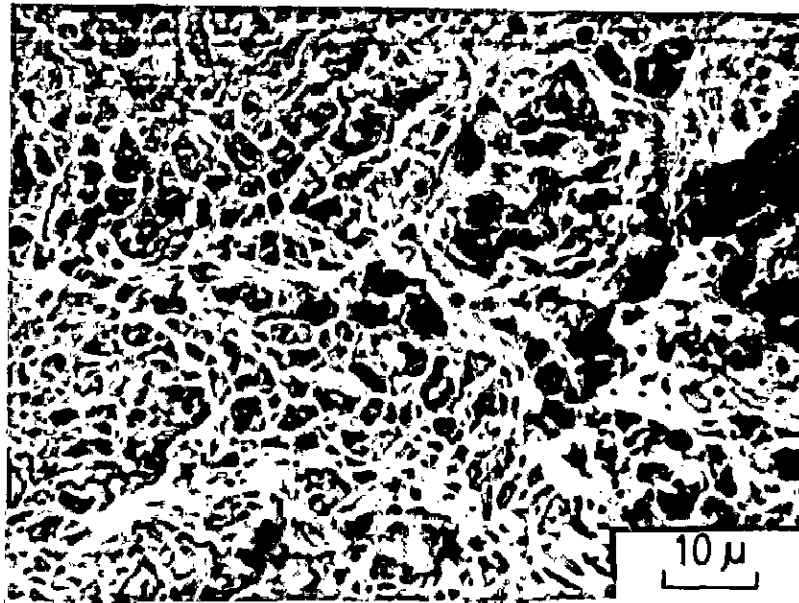
It is clearly seen that the fatigue cracks have a tendency to develop along the striations indicating the interaction of striations as an important parameter in the failure by fatigue. In the entire fracture surface there is no evidence of well defined dimple formation. A careful examination of the surface also reveals the formation of a network of fine secondary dimples around ill defined primary dimples. It is seen that the crack formation generally starts at locations of high striation density.

The TMA samples show a wide variation of structural characteristics on the fracture surfaces. Both ductile and quasi-cleavage type of regions are seen on the fracture surfaces. The striations in TMA specimens are in general more closely spaced as compared to as quenched and peak aged specimens. Figs. 4.32 and 4.33 respectively give the appearance of fracture surfaces of samples given TMA I and TMA II treatments. In both the cases it is seen that the fracture surface in most of areas contains fine loops of thick tangles of striations. As seen from Figs. 4.32 and 4.33 the striation loops are finer for TMA I treated samples as compared to TMA II treated samples. In TMA I treatment,





(a)

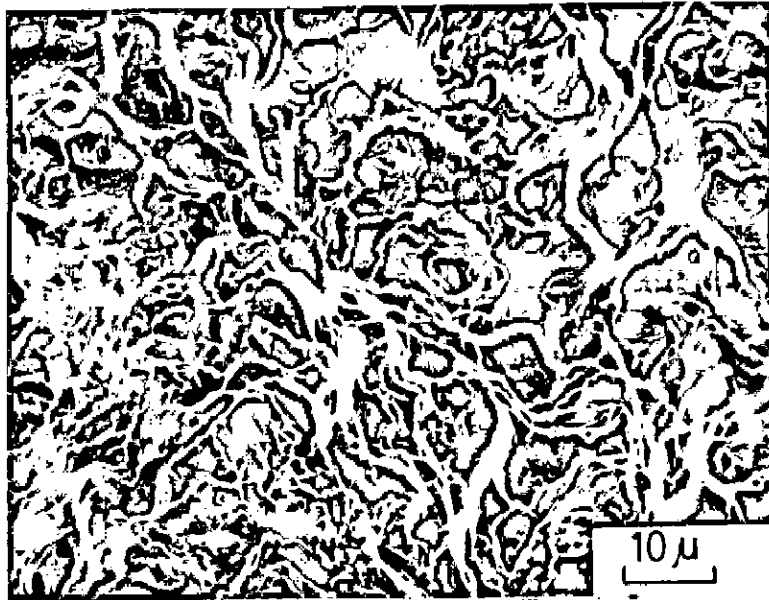


(b)

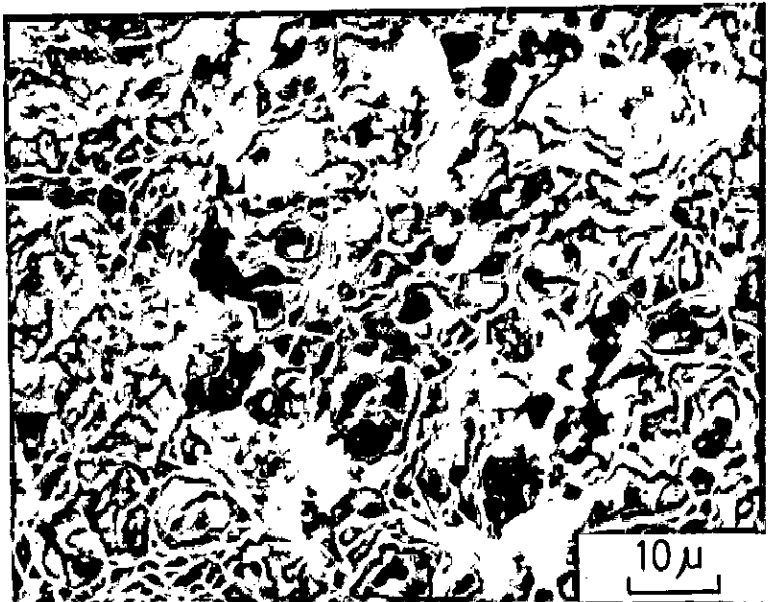
FIG.4.32 NET WORK OF CLOSE LOOP STRIATIONS IN FATIGUE TESTED SPECIMENS.

(a) TMA Ia

(b) TMA Ib



(a)

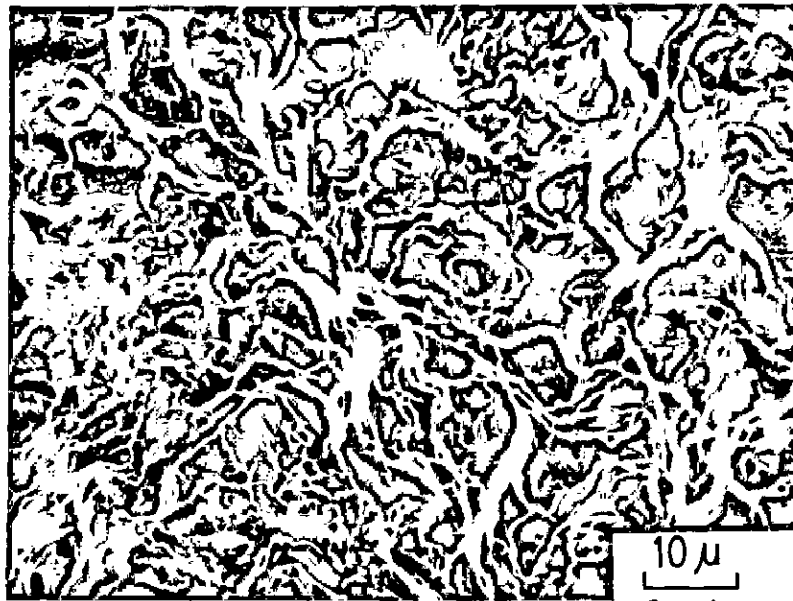


(b)

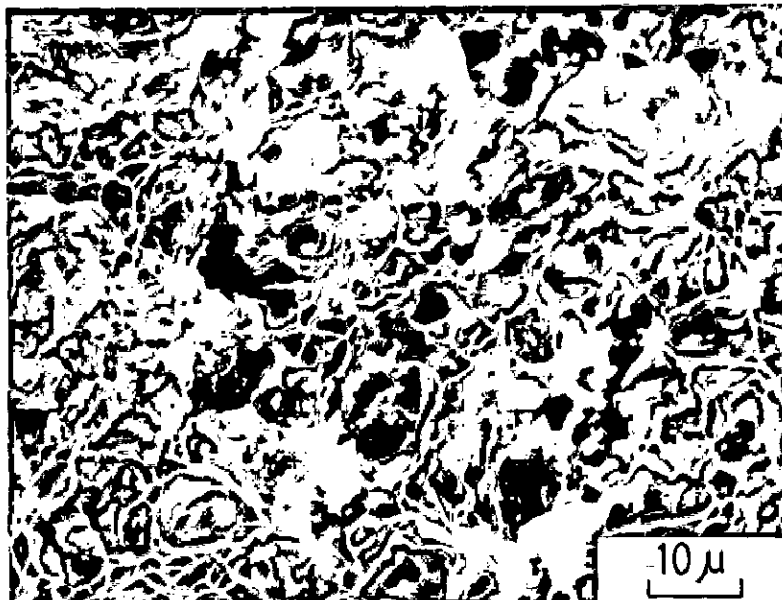
FIG. 4.33 CLOSE LOOP STRIATIONS IN FATIGUE TESTED SPECIMENS.

(a) TMA IIa

(b) TMA IIb



(a)



(b)

FIG. 4.33 CLOSE LOOP STRIATIONS IN FATIGUE TESTED SPECIMENS.

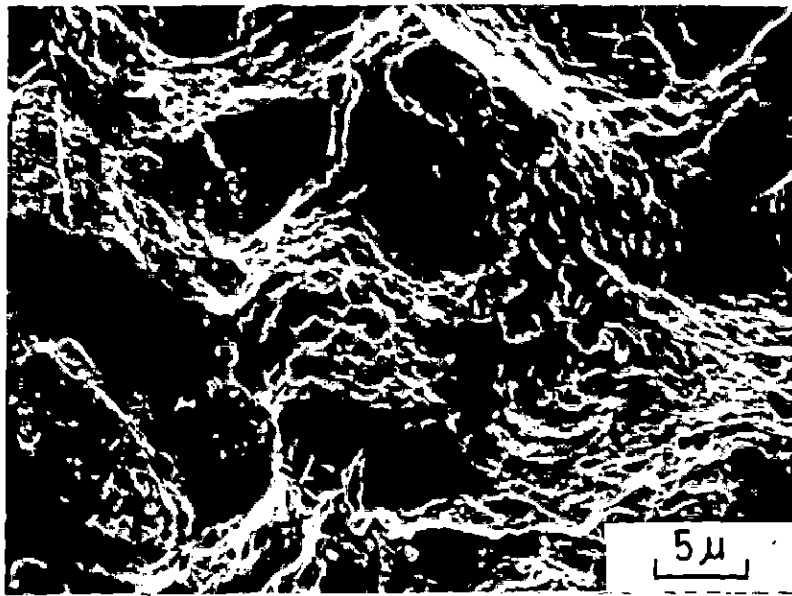
(a) TMA IIa

(b) TMA IIb

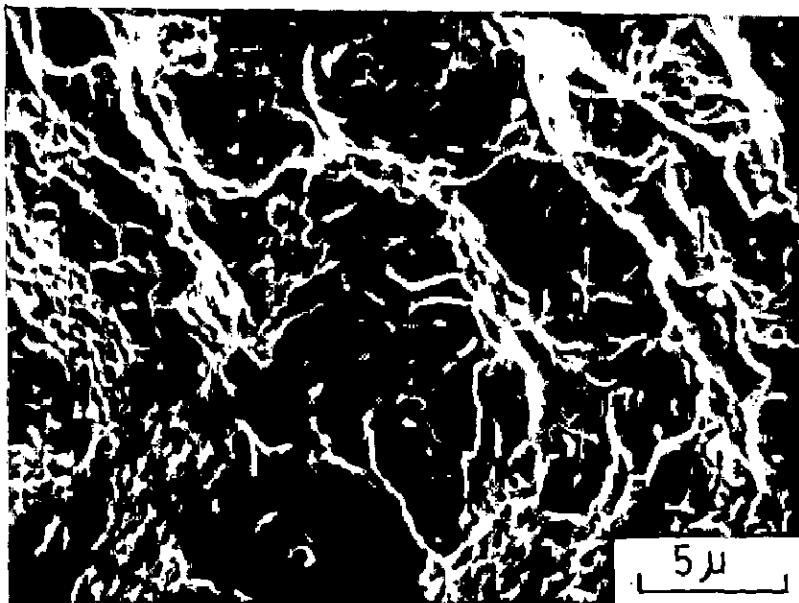
20 pct. deformation (TMA Ib) gives finer loop size than 10 pct. deformation (TMA Ia). Microcleavage type of striations are seen only at very few locations on the surface. Most of the regions indicate the existence of ductile type of striations. In the thermomechanically treated samples a fine network of secondary dimples is also observed decorated at primary dimple boundaries at several locations as seen in Fig.4.34.

The SEM fractographic study makes the effect of TMA clearly visible. In the as quenched and peak aged specimens the primary dimples are large and the dimple walls are smooth. The number of secondary dimples is very meagre. In the TMA specimens, on the other hand, the primary dimples are finer and the number of secondary or micro dimples is very large. In the as quenched and peak aged specimens the spacing between successive striations is sufficiently large and the striations may be distinguished separately, whereas in the TMA specimens the striations are extremely close and appear as thick tangles forming close loops. The striation loop size is finest for TMA Ib treated samples.

The mechanism of crack formation in the TMA specimens appears to be same as in the as quenched and peak aged ones. Fig.4.35 shows the formation of fatigue cracks along the striation tangles. In a number of adjacent fatigue striation patches, the cracks advanced on separate fronts



(a)

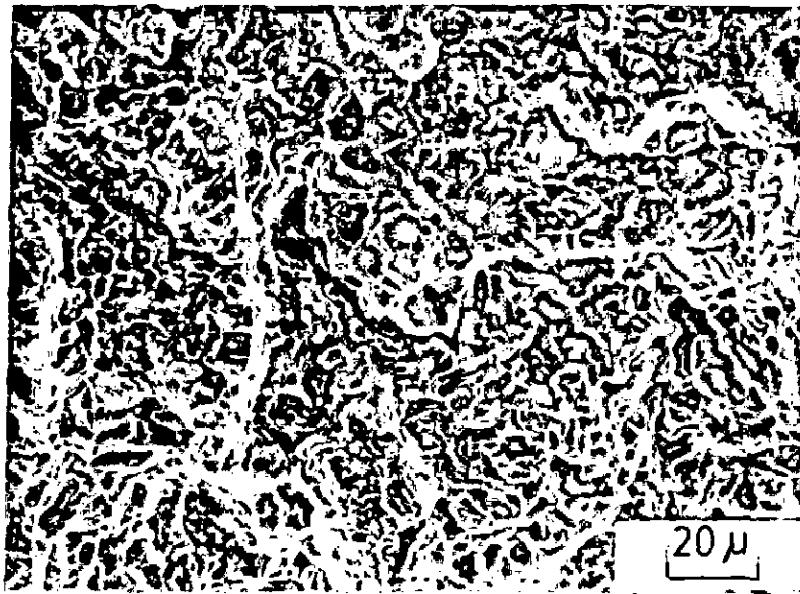


(b)

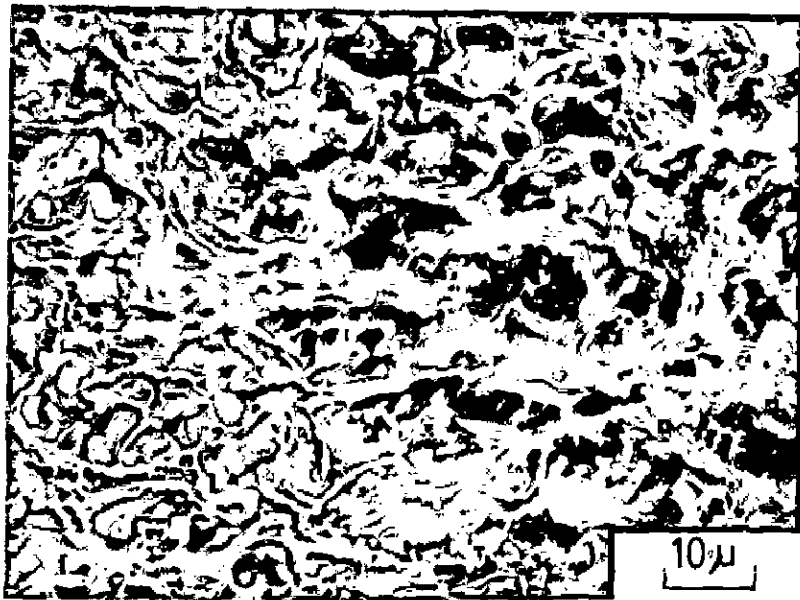
FIG. 4.34 FINE NETWORK OF SECONDARY DIMPLES ON WALLS OF PRIMARY DIMPLES.

(a) TMA Ia

(b) TMA IIa



(a)



(b)

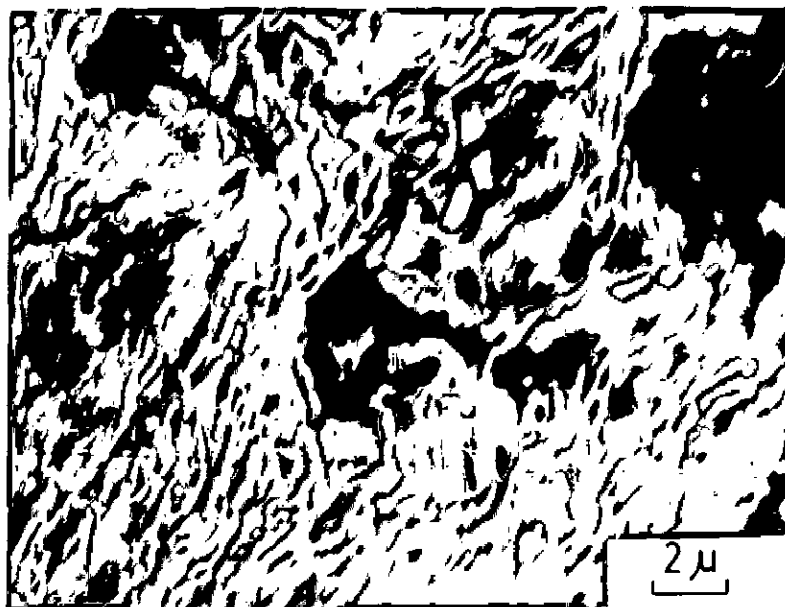
FIG. 4.35 FORMATION OF FATIGUE CRACKS ALONG TANGLES OF STRIATIONS IN TMA Ib TREATED SAMPLE.  
( a and b different locations )

are seen to meet together (Fig.4.36) resulting into formation of large voids. The final failure in all samples seems to be occurring by the coalescence of microvoids in front of advancing cracks as shown in Fig.4.37.

The presence of dispersoids has also been observed to play vital role in the fatigue properties of the various samples. At the fracture surfaces a large number of dispersoids have generally been observed as seen in Fig.4.38, specially in as quenched and peak aged samples. In the thermomechanically treated samples the quantity of dispersoids on fracture surfaces is observed to be much less than that in as quenched and peak aged conditions. The dispersoids cause formation of cracks preferentially at the interfaces with the matrix (Fig.4.39). In some locations breaking up of dispersoids during fatigue has been observed to occur which might also lead to fatigue failure (Fig.4.27).

#### 4.5 OPTICAL MICROSCOPIC STUDIES

The alloy samples after various treatments were prepared for metallographic examination and were observed under optical microscope. The studies reveal two types of particles which are usually called dispersoids [55-57]. These dispersoids are formed during homogenisation, hot rolling and solution heat treatment and are sometimes called 'high temperature precipitates'. Two types of dispersoids are distinguished from their shape and colour when viewed under optical microscope, one with a more rounded shape and smaller in size appears light gray and the other of a irregular shape and larger in size appears as



(a)



(b)

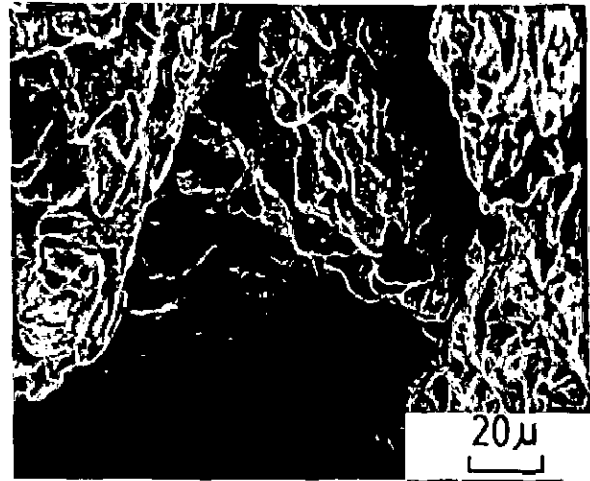
FIG. 4.36 FORMATION OF VOID DUE TO GROWTH OF CRACKS FROM DIFFERENT FRONTS IN TMA Ia TREATED SAMPLE.

( a and b different locations )

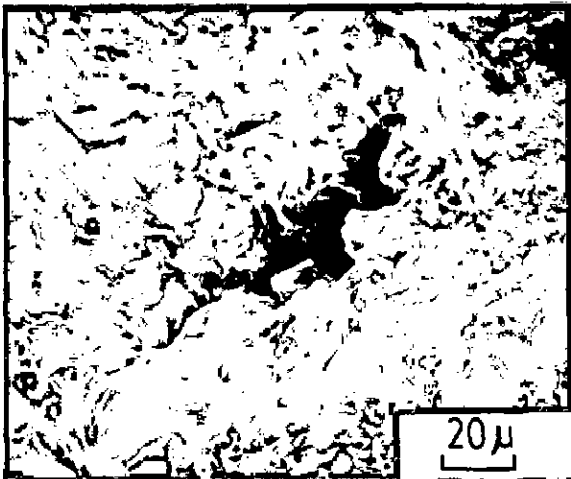




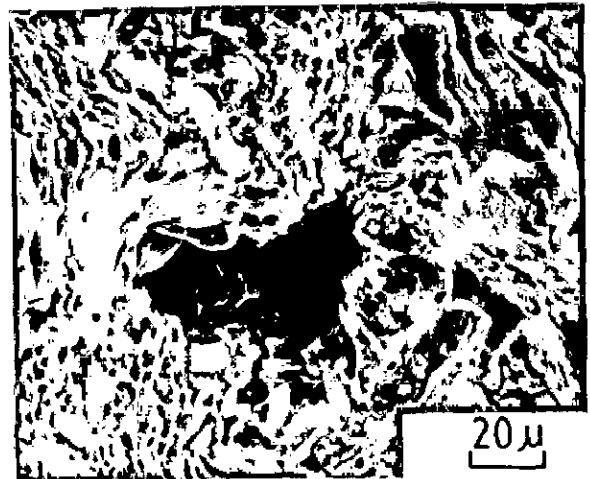
(a)



(b)



(c)

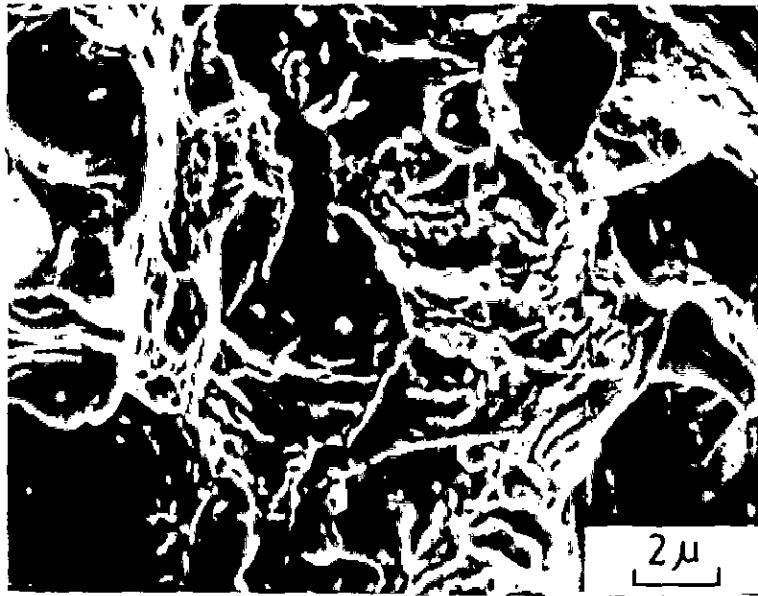


(d)

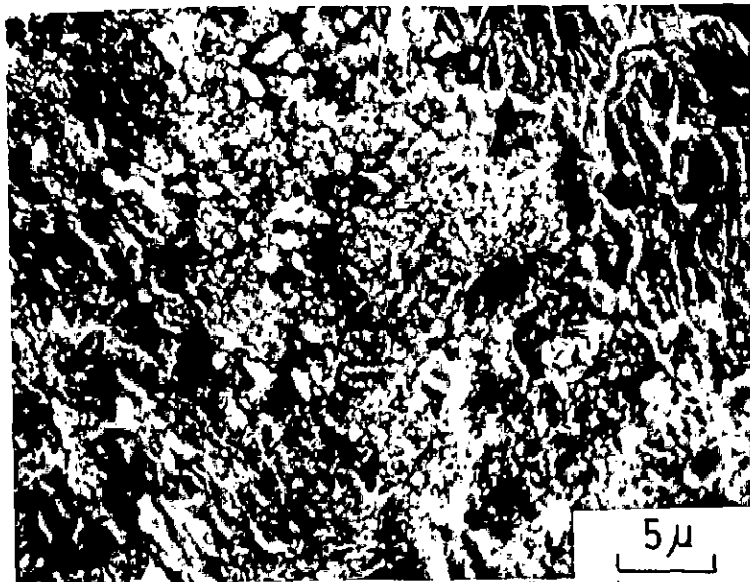
FIG. 4.37 COALESCENCE OF MICROVOIDS LEADING TO FAILURE

(a) AS QUENCHED (b) PEAK AGED

(c) TMA Ib (d) TMA IIb



(a)



(b)

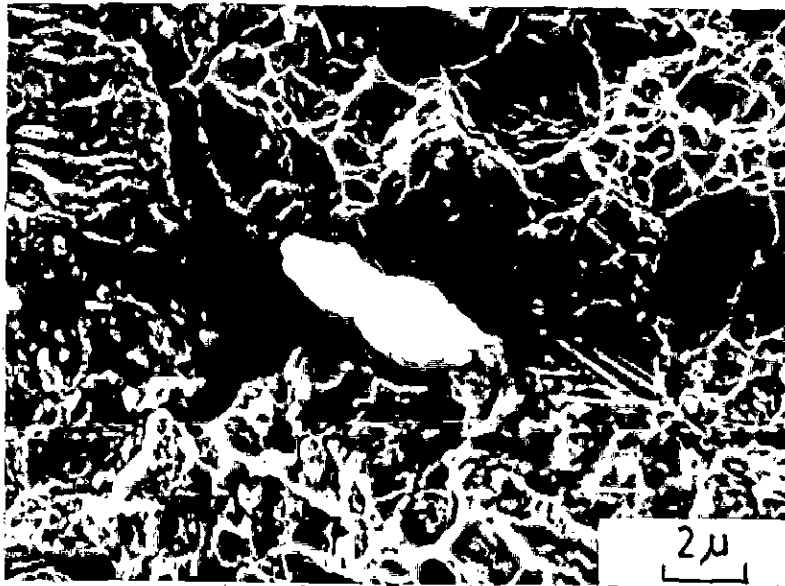
FIG. 4.38 DISPERSOIDS OBSERVED ON THE FRACTURE SURFACE.

(a) AS QUENCHED

(b) PEAK-AGED



(a)



(b)

FIG. 4.39 FORMATION OF CRACKS ALONG PARTICLE-MATRIX INTERFACES.

(a) AS QUENCHED.

(b) TMA Ia

dark gray. The light gray particles are identified as  $\text{Al}_4\text{CuMg}_5\text{Si}_4$  which has also been called as Q phase, whereas the dark gray particles are observed to have the composition  $\text{Al}_{12}(\text{Fe}, \text{Mn})_3\text{Si}$  [56, 57]. The presence of various elements in the dispersoids has been qualitatively verified by electron probe micro analysis as shown in fig.4.40. These particles are reported to have significant influence on various mechanical properties of aluminium alloys [55-57].

Figs. 4.41-4.43 show representative micrographs of the alloy samples after various treatments. It is observed that in the as quenched condition a high density of dispersoids exists in which the proportion of light gray dispersoid (Q phase) is much more than the dark constituent as seen in Fig.4.41a. Peak ageing treatment leads to partial dissolution of Q phase while the amount of dark etching dispersoids increases sharply (Fig.4.41b).

Thermomechanical treatment is observed to significantly influence the stability of both types of dispersoids. The deformation and subsequent ageing treatment in both TMA I and TMA II lead to preferential disappearance of Cu-rich constituent (Q phase) in comparison to the dark etching dispersoids. Accordingly it is observed that among the various thermomechanical treatments the TMA Ib gives minimum density of dark gray constituent with absolutely no traces of

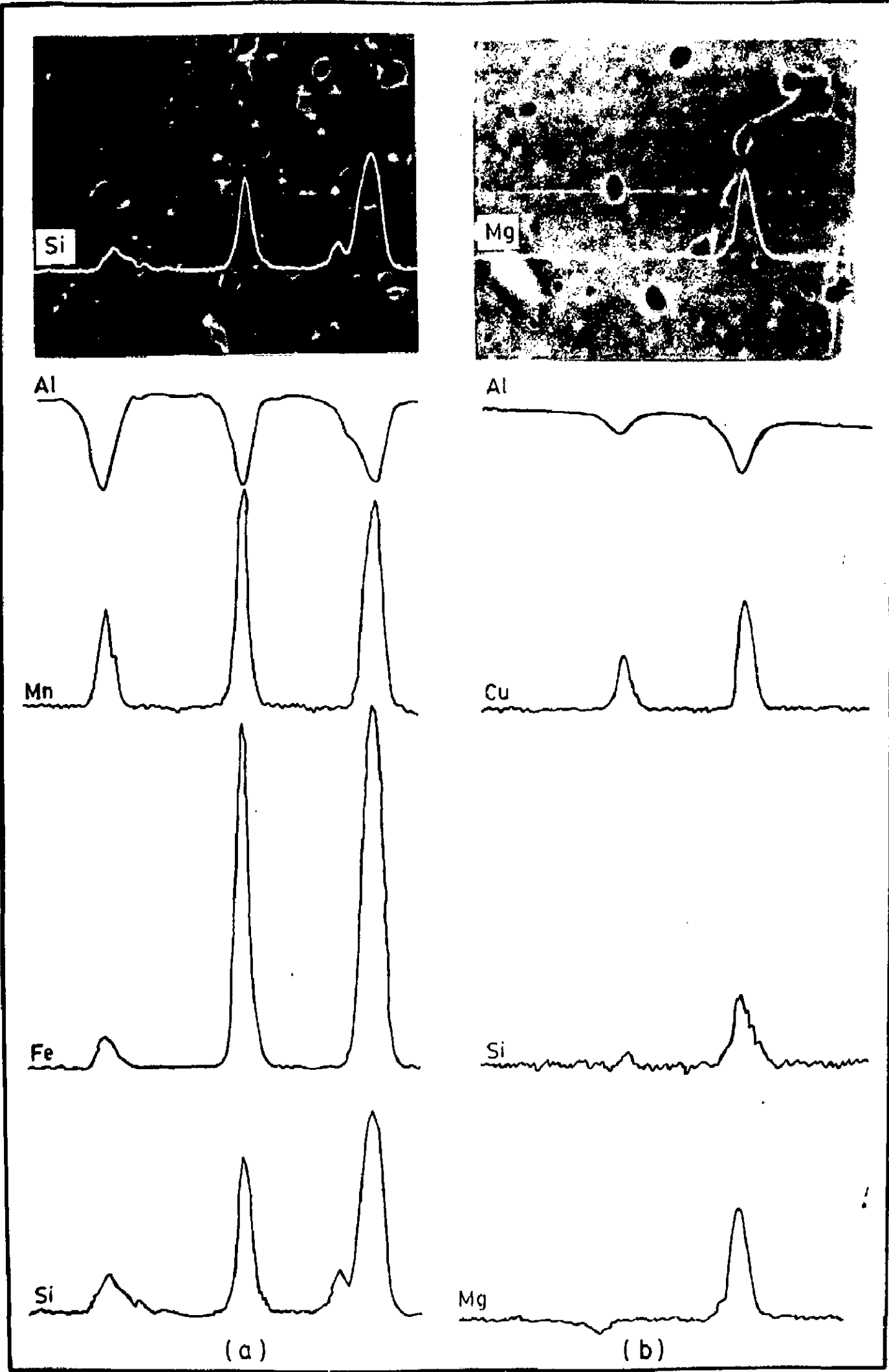
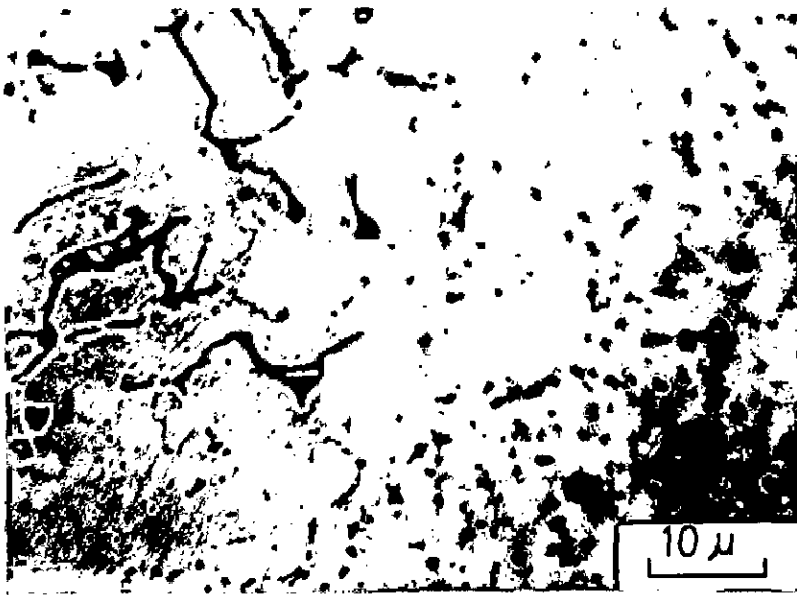
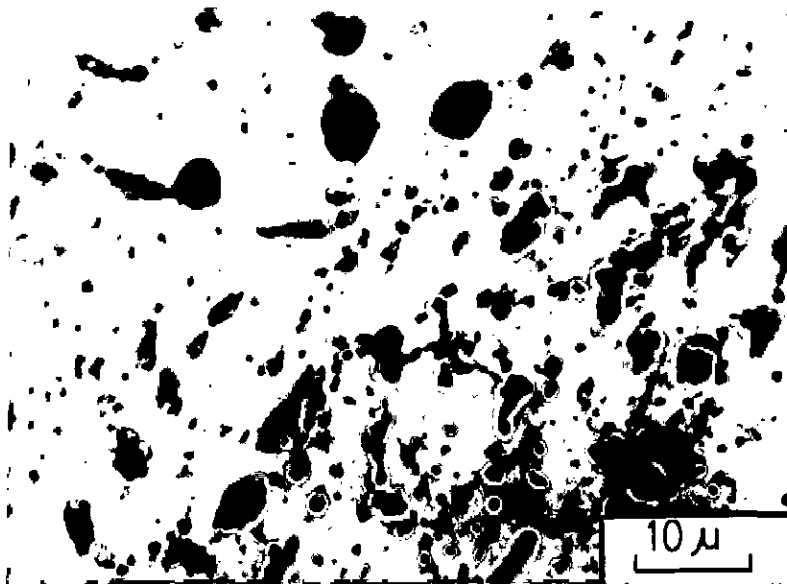


FIG. 4.40 LINE SCAN OF VARIOUS ELEMENTS IN DISPERSOIDS

(a)  $Al_{12}(Fe, Mn)_2Si$  (b)  $Al_4CuMg_5Si_4$ .



(a)



(b)

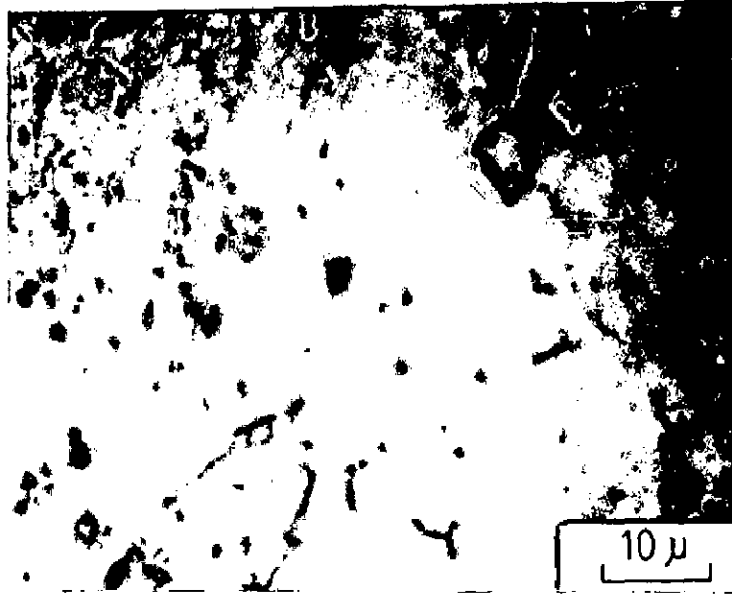
FIG. 4.41 OPTICAL MICROGRAPHS SHOWING (i) LIGHT ETCHING  $\text{Al}_4\text{CuMg}_5\text{Si}_4$  AND (ii) DARK ETCHING  $\text{Al}_{12}(\text{Fe},\text{Mn})_3\text{Si}$  DISPERSOIDS.

(a) AS QUENCHED

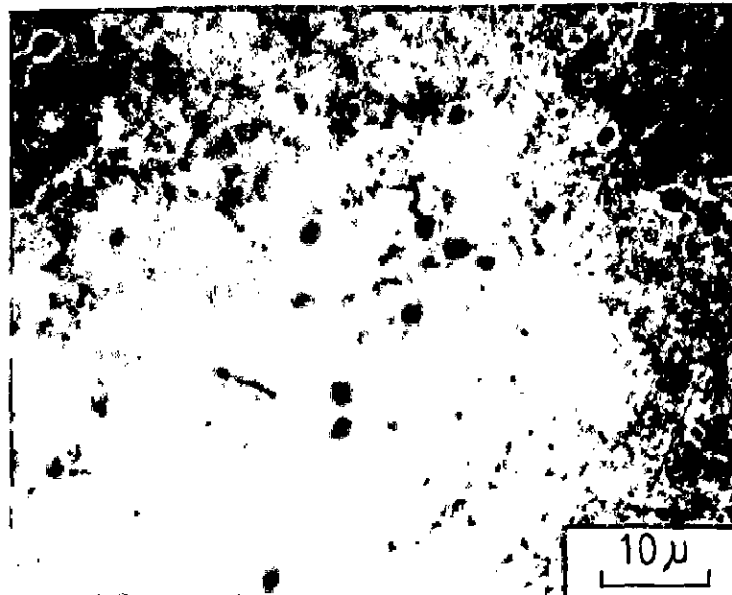
(b) PEAK AGED

the Q type of dispersoids (Fig.4.42b), as this treatment involves a large amount of deformation followed by an appreciable period of subsequent ageing. Strain induced effect on the stability of phases in various aluminium alloys has been reported in the literature [83,168].

The TMA Ia and TMA IIb treatments lead to a dispersoid density which is significantly higher than that obtained in the TMA Ib treatment (Fig.4.42 a and 4.43 b ). The dispersoid density obtained after the TMA IIa treatment (Fig.4.43 a) is still higher than that obtained in TMA Ia and TMA IIb, although in comparison to as quenched and peak aged conditions all the thermomechanical treatments result in lower density of dispersoids. There is no trace of Cu rich Q phase (light etching dispersoids) observed in TMA Ib and TMA IIb treated samples. In other thermomechanical treatments small traces of the Q phase are also observed.



(a)



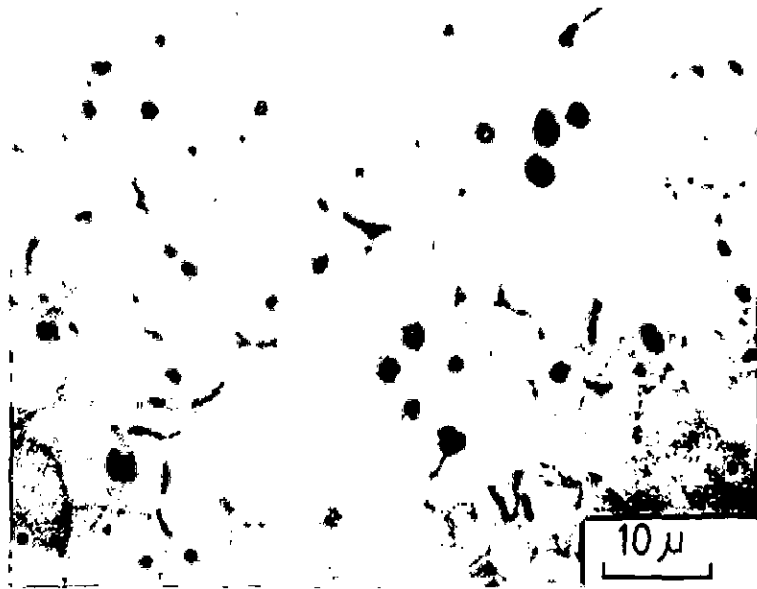
(b)

FIG. 4.42 OPTICAL MICROGRAPHS SHOWING DISPERSOIDS.

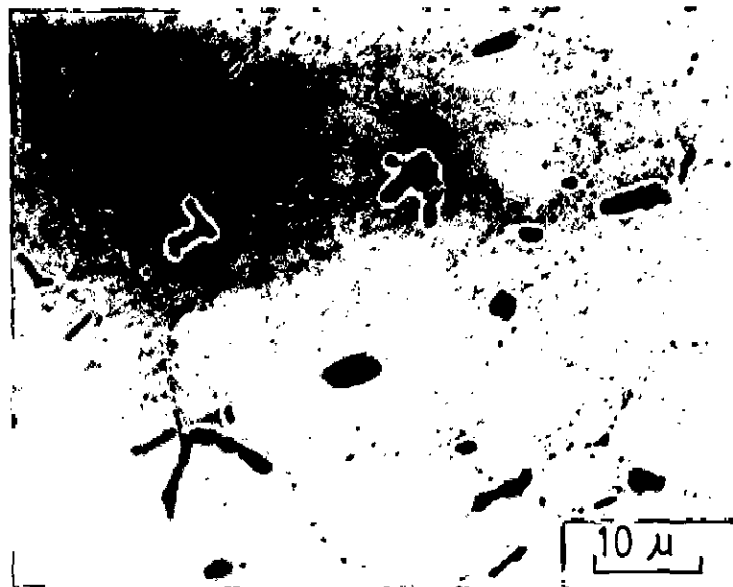
(a) TMA 1a

(b) TMA 1b





(a)



(b)

FIG.4.43 OPTICAL MICROGRAPHS SHOWING DISPERSOIDS.

(a) TMA IIa

(b) TMA IIb

suppression of  $\theta''$  formation during subsequent final ageing treatments. Any platelets of  $\theta''$  already formed prior to deformation also are converted to  $\theta'$  precipitates. There is, therefore, no evidence of  $\theta''$  platelets in the thermomechanically treated samples.

When we consider the combined effect of degree of preageing and degree of deformation, it would appear that the TMA Ib treatment should lead to maximum nucleation of  $\theta'$  precipitates among all the TMA treatments applied to the alloy under investigation. This treatment provides extremely high solute concentration in the matrix prior to deformation as well as a high degree of deformation prior to final ageing treatment. Accordingly, as seen from Fig.4.20, this treatment leads to the finest distribution of  $\theta'$  precipitates. In the TMA II treatment the solute concentration in the  $\alpha$ -matrix after the preageing treatment is very much depleted. The deformation treatment although provides additional nucleation centres, but the formation of additional  $\theta'$  precipitates is not significantly enhanced due to depleted solute concentration and only the previously formed  $\theta'$  particles are predominantly coarsened during the final ageing step. Due to the effect of dislocation on nucleation the TMA IIb yields a finer distribution of  $\theta'$  than the TMA IIa as seen in Fig.4.21.

The TMA treatments, besides affecting the ageing kinetics, also lead to precipitate-dislocation networks of

different magnitudes depending upon the amount of deformation and the duration of subsequent final ageing operations. As already discussed, in deformed alloys nucleation at lattice defects predominates. All dislocations serve as nucleation points for  $\theta'$  particles so that precipitation increases as the dislocation density increases. Dislocations generated during plastic deformation tend to rearrange and interact with precipitate particles during subsequent final ageing operations [63, 74, 109, 133, 176, 178, 181]. The rearrangement of dislocations is further complicated in that the deformation structure, the density, configuration and type of dislocations produced by the deformation, is not homogeneous. Due to difference in the deformation structure, regions with quite different dislocation-particle tangles are found in one and the same specimen. For pure metals the activation energy for rearrangement (climbing) of dislocations produced during deformation is equal to the activation energy for self-diffusion [182]. This can be increased by more than one order of magnitude by segregation of solute atoms in Al-Mn alloys [183] or by preferential precipitation on dislocations, as seen by the precipitation of  $\theta'$  in this study. As a result, the process of rearrangement of dislocations during final ageing operation becomes extremely difficult. The TEM studies have shown that no large angle boundaries are produced during final ageing step. The existing grain boundaries also are immobilised due to the formation of  $\theta'$  particles. In such a case the rearrangement

of dislocations can only occur by the formation or resolution of the precipitated particles. Precipitation may break down segregation of solutes at dislocations and hence facilitate their rearrangement. TEM studies in this alloy indicate that the dislocation structure produced by deformation dissolves the  $\theta''$  platelets during subsequent final ageing treatment which may help in the rearrangement of dislocations.

In view of the role of  $\theta''$  dissolution and  $\theta'$  precipitation in the rearrangement of dislocations during the final ageing operation, dislocation-particle tangles of different magnitudes have been observed after various TMA treatments as shown in Figs.4.22-4.25. Although same amount of deformation is given in TMA Ib and TMA IIb treatments, it is observed that the resultant dislocation-precipitate tangles are much thicker after TMA IIb. The duration of final ageing operation in TMA IIb is only 2.00 hours as against 5.50 hours in TMA Ib and hence the extent of annihilation and rearrangement of dislocations in TMA IIb is much less than that in TMA Ib. In addition, the microstructure at the beginning of final ageing step consists of higher density of  $\theta'$  particles, which also inhibits annihilation and rearrangement of dislocation in the TMA IIb treatment. Another factor which helps in annihilation of dislocations preferentially in TMA Ib is the release of dislocation energy due to nucleation of  $\theta'$  at the dislocations as already argued earlier. Thus the

resultant dislocations-particle tangles in TMA IIb treated samples are thicker as compared to TMA Ib treated samples. Similarly dense dislocation-particles are observed after TMA IIa as compared to TMA Ia treatment. The TEM observations in the present study reveal the thickest dislocation-particle tangles after TMA IIb treatment, which is in confirmation with the above discussion.

Among the various structural constituents, the presence of dispersoids as revealed by optical and transmission electron microscopy also plays an important role in influencing the mechanical properties including fatigue and fracture toughness. Thus it is important to note the effect of thermomechanical ageing on the stability and distribution of these dispersoids. As reported in Section 4.5 the light gray particles are identified as  $\text{Al}_4\text{CuMg}_5\text{Si}_4$  (also known as Q phase) and the dark gray particles as  $\text{Al}_{12}(\text{Fe},\text{Mn})_3\text{Si}$  as revealed in optical micrographs (Fig.4.41-4.43). The TEM studies also reveal the existence of these dispersoids as seen in Figs.4.18 and 4.21. The type of dispersoids, their size and distribution are observed to be significantly affected by the type of TMA treatment because of the following possible reasons:

- (i) variation in the solubility of different constituents, of which the dispersoids are formed, in the Al-matrix,
- (ii) the effect of deformation on the solubility of

different constituents, and

- (iii) the effect of deformation on conversion/dissolution of less stable dispersoid into either matrix or more stable dispersoids, as reported in other Al-alloy systems [54,55,83].

The constituents of the alloy under consideration can be divided into two groups, viz., soluble constituents Cu, Mg and Si; and relatively insoluble constituents Fe and Mn. This affects the stability of the dispersoids to different extents. As revealed in this study, the as quenched specimen possess predominantly  $Al_4CuMg_5Si_4$ , whereas samples peak aged at  $160^\circ C$  contain mainly  $Al_{12}(Fe,Mn)_3Si$  particles. These dispersoids tend to disappear after TMA treatments. These observations show that both these types of dispersoid are metastable in character. The  $Al_4CuMg_5Si_4$  phase appears to be relatively more stable at high temperature ( $\sim 500^\circ C$ ) whereas at temperatures close to the ageing temperature ( $160^\circ C$ ), the  $Al_{12}(Fe,Mn)_3Si$  particles are more stable. This is the reason why the as quenched sample contains a higher proportion of the high temperature phase  $Al_4CuMg_5Si_4$ , whereas in the normal peak ageing treatment the high temperature phase tends to disappear and the insoluble elements like Fe and Mn in the matrix tend to grow in the form of  $Al_{12}(Fe,Mn)_3Si$  dispersoids.

The deformation structure produced during TMA treatments decreases the stability of both types of

dispersoids. Since at the ageing temperature ( $160^{\circ}\text{C}$ ), the stability of  $\text{Al}_4\text{CuMg}_5\text{Si}_4$  particles is already much less than that of  $\text{Al}_{12}(\text{Fe},\text{Mn})_3\text{Si}$  particles, the elimination of former type of dispersoids occurs much faster during the final ageing operation. In agreement with this reasoning it is observed that among the various TMA treatments, TMA Ib gives minimum density of dark etching  $\text{Al}_{12}(\text{Mn},\text{Fe})_3\text{Si}$  constituent with absolutely no traces of the light etching  $\text{Al}_4\text{CuMg}_5\text{Si}_4$  phase (Fig.4.42 b) ; since this treatment involves a higher degree of deformation followed by an appreciable period of subsequent final ageing. The high temperature phase  $\text{Al}_4\text{CuMg}_5\text{Si}_4$  is also eliminated at fast rate because during final ageing operation in TMA Ib treatment enhanced nucleation of  $\theta'$  precipitates takes place which causes depletion of Cu concentration in the matrix, which, in turn, makes the Cu bearing dispersoid  $\text{Al}_4\text{CuMg}_5\text{Si}_4$  more unstable. As the stability of the dispersoids is directly affected by the amount of deformation, it is observed in the present investigation that, at any preageing, 20 pct. deformation leads to the elimination of dispersoids to a greater extent than 10 pct. deformation in all the TMA treatments employed.

## 5.2 EFFECT OF THERMOMECHANICAL AGEING (TMA) ON STRENGTHENING BEHAVIOUR

The strengthening effects in the 2014 Al-alloy after various TMA treatments may be considered to be due to (i) coherent

precipitates  $\theta''$ , (ii) partially coherent  $\theta'$  precipitates, (iii) dislocation substructure and (iv) the presence of dispersoids. According to TEM observations, the GP II ( $\theta''$ ) is formed only in peak ageing treatment. The increase in strength due to various thermomechanical treatments in the alloy under investigation may be attributed to the presence of  $\theta'$  precipitates, as has been observed by other investigators [51,56] also. The degree of strengthening resulting from the  $\theta'$  precipitates depends on their size, mean interparticle spacing, volume fraction and their distribution in the matrix. All these factors are interrelated so that one factor cannot be changed without affecting the other. The  $\theta'$  particles may be cut by the dislocations at stress levels much above those required to move dislocations through the matrix phase. On the other hand the  $\theta'$  particles may also resist cutting and the dislocations may be forced to take a path around the obstacles, i.e. they can act as strong impenetrable particles through which the dislocations can move only by sharp changes in curvature of dislocations. While it is difficult to observe these interactions even in the electron microscope, it is believed that the first mechanism is operative only in the presence of GP I and GP II zones ( $\theta''$ ) while in the presence of semicoherent  $\theta'$  particles the second mechanism appears to be operative. A dislocation may, in passing through the matrix, be arrested by the dispersion of  $\theta'$  particles. The stress required to bulge round



the particles is given by the expression

$$\bar{\tau} = 2Gb / \lambda \quad \dots (5.1)$$

where  $G$  is shear modulus,  $b$  is Burgers vector and  $\lambda$  is interparticle spacing. This relation clearly shows that for a given volume fraction of  $\theta'$ , a higher stress  $\bar{\tau}$  is required for a finer size of precipitate particles because this would result in a smaller interparticle spacing  $\lambda$ . After bulging through between the particles, the dislocation line re-forms, leaving a dislocation loop around the particles, effectively increasing its size and decreasing the spacing between nearby particles, so that an ever increasing stress is required to push successive dislocations through.

Besides the contribution of  $\theta'$  particles, the dislocation substructure produced in the TMA treatments also plays a vital role in overall strengthening mechanism. The dislocation substructures produced during various TMA treatments consist of tangles of dislocations and dislocation cells as shown in Figs. 4.22-4.25. The strengthening is caused due to work hardening effects produced between moving dislocations and the dislocation substructure. Staker and Holt [184] gave the following flow stress relationship.

$$\bar{\tau} = \alpha Gb \sqrt{\rho}, \quad \dots (5.2)$$

where  $\alpha$  is a constant of the order 0.5,  $G$  the shear modulus,

will be high when fine  $\theta'$  particles are formed in dense dislocation cell structure.

The average diameters of  $\theta'$  plates after various treatments have been estimated from TEM studies as follows.

Peak aged	: 850 $\overset{\circ}{\text{A}}$
TMA Ia	: 650 $\overset{\circ}{\text{A}}$
TMA Ib	: 400 $\overset{\circ}{\text{A}}$
TMA IIa	: 750 $\overset{\circ}{\text{A}}$
TMA IIb	: 600 $\overset{\circ}{\text{A}}$

Bonfield and Datta [51] have established that the peak hardness in Al-Cu-Si-Mg alloy is associated with the presence of  $\theta'$  precipitates of diameter upto 750  $\overset{\circ}{\text{A}}$  and an increase of diameter beyond 850  $\overset{\circ}{\text{A}}$  causes overageing effects. In the present study the diameter of  $\theta'$  particles in the peak aged samples is approximately 850  $\overset{\circ}{\text{A}}$ . The peak hardness in peak aged condition is associated with the presence of  $\theta''$  and  $\theta'$ . In all the thermomechanically aged samples the peak hardness is associated only with  $\theta'$  as no evidence of  $\theta''$  is seen in these samples. Since the diameter of  $\theta'$  precipitates in all the thermomechanically aged samples is less than 850  $\overset{\circ}{\text{A}}$ , it would appear that strengthening after various TMA treatments would be significantly governed by the nature of dislocation substructures. As revealed from TEM study, the dislocation density  $\rho$  is maximum

the particles is given by the expression

$$\bar{\tau} = 2Gb / \lambda \quad \dots (5.1)$$

where  $G$  is shear modulus,  $b$  is Burger's vector and  $\lambda$  is interparticle spacing. This relation clearly shows that for a given volume fraction of  $\theta'$ , a higher stress  $\bar{\tau}$  is required for a finer size of precipitate particles because this would result in a smaller interparticle spacing  $\lambda$ . After bulging through between the particles, the dislocation line re-forms, leaving a dislocation loop around the particles, effectively increasing its size and decreasing the spacing between nearby particles, so that an ever increasing stress is required to push successive dislocations through.

Besides the contribution of  $\theta'$  particles, the dislocation substructure produced in the TMA treatments also plays a vital role in overall strengthening mechanism. The dislocation substructures produced during various TMA treatments consist of tangles of dislocations and dislocation cells as shown in Figs.4.22-4.25. The strengthening is caused due to work hardening effects produced between moving dislocations and the dislocation substructure. Staker and Holt [184] gave the following flow stress relationship.

$$\bar{\tau} = \alpha Gb \sqrt{\rho}, \quad \dots (5.2)$$

where  $\alpha$  is a constant of the order 0.5,  $G$  the shear modulus,

b the Burger's vector, and  $\rho$  the dislocation density. According to Thompson [100] the flow stress is also related to the dislocation cell size as follows:

$$\bar{\tau} = \alpha K G b d^{-1} \quad \dots (5.3)$$

Here d is the dislocation cell size, k is a constant for a given material and  $\alpha$ , G and b have the same meanings as in Eq. 5.2. Higher flow stresses have been observed in smaller cells in accordance with this equation [6].

The existence of  $Al_4CuMg_5Si_4$  and  $Al_{12}(Fe, Mn)_3Si$  dispersoids contribute to the strengthening of the alloy only weakly and in contrast to the contribution of  $\theta'$  and dislocation substructure, their effect on overall strengthening may be neglected. These dispersoids are very coarse in size [57] and can be easily seen under optical microscope at low magnifications. Hence, their effect on strengthening is insignificant as compared to the effect of  $\theta'$ , which is distributed at a much finer level. The dispersoids are also mechanically weak particles and are observed to break at low stresses [57].

Thus from the above discussion it is clear that strengthening in the alloy under investigation will be observed in a thermomechanical treatment which combines the effects of  $\theta'$  distribution and strain hardening due to dislocation substructure. Since the nucleation of  $\theta'$  particles is enhanced by the presence of dislocations, the strength

will be high when fine  $\theta'$  particles are formed in dense dislocation cell structure.

The average diameters of  $\theta'$  plates after various treatments have been estimated from TEM studies as follows.

Peak aged	: 850 $\overset{\circ}{\text{A}}$
TMA Ia	: 650 $\overset{\circ}{\text{A}}$
TMA Ib	: 400 $\overset{\circ}{\text{A}}$
TMA IIa	: 750 $\overset{\circ}{\text{A}}$
TMA IIb	: 600 $\overset{\circ}{\text{A}}$

Bonfield and Datta [51] have established that the peak hardness in Al-Cu-Si-Mg alloy is associated with the presence of  $\theta'$  precipitates of diameter upto 750  $\overset{\circ}{\text{A}}$  and an increase of diameter beyond 850  $\overset{\circ}{\text{A}}$  causes overageing effects. In the present study the diameter of  $\theta'$  particles in the peak aged samples is approximately 850  $\overset{\circ}{\text{A}}$ . The peak hardness in peak aged condition is associated with the presence of  $\theta''$  and  $\theta'$ . In all the thermomechanically aged samples the peak hardness is associated only with  $\theta'$  as no evidence of  $\theta''$  is seen in these samples. Since the diameter of  $\theta'$  precipitates in all the thermomechanically aged samples is less than 850  $\overset{\circ}{\text{A}}$ , it would appear that strengthening after various TMA treatments would be significantly governed by the nature of dislocation substructures. As revealed from TEM study, the dislocation density  $\rho$  is maximum

after TMA IIb treatment and decreases after various treatments in the order

$$\rho_{TMA IIb} > \rho_{TMA Ib} > \rho_{TMA IIa} > \rho_{TMA Ia} > \rho_{peak\ aged}.$$

Thus strengthening after various thermomechanical treatments is also expected to be in this order. This explains the observations of hardness, YS and UTS after various treatments as given in Figs.4.4, 4.5 and 4.7. The TMA IIb treatment, therefore, provides maximum increase in hardness, YS and UTS. The peak ageing treatment results in poorest mechanical properties due to coarsest  $\theta'$  particle size and absence of dislocation-particle tangles. In the present study, the TMA IIb treatment raises the YS of 2014 Al-alloy from  $313.82 \text{ N/mm}^2$  (45.3 Ksi) (achieved in the normal peak aged condition) to  $392.28 \text{ N/mm}^2$  (56.9 Ksi) and UTS from  $372.12 \text{ N/mm}^2$  (54.4 Ksi) to  $431.50 \text{ N/mm}^2$  (62.6 Ksi). Pattanaik et al [6] observed a decrease in the room temperature YS and UTS in the 2024-Al-alloy after various thermomechanical processings. Thompson et al [123,124] achieved a goal of  $380 \text{ N/mm}^2$  (55 Ksi) YS and  $480 \text{ N/mm}^2$  (70 Ksi) UTS in 2048 Al-alloy through thermomechanical treatments. Thus the achievements of the present investigation in strengthening the 2014 Al-alloy are quite considerable.

Attempts have also been made by several workers [4,6,100] to improve high temperature performance of Al-alloys by providing through TMA treatments a dislocation substructure

which is stable at elevated temperatures. Such a substructure should be a source of strength at elevated temperatures. Figs. 4.8 -4.10 show the variation in UTS, YS and elongation respectively after an exposure of 100 hours at various temperatures. These results have been replotted in Figs.5.2, 5.3 and 5.4 as pct. change in the room temperature values of UTS, YS and elongation respectively after 100 hour exposure at various temperatures. It is seen that the stabilisation of UTS and YS values is directly linked to the dislocation density in the dislocation substructures produced by different TMA treatments. Maximum stabilisation in UTS and YS at elevated temperatures is observed in the alloy after TMA IIb treatment which produces thickest dislocation-particle tangles. The alloy after this treatment shows a 20 pct. fall of UTS and YS values after 100 hour exposure at 250°, whereas in the alloy after peak ageing the drop in these properties is by 50 pct. Figs.5.2-5.4 show that exposure at elevated temperatures increases the elongation very steeply at the expense of small drops in the tensile strength.

The stabilisation of strength properties at elevated temperatures is considered to be due to the presence of fine  $\theta'$  particles in the deformed structure, which inhibit recrystallization. The subboundaries of dislocation cell structure are invariably held by the fine  $\theta'$  precipitate particles, which finally inhibits the movement of dislocations and slows down the recrystallisation. TEM studies

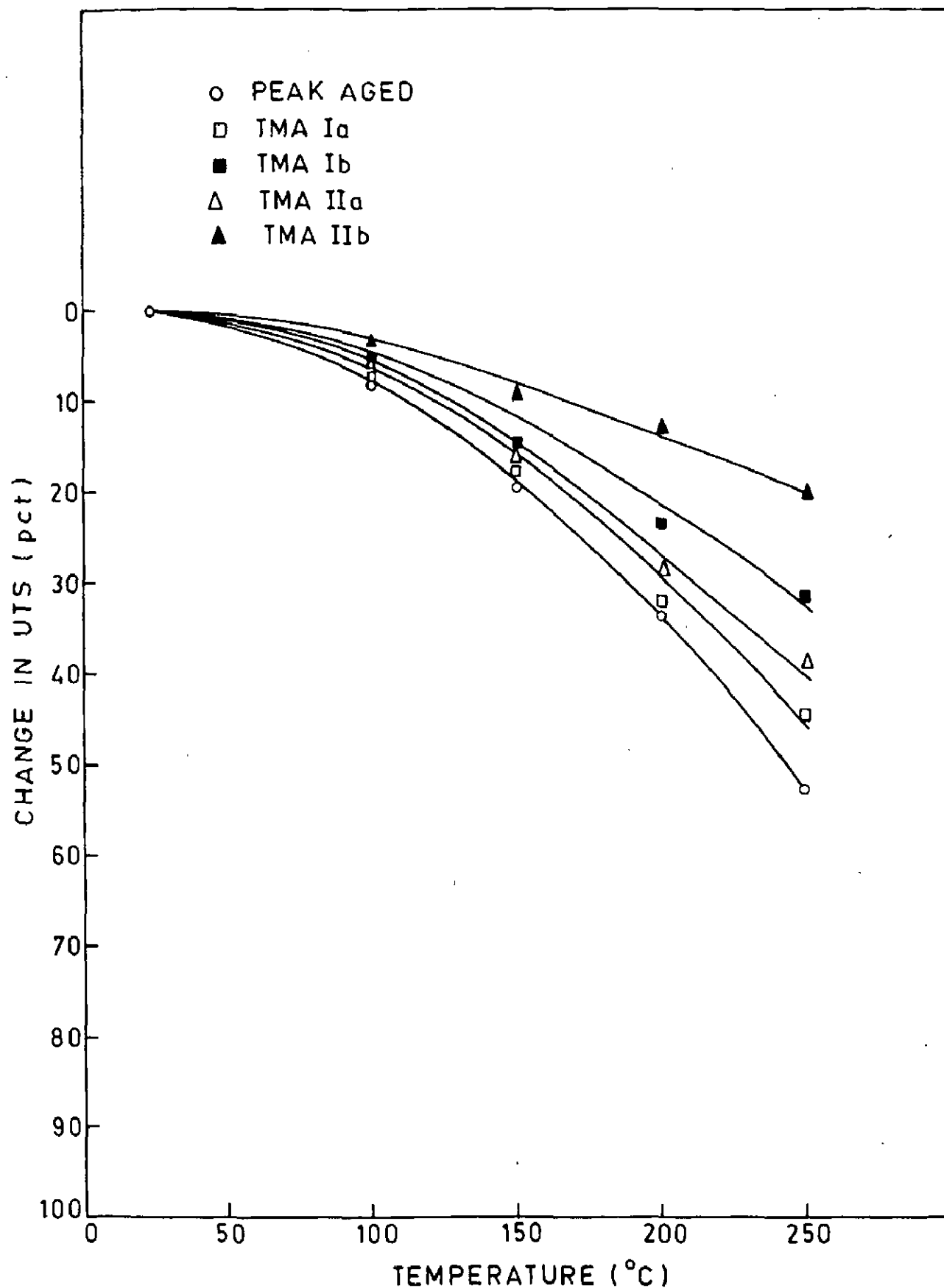


FIG.5.2 CHANGE IN PEAK UTS VALUES AFTER 100 HOUR EXPOSURE AT DIFFERENT TEMPERATURES.



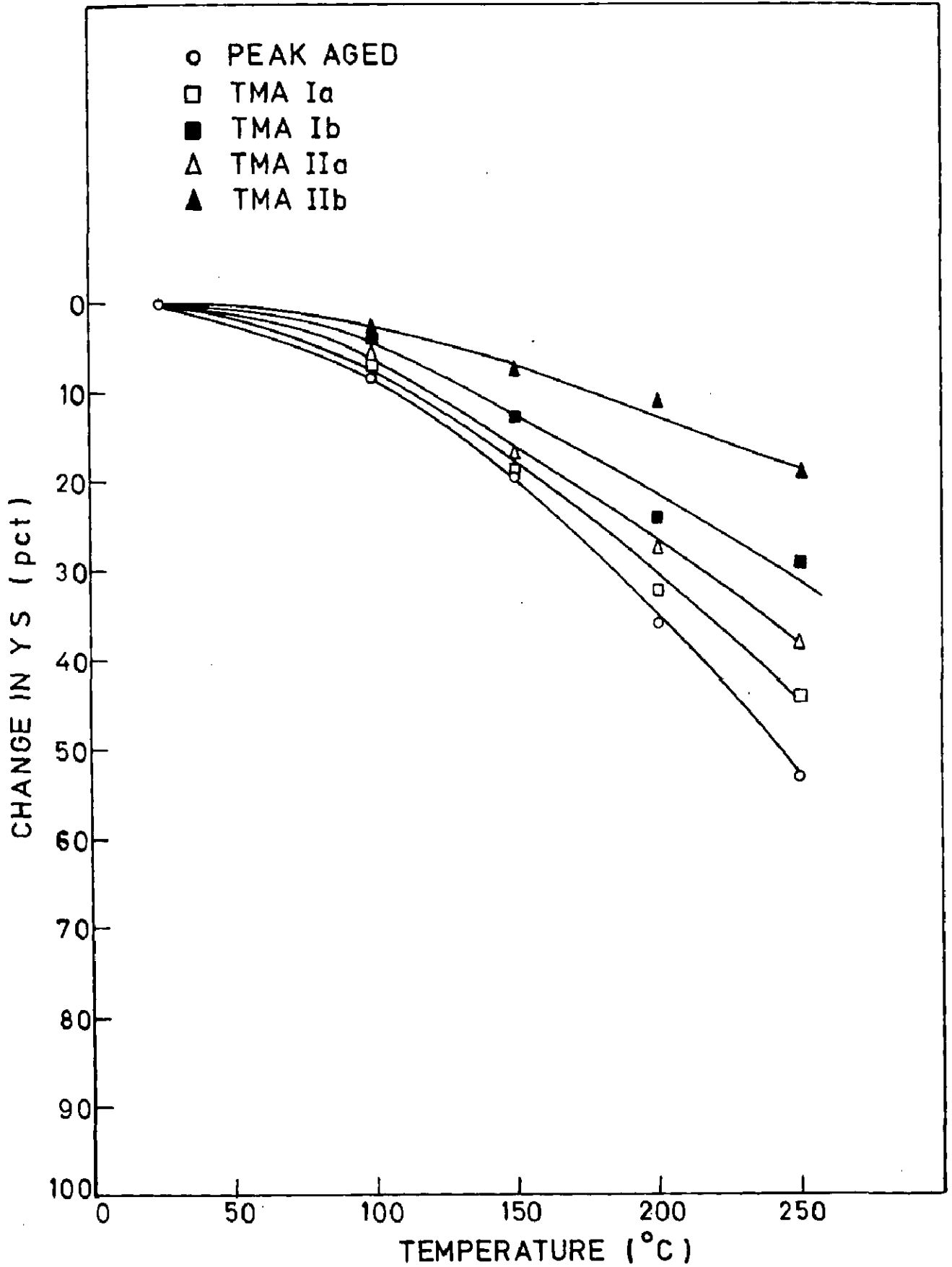


FIG.5.3 CHANGE IN PEAK YS VALUES AFTER 100 HOUR EXPOSURE AT DIFFERENT TEMPERATURES.

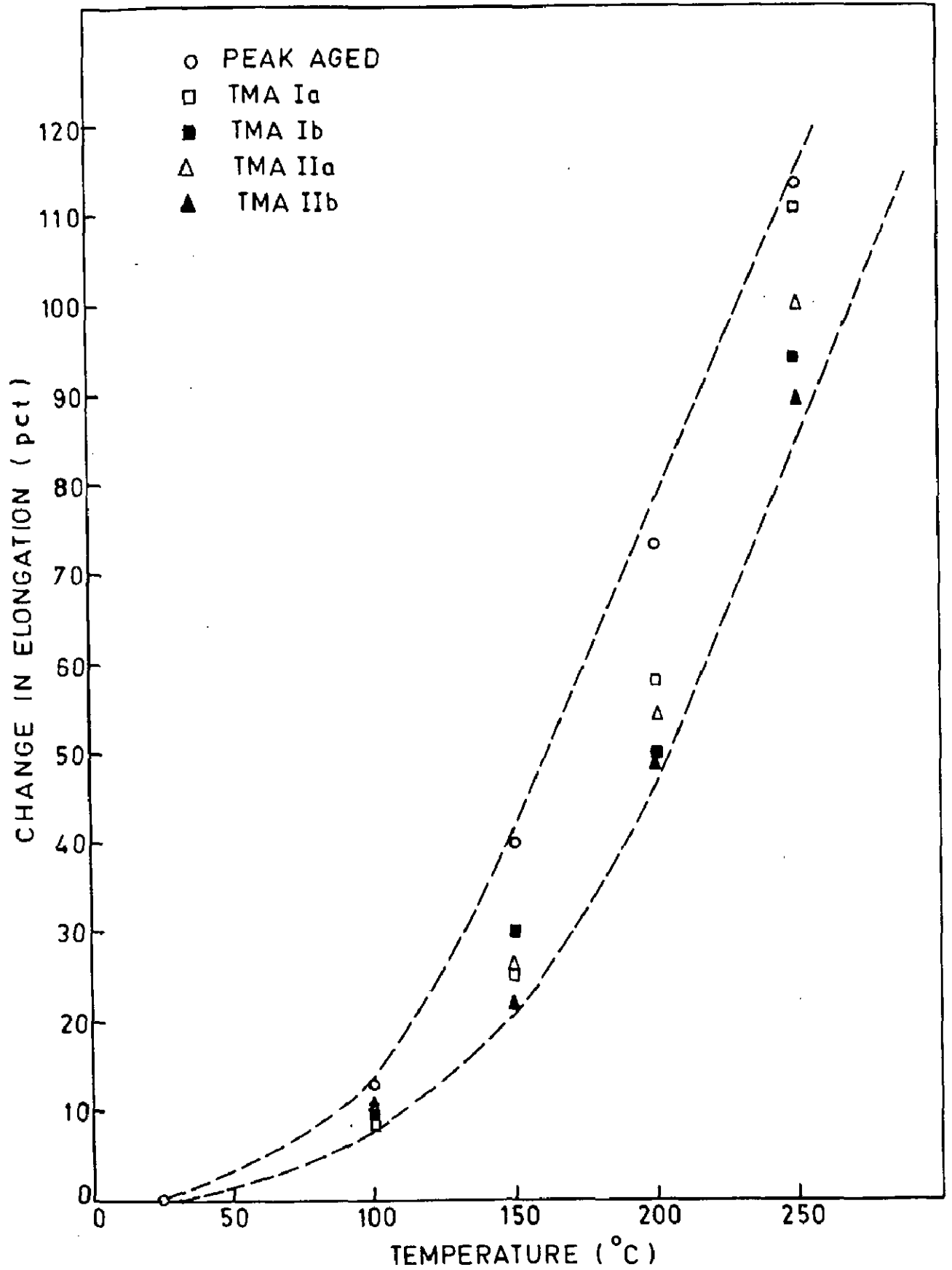


FIG. 5.4 CHANGE IN PEAK VALUES OF ELONGATION AFTER 100 HOUR EXPOSURE AT DIFFERENT TEMPERATURES.

show practically no change in dislocation configuration of the TMA I Ib treated alloy after 100 hour exposure at 250°C. The interparticle spacing in all the thermo-mechanically treated samples ranges between 0.1 $\mu$  and 0.2 $\mu$ . This is in agreement with the observations of Doherty and Martin [185] and Pattanaik et al [6] that recrystallisation in Al-Cu alloys containing  $\theta'$  is slowed down when the interparticle spacing is less than 1 $\mu$ .

In the light of the above discussion and on the basis of TEM observations it is concluded that the TMA I Ib treatment not only provides maximum strengthening to 2014 Al alloy but also provides a dislocation-precipitate structure which is most effective in stabilising the tensile strength at elevated temperatures.

### 5.3 EFFECT ON FATIGUE PROPERTIES

The total life time during fatigue generally can be divided into two regimes: one for crack initiation and the other for crack propagation. In the case of precipitation hardened alloys both regimes are influenced markedly by the microstructure of the material [150,186-188]. In the commercial Al-alloys the crack initiation during fatigue is promoted or caused due to structural inhomogeneities like precipitates, dispersoids or inclusions and persistent slip bands (PSBs). Fatigue crack propagation can be divided into two stages. The Stage I involves crystallographic

crack growth on slip planes, whereas in Stage II the crack follows a macroscopically non-crystallographic plane whose normal is parallel to the axis of maximum tensile stress. The stage I crack propagates along crystallographic slip planes, which experience maximum shear stress [189,190], into PSBs [154,191] which are continually formed ahead of the crack tip due to inhomogeneous stress state existing in that region [148,149,189]. The stage I crack may extend for only a few grain diameters before the crack propagation changes to stage II. The rate of crack propagation in Stage I is generally very low, of the order of angstroms per cycle, compared with crack propagation rates of microns per cycle in stage II. The fracture surface of stage I fractures is practically featureless. Despite the non-crystallographic macroscopic appearance of the crack plane in stage II, the fracture surface of stage II crack propagation frequently shows crystallographic fracture facets, i.e. a pattern of ripples or fatigue fracture striations [135,142] as shown in SEM fractographs (Figs.4.27-4.39) Each striation represents the successive position of an advancing crack front, produced by a single cycle of stress.

Important microstructural features, which significantly affect the fatigue properties of 2014 Al-alloy after various TMA treatments, are mainly (i) dispersoids, (ii) strengthening precipitates ( $\theta'$ ), and (iii) dislocation

networks. Of all the factors, the presence of dispersoids is known to play a dominant role in fatigue crack nucleation in Al-alloys [56,57,119,127,147,150,186-188]. Their importance in nucleating fatigue cracks relates to three factors: (i) a hard dispersoid can act as a stress concentrator, thereby localizing deformation in much the same way as notch, (ii) debonding may occur along the dispersoid-matrix interface, (iii) the relative brittleness of intermetallic compounds allows the possibility of precracking during forming operation (Fig.4.27). In addition to their effect on nucleation, dispersoids can also increase the rate of stage II crack propagation by nucleating cracks ahead of the main advancing crack [127] as shown in Fig.4.39. The present study confirms the vital role played by dispersoid particles in affecting the fatigue properties. The optical microscopic examination reveals the existence of large concentrations of dispersoids in as quenched and peak aged samples, which, as shown in Fig.4.11 also depict poor fatigue properties. Existence of large number of dispersoids at the fracture surfaces of as quenched and peak aged samples is also supported by SEM fractographs (Fig. 4.38). The improvement in fatigue properties after various TMA treatments can be mainly attributed to the drastic reduction in the concentration of these dispersoids as is revealed by optical metallographic observations (Figs.4.41 and 4.42).

Structural heterogeneities developed due to cyclic deformation also play considerably vital role in the fatigue mechanism. The Persistent Slip Bands (PSBs) contribute significantly to fatigue crack nucleation, which is caused by the mechanism of band-matrix decohesion [150,189]. A highly heterogeneous deformation structure consisting of PSBs and cell walls provides paths along which crack growth is facilitated. In view of this, a material capable of a high degree of dynamic recovery would be expected to behave poorly in fatigue, since the recovery accelerates the formation of intense cell walls and slip bands.

Since the  $\theta'$  precipitates nucleate preferentially at dislocations and significantly control the deformation structure in the 2014 Al-alloy, they also play important role in influencing the fatigue properties of this alloy after various TMA treatments. Fine  $\theta'$  precipitates will lead to better fatigue properties, because fine size precipitates inhibit dynamic recovery and thus the formation of PSBs and intense cell walls.

Another factor affecting fatigue is impact of cyclic loading on the precipitation structure of age hardenable Al-alloys as put forward by several investigators [150,192-198]. Generally the fatigue stresses applied are much lower than the yield stress of the material. Thus a single application of fatigue stress has very little probability of causing any significant dislocation movement, but if the

stress is applied many times, there is a chance that eventually some local slip will occur. Local dislocation movements generate vacant lattice sites, thus increasing the local diffusion rates. This increased local diffusion causes localised effects similar to high temperature ageing. This phenomenon results in localised coherent precipitation in solution treated specimens and further ageing in partially aged alloy. This will also cause overageing in fully hardened specimens. In this view, maximum overageing effects are expected in the peak aged specimens, since the  $\theta'$  precipitates are maximum coarse in peak aged condition only. This overageing effect causes  $\theta'$  precipitates to behave in the same way as the dispersoids in nucleating and propagating fatigue crack. Thus the fatigue properties of peak aged samples, which are already very poor due to the presence of dispersoids, are further deteriorated due to coarsening of  $\theta'$  precipitates caused by cyclic stresses.

The SEM studies in the present investigation show striations on the fracture surface. Striations correspond to cycle to cycle crack growth, each striation being indicative of successive positions of the crack front. These striations are related to the formation of PSBs which are continually formed ahead of the crack tip. Earlier TEM studies of the deformation structure adjacent to the fracture surfaces have established that striations are related to the nonuniform dislocation substructure [199]. In a recent

investigation, Nix and Flower [190] using combined SEM/TEM observations have shown that the dislocation band spacing corresponds to that of the surface striations and that the dislocation bands also correspond to the position of the fatigue crack front at some stage during the fatigue cycle. Thus existence of striations on the SEM fractographs can be correlated with that of high density dislocation bands produced during fatigue. Since such bands lead to band-matrix decohesion due to high stress concentration, cracks would also be detected at dense striation walls in the SEM fractographs as shown in Figs.4.30, 4.31 and 4.35. The occurrence of well defined, regular striations observed in the as quenched condition (Fig.4.27) is attributed to a large number of available slip systems and the ease of cross slip allowing the material to perfectly accommodate the deformation required by an irregular crack front. The striations in the peak aged sample, however, are wavy and ill defined due to the presence of large dispersoids and overageing of  $\theta'$  particles as described earlier (Fig.4.31). The fractographs of samples after various TMA treatments show fine networks of close loop striations (Figs.4.32 and 4.33), because the plastic deformation is localised due to the presence of fine size  $\theta'$  precipitates, which is indicative of high fatigue strength. Fine  $\theta'$  particles inhibit cross slip and thus localize the plastic deformation occurring at the crack tip of the



advancing front. The alloy after TMA Ib treatment yields finest distribution of  $\theta'$  precipitates and accordingly the striation loops formed in the sample after this treatment are also finest (Fig.4.32b).

On the basis of the above discussion it is found that in the 2014 Al-alloy under investigation, fatigue properties will be improved by a thermomechanical treatment, which would (i) reduce the concentration of dispersoids, (ii) provide a relatively uniform deformation structure and (iii) produce a fine distribution of  $\theta'$  precipitates. The maximum improvement in fatigue properties after the TMA Ib treatment is in agreement with this discussion. This treatment produces finest distribution of  $\theta'$  precipitates, lowest density of dispersoids and a relatively uniform dislocation substructure. Among all the TMA treatments poorest fatigue properties are observed in TMA IIa treatment because this gives a very coarse  $\theta'$  precipitate distribution, high density of dispersoids and a relatively heterogeneous deformation structure. Thus in agreement with the above reasoning it is also observed that all TMA treatments result into better fatigue properties than in as quenched and peak aged conditions as given in Fig.4.12. The relative difference in fatigue life after various treatments is due to the combined effect of various controlling parameters.

The present investigation also shows that, in general, the improvement in static strength is more pronounced, after

various TMA treatments, than the fatigue strength. This fact can be seen from Fig.5.5 in which fatigue ratio, i.e. the ratio of endurance strength to UTS, is plotted against fatigue life. It is seen from this figure that the fatigue ratios for peak aged and all the TMA treated samples lie in a narrow band which is below the curve for as quenched alloy. Thus the fatigue ratios of the various TMA treatments remain practically unaltered. This also shows that the structure alterations achieved through various thermo-mechanical treatments may affect the static strength of 2014 Al-alloy to a much greater extent than the fatigue strength.

#### 5.4 EFFECT ON FRACTURE TOUGHNESS

Fracture toughness has been measured in two different forms, i.e. plane strain fracture toughness designated as  $K_{Ic}$  and dynamic fracture toughness designated as  $K_{Id}$ . Both these values are expressed in units of  $(\text{stress}) \times (\text{length})^{1/2}$ . Fracture toughness is analogous to the strength of materials. In exact words, it is the internal resistance of material which resist or check the crack growth, and is measured in terms of the opening-mode stress intensity factor  $K_I$ . The distinction between notch toughness or crack toughness and stress intensity factor ( $K_I$ ) is important, and is comparable to the distinction between strength and stress. To determine a  $K_{Ic}$  value, a crack-notched specimen of

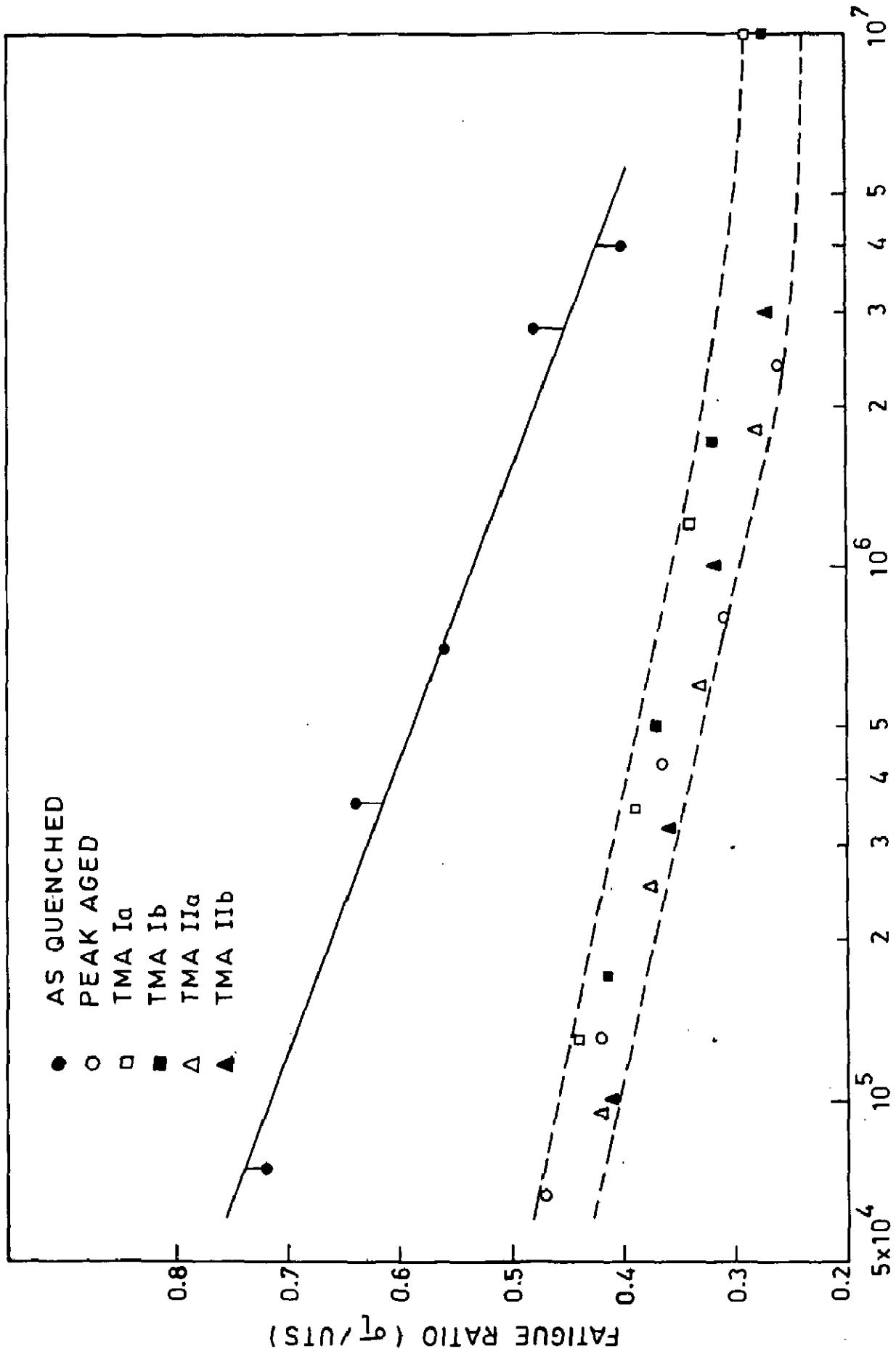


FIG. 5.5 RELATIONSHIP BETWEEN FATIGUE RATIO AND FATIGUE LIFE.

suitable dimensions is increasingly loaded until the crack becomes unstable and extends abruptly. The  $K_I$  value, corresponding to the load at which unstable crack extension is observed, is termed as  $K_{Ic}$ . Under certain conditions the  $K_{Ic}$  level of a material can be used to estimate the load that a structural member containing a crack of specified dimensions could sustain without fracture. The  $K_{Id}$  values correspond to the fracture toughness under dynamic loading.

This investigation shows that with appropriate choice of thermomechanical treatment, it is possible to achieve high notch toughness in 2014 Al-alloy without sacrificing its tensile strength. This improvement in the notch toughness at high strength levels after various TMA treatments is attributed to structural modifications. The various structural parameters, which are likely to affect notch toughness of age hardenable high strength Al-alloys, may be (i) size, shape and distribution of dispersoids, (ii) size and distribution of strengthening precipitates and (iii) dislocation substructure.

During testing of fracture toughness, in most of the high strength Al-alloys, the fracture occurs by a process called plastic fracture [57]. In plastic fracture microscopic voids nucleate at impurity particles, and the growth and coalescence of these voids cause final rupture. It has been shown by various investigations [56, 57, 63, 79, 106, 110, 130, 200-203] that coarse,  $1\mu$  to  $100\mu$ , dispersoid

particles can serve as effective crack initiation sites in high strength Al-alloys. Thus the fracture toughness of these alloys may be affected strongly by the density and distribution of dispersoids, which normally do not contribute to the strength. Recently, similar effect of inclusions on crack initiation has been observed in steel and in other alloy system [204-206]. As reported in Section 4.5 two types of dispersoids have been identified in the alloy under investigation, i.e. large irregular shaped  $Al_{12}(Fe,Mn)_3Si$  particles and small, more rounded  $Al_4CuMg_5Si_4$  particles. Tanaka et al [57] have shown that both type of dispersoids crack during mechanical working with no apparent difference in cracking behaviour. The large particles tend to crack first. The Fe containing dispersoids  $Al_{12}(Fe,Mn)_3Si$  are observed to crack preferentially as compared to the high Si dispersoids  $Al_4CuMg_5Si_4$  [57].

To increase fracture toughness, it would be desirable to simultaneously decrease the size ( $d$ ), and increase the spacing ( $\lambda$ ) between the void nucleating dispersoid particles. The extent of void growth is controlled by the spacing to size ratio ( $\lambda/d$ ) of these particles. Reduction in the particle size decreases the initial void size, while increase in the particle spacing will permit the voids to grow to large sizes before coalescence and thereby improve toughness. The volume fraction of the second phase particles also affects the fracture toughness of high strength Al-alloys by affecting the number of void initiation

centres and spacing between the two successive voids. Thus, decrease in volume fraction of the second phase particles increases the fracture toughness. In addition to the dispersoids, the presence of  $\theta'$  precipitates and dislocation substructure, which is observed to strengthen the matrix, also causes an improvement in the notch toughness because by their presence the crack growth is retarded. In the case of plane strain fracture toughness ( $K_{IC}$ ), due to slow rate of loading, the relative effect of dispersoids,  $\theta'$  and dislocation substructure will be almost the same as in the case of tensile properties because of similarities in the nature and mode of deformation in both the cases. In a recent study Ritchie and Thompson [207] have also established that the metallurgical factors which specifically influence yield strength can have a far greater influence on crack growth toughness compared to crack initiation toughness. Thus  $K_{IC}$  will be largely governed by the presence of  $\theta'$  and dislocation substructure in comparison to the dispersoids. In the case of dynamic fracture toughness ( $K_{ID}$ ), however, the situation is different. In this case, because of impact loading, instantaneous opening of dispersoid-matrix interfaces takes place and, therefore, the effect of dispersoid particles will be stronger than in case of  $K_{IC}$ .

The results of the present investigation are in agreement with the above discussion. Since in plane strain

fracture toughness ( $K_{IC}$ ) the effect of dispersoids,  $\theta'$  and dislocation substructure is identical to their effect on tensile properties, it is observed, as shown in Fig.4.13, that there is a close relationship between  $K_{IC}$  and YS after various treatments. The TMA I Ib treatment results into maximum improvement in  $K_{IC}$  value due to the presence of fine  $\theta'$  precipitate and a high density dislocation substructure'. The variation of  $K_{IC}$  as a function of dispersoid particle spacing ( $\lambda$ ) is given in Fig.5.6 for various treatments. It is seen that as  $\lambda$  increases, the  $K_{IC}$  also improves. The sudden drop in the  $K_{IC}$  from peak age (PA) value to as quenched (AQ) value is due to the absence of strengthening precipitate  $\theta'$  in the as-quenched condition. This observation confirms the key role played by  $\theta'$  precipitates in improving the plane strain fracture toughness of 2014 Al-alloy.

Since in the case of dynamic fracture toughness the dispersoids also play a major role, the effect of  $\theta'$  precipitates has to be considered in relation to the  $\lambda/d$  ratio of dispersoid particles. At very low values of  $\lambda/d$ , the dispersoids will be very close to each other and the concentration of  $\theta'$  precipitates will be very low in between two successive dispersoid particles. Since during dynamic loading dispersoid-matrix interfaces open up very fast, the thin layers of  $\theta'$  will be rather ineffective in controlling coalescence of voids nucleated at various

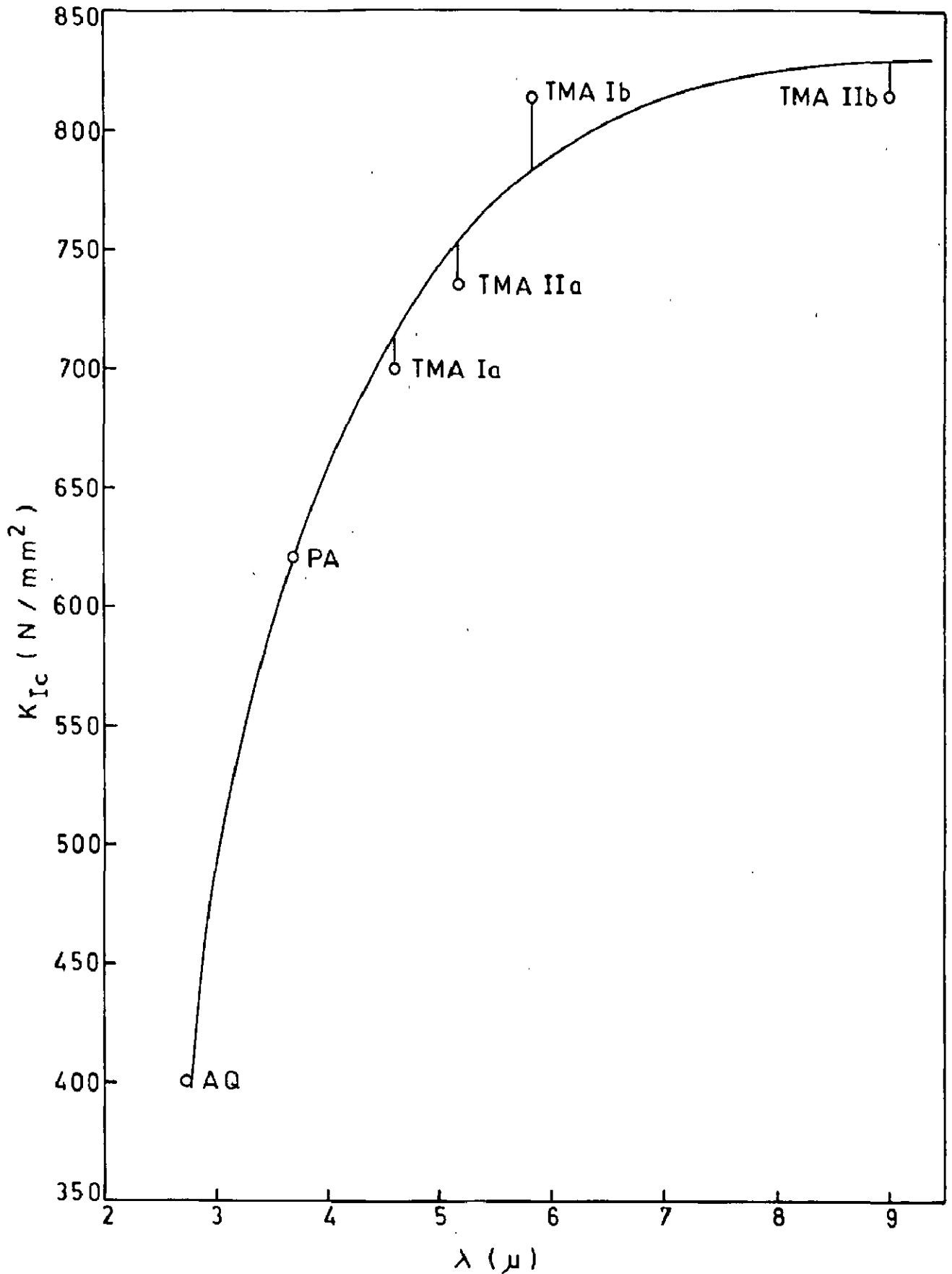


FIG. 5.6  $K_{Ic}$  AS A FUNCTION OF CENTER TO CENTER SPACING  $\lambda$  OF DISPERSOIDS.



points at the dispersoid-matrix interfaces. At large  $\lambda/d$  values, on the other hand, the gaps in between dispersoids are large and the concentration of  $\theta'$  in between dispersoids will be sufficient to provide a check on crack growth. In Fig.5.7, the variation of  $K_{I_d}$  is shown as a function of  $\lambda/d$  of dispersoids. It is seen that the dynamic fracture toughness in peak aged condition is lower than that in as quenched condition inspite of the fact that a fairly high density of  $\theta'$  is formed on peak ageing and the as-quenched alloy is completely deprived of the presence of strengthening  $\theta'$  precipitates. The  $\lambda/d$  values in the as-quenched and peak aged conditions are less than 3 (Fig.5.7) and, therefore, the fracture toughness is primarily determined by dispersoids only. The  $\lambda/d$  value for peak aged samples is observed to be 1.42 as against 2.67 in the as quenched condition. Another contributory factor for higher dynamic fracture toughness in as quenched condition in comparison to peak aged condition is the relative influence of constituent elements of dispersoids. In the as quenched condition a much higher proportion of rounded shaped Si rich  $Al_4CuMg_5Si_4$  dispersoids are formed, whereas in peak aged samples the proportion of the irregular form Fe rich  $Al_{12}(Fe, Mn)_3Si$  particles is much higher. Since presence of Fe is detrimental to fracture toughness, the improvement in the dynamic fracture toughness by the presence of strengthening  $\theta'$  precipitates is outweighed by the detrimental effect

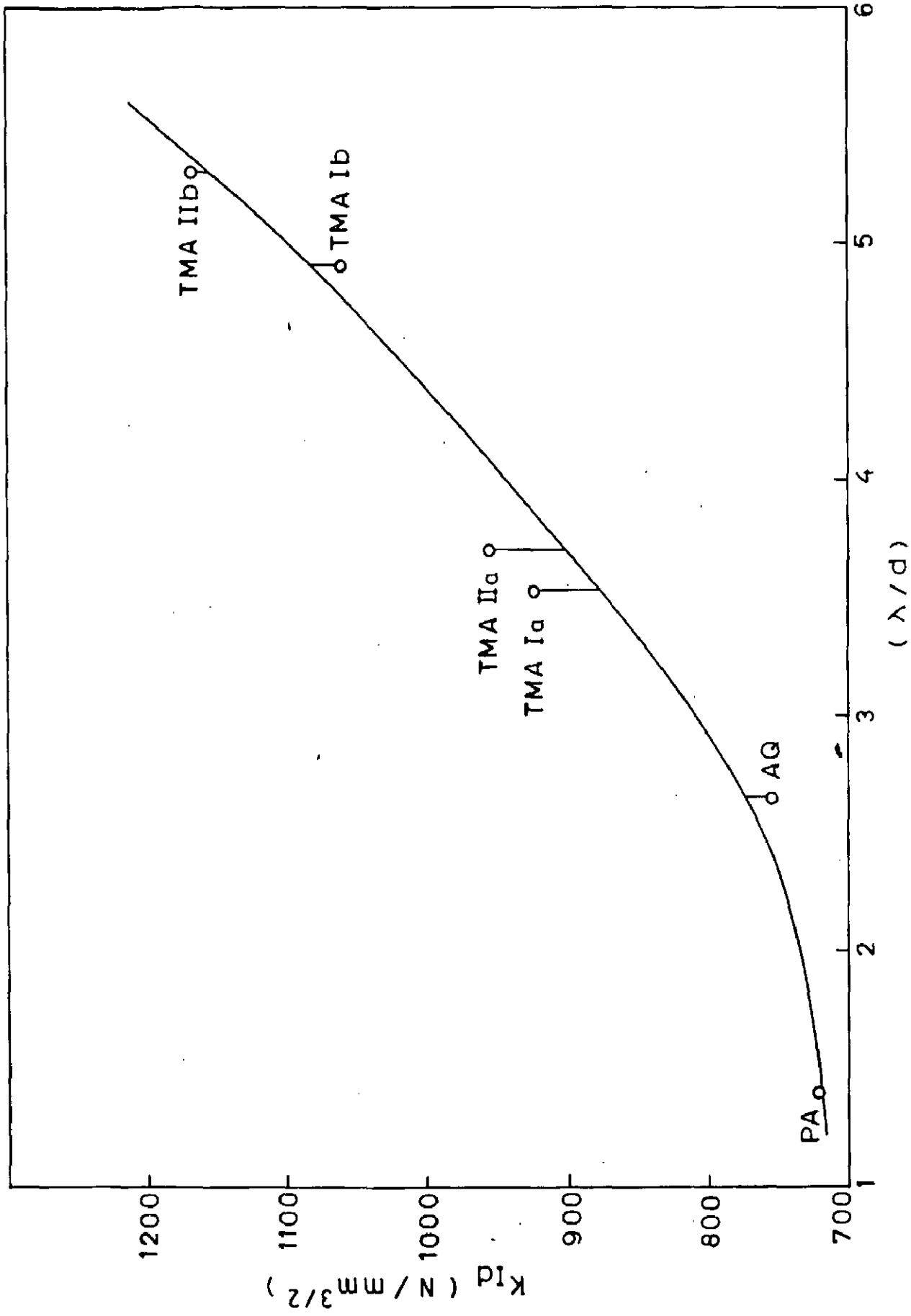


FIG. 5.7 EFFECT OF SPACE-TO-SIZE RATIO  $\lambda/d$  OF DISPERSOIDS ON  $K_{Id}$ .

of Fe rich dispersoid particles having a high dispersion corresponding to a very low  $\lambda/d$  value in peak aged condition. The  $K_{Id}$  values are significantly improved by various TMA treatments as shown in Figs. 4.14, 4.16 and 5.7. It is seen from these figures that the improvement in  $K_{Id}$  after various TMA treatments is due to the combined effects of  $\lambda/d$  value of dispersoids, and the modifications in strengthening precipitates  $\theta'$  and dislocation substructure produced by these treatments. The TMA IIb treatment provides maximum improvement in both  $K_{Ic}$  and  $K_{Id}$  values.

A comparison of Figs. 4.15 and 4.16 shows that dynamic fracture toughness ( $K_{Id}$ ) values are higher than the corresponding  $K_{Ic}$  values in case of all treatments, because the strain rate effect associated with the dynamic test is shown to increase the fracture toughness for most alloys [166, 167]. In the literature it is reported that this effect is due to the presence of adiabatic plastic zone ahead of the advancing crack, whereas in case of plane strain fracture testing with a slow rate of loading, an isothermal plastic zone exists ahead of the advancing crack which may cause a time dependent embrittlement of material just ahead of crack tip, and thus lower the fracture toughness ( $K_{Ic}$ ) values.

#### 5.5 CHOICE OF THERMOMECHANICAL AGEING TREATMENT

A critical analysis of the results obtained in this investigation shows that by selecting an appropriate TMA treatment,

the mechanical properties of 2014 Al-alloy can be significantly improved. By a suitable combination of deformation-ageing cycle it is possible to attain a considerable improvement in fatigue and fracture toughness properties in addition to improvement in tensile properties at room temperature as well as at elevated temperature. The factors responsible for affecting various properties are the modifications in the structure of the alloy involving formation and distribution of  $\theta'$  precipitates, dispersoids, and dislocation-particle tangles. The general requirement to improve various mechanical properties is the generation of a structure consisting of (i) fine distribution of  $\theta'$  precipitation, (ii) minimum size and density of dispersoids and (iii) thick, stabilised and uniformly distributed dislocation-particle tangles.

A summary of the effects of various treatments on mechanical properties of 2014 Al-alloy is given in Fig.5.8. It is observed that, among all the TMA treatments, the TMA IIB has maximum influence on hardness,  $K_{Ic}$ ,  $K_{Id}$  and UTS at room temperature and at elevated temperature. Only in case of fatigue does this treatment show somewhat lower value of endurance limit than in TMA IB treatment, which is observed to be next best thermomechanical treatment. Taking the peak age values as base it is observed that TMA IIB treatment provides maximum influence in stabilising high temperature strength and considerable improvement in dynamic fracture toughness and other mechanical properties.

## CHAPTER-6

### CONCLUSIONS AND SUGGESTIONS FOR FUTURE WORK

#### 6.1 CONCLUSIONS

The present investigation has been carried out to study the effect of various thermomechanical ageing treatments on the structure and mechanical properties of 2014 Al-alloy. The main conclusions of this study are as follows.

(1) In the peak aged condition the structure is characterised by the existence of large amount of  $\theta''$  platelets with a very small amount of  $\theta'$  precipitates. All the TMA treatments suppress the formation of  $\theta''$  and accelerate the formation of  $\theta'$  precipitate. In general, TMA I treatments produce finer distribution of  $\theta'$  than TMA II treatments at any degree of deformation. Two types of dispersoids have been identified, dark etching irregular shape  $Al_{12}(Fe,Mn)_3Si$  and light etching nearly rounded  $Al_4CuMg_5Si_4$ . The TMA treatments reduce the size and density of these dispersoids, the effect of TMA Ib being maximum. Although the TMA II treatments generate higher density of dislocations in the structure as compared to the TMA I treatments at any degree of deformations, the TMA I treatments produce relatively more uniform deformation

the mechanical properties of 2014 Al-alloy can be significantly improved. By a suitable combination of deformation-ageing cycle it is possible to attain a considerable improvement in fatigue and fracture toughness properties in addition to improvement in tensile properties at room temperature as well as at elevated temperature. The factors responsible for affecting various properties are the modifications in the structure of the alloy involving formation and distribution of  $\theta'$  precipitates, dispersoids, and dislocation-particle tangles. The general requirement to improve various mechanical properties is the generation of a structure consisting of (i) fine distribution of  $\theta'$  precipitation, (ii) minimum size and density of dispersoids and (iii) thick, stabilised and uniformly distributed dislocation-particle tangles.

A summary of the effects of various treatments on mechanical properties of 2014 Al-alloy is given in Fig.5.8. It is observed that, among all the TMA treatments, the TMA IIb has maximum influence on hardness,  $K_{Ic}$ ,  $K_{Id}$  and UTS at room temperature and at elevated temperature. Only in case of fatigue does this treatment show somewhat lower value of endurance limit than in TMA Ib treatment, which is observed to be next best thermomechanical treatment. Taking the peak age values as base it is observed that TMA IIb treatment provides maximum influence in stabilising high temperature strength and considerable improvement in dynamic fracture toughness and other mechanical properties.

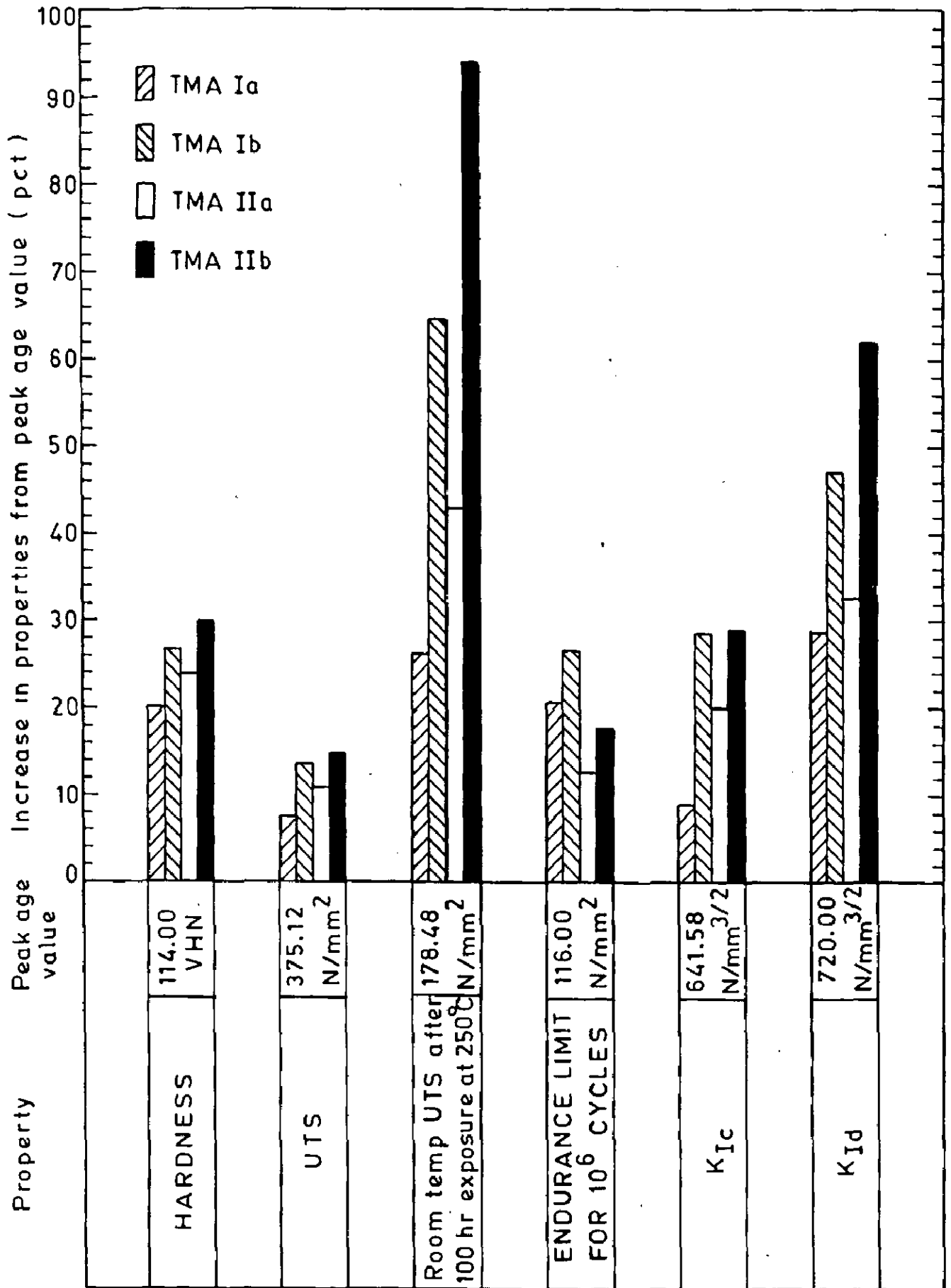


FIG. 5.8 PERCENT INCREASE IN VARIOUS PROPERTIES FROM PEAK AGE VALUE AFTER DIFFERENT TMA TREATMENTS.

## CHAPTER-6

### CONCLUSIONS AND SUGGESTIONS FOR FUTURE WORK

#### 6.1 CONCLUSIONS

The present investigation has been carried out to study the effect of various thermomechanical ageing treatments on the structure and mechanical properties of 2014 Al-alloy. The main conclusions of this study are as follows.

(i) In the peak aged condition the structure is characterised by the existence of large amount of  $\theta''$  platelets with a very small amount of  $\theta'$  precipitates. All the TMA treatments suppress the formation of  $\theta''$  and accelerate the formation of  $\theta'$  precipitate. In general, TMA I treatments produce finer distribution of  $\theta'$  than TMA II treatments at any degree of deformation. Two types of dispersoids have been identified, dark etching irregular shape  $Al_{12}(Fe, Mn)_3Si$  and light etching nearly rounded  $Al_4CuMg_5Si_4$ . The TMA treatments reduce the size and density of these dispersoids, the effect of TMA Ib being maximum. Although the TMA II treatments generate higher density of dislocations in the structure as compared to the TMA I treatments at any degree of deformations, the TMA I treatments produce relatively more uniform deformation



structure as compared to TMA II treatments because of the difference in the subsequent ageing periods.

(ii) The general strengthening of the alloy is attributed mainly to the existence of  $\theta''$ ,  $\theta'$  and dislocation-particle tangles. The dispersoids do not have any significant effect on strengthening. In the peak aged material the hardening occurs predominantly due to  $\theta'$  platelets, whereas after TMA treatments the strengthening is mainly controlled by fine distribution of  $\theta'$  precipitates and density of dislocations. The alloy after TMA IIb treatment exhibits maximum improvement in hardness and tensile properties. Maximum stabilisation of tensile properties is observed after 100 hour exposure at 250°C, through TMA IIb treatment, due to the presence of thickest dislocation-precipitate tangles and smaller interparticle spacing which inhibit recrystallisation.

(iii) It is observed that fatigue properties are improved by lowering the density of dispersoids, increasing the fineness of  $\theta'$  distribution and by generating a uniform dislocation substructure. The best fatigue properties are observed after TMA Ib treatment. Peak aged material exhibits the poorest fatigue properties due to very high density of dispersoids.

(iv) The fracture toughness of the alloy under investigation is observed to be controlled by the presence of dispersoids, strengthening  $\theta'$  precipitates and dislocation

substructure. The effect of  $\theta'$  and dislocation substructure is more significant as compared to that of dispersoids on  $K_{Ic}$  values; whereas the effect of dispersoids is equally significant in case of dynamic fracture toughness. An improvement in fracture toughness is observed after all TMA treatments. Maximum improvement in both  $K_{Ic}$  and  $K_{Id}$  values is observed after TMA IIB treatment.

## 6.2 SUGGESTIONS FOR FUTURE WORK

On the basis of the present study, further work is proposed on the following lines:

- (i) Present study has shown that dispersoids play a major role in affecting fatigue and fracture toughness properties. In order to identify the role of dispersoids, study may be conducted to clearly understand their nature. 2014 Al-alloys with varying impurity levels may be prepared in order to produce various types of dispersoids. Systematic investigations are required to understand the exact effect of shape, size, distribution and composition of dispersoids.
- (ii) The effect of thermomechanical treatment on the fatigue properties has been studied in this investigation. There is, however, ample scope to undertake studies on the mechanisms of fatigue crack growth. Such an investigation would involve combined TEM/SEM study of the fracture surfaces.
- (iii) Another field of further investigation would be

fracture toughness study with the help of instrumented V-notch Charpy test. Such a study will provide information about the energies required for crack initiation and for complete fracture and will, in turn, identify more clearly the factors affecting the fracture toughness of age hardenable Al-alloys.

(iv) The high strength Al-alloys are, in many applications, required to be used in corrosive atmospheres and under cryogenic conditions. Suitable thermomechanical treatments may be developed for producing Al-alloys suitable for such applications.

\*\*\*\*\*

## REFERENCES

\*\*\*\*\*

\*\*\*\*\*

## CHAPTER 6

### CONCLUSIONS AND SUGGESTIONS FOR FUTURE WORK

\*\*\*\*\*

## REFERENCES

1. N.Ryum, B.Haegland and T.Lindveit,  
Z.Metallkunde 58(1967) 28.
2. N.Ryum,  
Acta Met.16(1968) 327.
3. N.Ryum,  
Acta Met.17 (1969) 821.
4. H.A.Lipsitt and C.M.Sargent,  
Proc. 2nd Int. Conf. on Strength of Metals and Alloys,  
ASM (1970) 937.
5. H.A.Lipsitt,  
Met.Trans.2A(1971) 1739.
6. S.Pattanaik, V.Srinivasan and M.L. Bhatia,  
Scripta Met.6(1972) 191.
7. A.Wilm,  
Metallurgie 8 (1911) 225.
8. A.Wilm,  
Metallurgie 8 (1911) 650
9. P.D.Merica, R.C.Walthernberg and H.Scott,  
Trans. Met.Soc. AIME 64 (1921) 3.
10. S. Konno,  
Science Reports Tohoku Imperial University 11 (1922)  
269.
11. W.Franknel and E.Scheuer,  
Z.Metallkunde 14 (1922) 49.

12. M.L.V.Gayler and G.P.Preston,  
J.Inst. Metals 41 (1929) 191.
13. W.Rosenhein,  
J.Inst. Metals 44(1930) 226.
14. G.Tammann,  
Z.Metallkunde 22(1930) 365.
15. P.D.Merica,  
Trans. Met.Soc. AIME 99 (1932) 131.
16. C.H.M.Jenkins and E.M.Bucknall,  
J.Inst.Metals 57 (1935) 141.
17. W.De Sorbo, H.N.Treafitis and D.Turnbull,  
Acta Met.6 (1958) 401.
18. D.Turnbull, H.S.Rosenbaum and H.N. Treafitis,  
Acta Met. 8 (1960) 277.
19. A.Guinier,  
Ann.Physique 12 (1939) 161.
20. G.P.Preston,  
Proc. Royal Society A161 (1938) 526.
21. A.Guinier,  
Acta Met.3 (1955) 510.
22. A.Guinier,  
'X-ray Diffraction', W.H.Freeman, San Fransisco (1963).
23. V.Gerold,  
Phys. Status Solidi 1 (1961) 37.
24. G.Borelius,  
'Defects in Crystalline Solids', Physical Society  
(1955) 169.

25. G.Borelius, L.E. Larsson,  
'The Mechanism of Phase Transformation in Metals',  
Inst. Metals (1956) 285.
26. H.Herman and J.B. Cohen,  
Nature 191 (1961) 63.
27. H.Haberkrone and V.Gerold,  
Phys. Status Solidi 15 (1966) 167.
28. F.R.N. Nabarro,  
Proc. Phys.Soc. 52 (1940) 90.
29. F.R.N. Nabarro,  
Proc.Roy.Soc. A175 (1940) 519.
30. N.F.Mott and F.R.N. Nabarro,  
Proc. Phys.Soc. 52(1940) 86.
31. R.C.Baker, D.G.Braddon, and J.Nutting,  
Phil.Mag [8] 4(1959) 1339.
32. C.Zener,  
Proc. of Inst.Conf. on Physics of Metals,  
Amsterdam (1948) 117.
33. F.Seitz,  
'L'Etat Solide', Inst.Intern.Phys.Solvay, R.Stoops(1952)  
401.
34. T.Federighi,  
Acta Met. 6 (1958) 379.
35. H.Herman,  
Met. Trans. 2A(1971) 16.
36. E.W.Hart,  
Acta Met. 6(1958) 533.
37. T.Federighi and G.Thomas,  
Phil.Mag. [8] 7 (1962) 127.



38. A.Kelly and R.B.Nicholson,  
'Progress in Material Science', Pergamon Press,  
Oxford 10 (1966) 151.
39. J.Friedel,  
'Les Dislocations', Gauthier Villars (1956).
40. H.Brooks,  
'Metal interfaces', ASM(1952) 20.
41. H.K. Hardy and T.J. Heal,  
'Progress in Metal Physics', Pergamon Press,  
Oxford 5(1954) 143.
42. A.Guinier,  
J.Phys. Radium 8(1942) 122.
43. A.Guinier,  
Acta Cryst. 5(1952) 51.
44. V.Gerold,  
Z.Metallkunde 45 (1954) 593.
45. J.M.Silcock, T.J.Heal and H.K. Hardy,  
J.Inst. Metals 82 (1953) 239.
46. V.Gerold and H.Haberkron,  
Z.Metallkunde 50 (1959) 568.
47. H.Lambot,  
Rev.Met. 47(1950) 709.
48. J.M.Silcock,  
J.Inst. Metals 89 (1960) 203.
49. R.N. Wilson,  
J.Inst.Metals 97(1969) 80.
50. R.N.Wilson, D.M.Moore and P.J.E.Forsyth,  
J.Inst.Metals 95 (1967) 177.
51. W.Bonfield and P.K. Datta,  
J.Mater. Sci. 11(1976) 1661.

52. W. Bonfield and P.K. Datta,  
J.Mater. Sci. 12 (1977) 1050.
53. W. Bonfield and P.K. Datta,  
J.Mater. Sci. 15(1980) 3166.
54. L.F. Mondolfo,  
'Aluminium alloys: Structure and Properties',  
Butterworths and Co.(Publishers) Ltd., London(1976).
55. Kent R. Van Horn,  
'Aluminium', ASM, Metals Park, Ohio 1(1968).
56. R.H. Van Stone, R.H. Merchant and J.R. Low, Jr.  
ASTM STP 556, Amer.Soc. for Testing and Materials(1974)93.
57. J.P. Tanaka, C.A. Pampillo and J.R. Low, Jr.  
ASTM STP 463, Amer.Soc. for Testing and Materials (1970)191.
58. R.E. Smallman,  
'Modern Physical Metallurgy', Butterworths and Co.  
(Publishers) Ltd., London (1963).
59. J.W. Martin,  
'Precipitation hardening', Pergamon Press Ltd., Oxford(1968).
60. W.E. Duckworth,  
J.Metals 8 (1966) 915.
61. V.S. Ivanova,  
Met. Sci. Heat treatment 2 (1967) 339.
62. W. Gruhl,  
Aluminium 38 (1962) 775.
63. H.J. Rack and R.W. Krenzer,  
Met. Trans. 8A(1977) 335.

64. A.Berghezan,  
Competus Rendus 232(1951) 1560.
65. R.Graf,  
Publs. Sci. et tech.ministere air No.315(1956).
66. Y.Murakami and O.Kawano,  
Mem. Faculty Eng. Kyoto Univ.21 (1959) 393.
67. J.M.Silcock,  
Acta Met.8 (1960) 589.
68. A.Guinier,  
'Solid State Physics', Academic Press, New York 9 (1959).
69. R.Graf and A.Guinier,  
Competus Rendus 238 (1954) 819.
70. R.Graf and A.Guinier,  
Competus Rendus 239 (1954) 2175.
71. G.Thomas and J.Nutting,  
Acta Met.7 (1959) 515.
72. G.M.K. Sarma and T.R.Anantharaman,  
Trans. I.I.M. 18 (1965) 151.
73. C.Laird and H.I. Aaronson,  
Trans.AIME 242 (1968) 591.
74. P.Guyot and M.Wintenberger,  
J.Mater. Sci. 9 (1974) 614.
75. W.D.Robertson,  
Trans AIME. 166 (1946) 216.
76. H.A.Holl,  
Metal Sci. J., 1(1967), 111.

77. J.Nutting,  
Met. Trans. 2A (1971) 45.
78. Y.Takeuchi,  
Aluminium 47 (1971) 665.
79. D.S.Thompson, S.A.Levy and D.K. Benson,  
Proc. of 3rd Int. Conf.on Strength of Metals and  
Alloys, Cambridge, England 1 (1973) 119.
80. C.M.Wan, M.T.Jahn, T.Y.Chen and L.Chang,  
J.Mater. Sci. 13 (1978) 2059.
81. C.M. Wan, W.Y.Wei and M.T.Jahn,  
J.Mater. Sci. 16 (1981) 1097.
82. N.C.Danh, Krishna Rajan and W.Wallace,  
Met. Trans. 14A (1983) 1843.
83. D.B.Goel, P.Furrer and H.Warlimont,  
Aluminium 50 (1974) 511.
84. P.C.Varley, M.K.B.Day and A.Sendorek,  
J.Inst. Metals 86 (1957) 337
85. H.S. Rosenbaum and D.Turnbull,  
Acta Met. 6 (1958) 653.
86. H.S.Rosenbaum and D.Turnbull,  
Acta Met.7(1959) 664.
87. J.D.Embury and R.B.Nicholson,  
J.Aust. Inst. Metals 8 (1963) 76.
88. J.D.Embury and R.B.Nicholson,  
Acta Met.13(1965) 403.
89. G.W.Lorimer and R.B. Nicholson,  
Acta Met.14 (1966) 1009.

90. E.A.Strake,  
J.Metals 22 (1970) 54.
91. N.Ryum,  
Z.Metallkunde 66 (1975) 338.
92. K.Welpmann, G.Lutjering and W.Bunk,  
Aluminium 50 (1974) 263.
93. W.F.Smith and N.J. Grant,  
Trans. ASM 62(1969) 724.
94. A.J.McEvily, R.L. Snyder and J.B. Clark,  
Trans AIME 227 (1963) 452.
95. A.J.McEvily, J.B.Clark and A.P.Bond,  
Trans. ASM 60 (1967) 661.
96. N.K. Srinivasan and V.Ramachandran,  
Indian J.of Tech.11 (1973) 555.
97. P.N.T.Unwin, G.W.Lorimer and R.B.Nicholson,  
Acta Met. 17 (1969) 1363.
98. R.B.Nicholson,  
'Nucleation at imperfections in phase transformation',  
ASM, Metals Park, Ohio (1970).
99. K.Welpmann, G.Lutjering and W.Bunk,  
Proc. of 4th Int. Conf. on Fracture, Waterloo, Canada  
2A(1977) 105.
100. A.W.Thompson,  
Met. Trans. 8A (1977) 833.
101. L.Anand and J.Gurland,  
Met. Trans. 7A (1976) 610.
102. R.J.Price and A.Kelly,  
Acta Met. 10 (1962) 980.

103. G.Greetham and R.W.K.Honeycombe,  
J.Inst. Metals. 8(1960) 13.
104. D.Dew-Hughes and W.D.Robertson,  
Acta Met. 8(1960) 147 and 156.
105. C.J. Beevers and R.W.K.Honeycombe,  
Acta Met. 10 (1962)17.
106. D.S. Thompson and S.A. Levy,  
Light Metal Age, August (1977) 11.
107. A.W.Sommer, N.E. Paton and D.G.Folgnier,  
Air Force Materials Laboratory Technical Report  
No.AFML-TR-72-5 February (1972).
108. H.J.Rack,  
Mater. Sci. Eng. 29(1977) 179.
109. H.J. Rack,  
Scripta Met. 12 (1978).777.
110. Joseph S.Santner,  
Met. Trans. 9A (1978). 769.
111. R.E.Sanders, Jr. and E.A.Strake, Jr.,  
Met. Trans. 9A (1978) 1087.
112. N.E.Paton and A.W. Sommer,  
Proc. of 3rd Int. Conf. on Strength of Metals and  
Alloys, Cambridge, England 1(1973) 101.
113. E.Di Russo, M.Conserva, M.Buratti and F.Gatto,  
Mater. Sci. Eng. 14 (1974) 23.
114. J.Waldman, H.Sulinski and H.Markus,  
Met. Trans. 5A (1974) 573.
115. J.W.Evancho and J.T.Staley,  
Met. Trans. 5A (1974) 43.

116. M.Conserva and M.Leoni,  
Met. Trans. 6A (1975) 189.
117. S.V.S. Narayana, C.S.Harendranath and A.K. Mallik,  
Trans. I.I.M. 35 (1982) 421.
118. R.I. Ganguly, B.K. Dhindaw and P.R.Dhar,  
Met. Trans. 8A (1977) 363.
119. K. Tanaka and T.Mura,  
Met. Trans. 13A (1982) 117.
120. V.Sijacki-ZeraVcic, M.Rogulic and V.Milenkovic,  
Aluminium 59 (1983) 379.
121. R.E.Sanders, Jr., T.H.Sanders, Jr. and J.T.Staley,  
Aluminium 59 (1983) 13.
122. R.E.Sanders, Jr., T.H.Sanders, Jr. and J.T.Staley,  
Aluminium 59 (1983) 143.
123. D.S.Thompson, S.A.Levy and G.E.Spangler,  
Aluminium 50 (1974) 647.
124. D.S.Thompson, S.A.Levy and G.E.Spangler,  
Aluminium 50 (1974) 719.
125. M.Conserva, E.DiRusso and F.Gatto,  
Aluminium 37 (1968) 441.
126. F.Ostermann,  
Met. Trans. 2A(1971) 2897.
127. F.G.Ostermann and W.H. Reimann,  
ASTM STP 467, Amer.Soc. for Testing and Materials(1970) 162.
128. W.H.Reimann and A.W.Brisbane,  
Eng. Fracture Mechanics 5 (1973) 67.

129. E.DiRusso, M.Conserva, F.Gatto and H.Markus,  
Met. Trans. 4A (1973) 1133.
130. S.A.Levy, D.S.Thompson and G.E.Spangler,  
Metals Eng., Quart.May (1975) 21.
131. Morris E.Fine and Joseph S.Santner,  
Scripta Met. 9 (1975) 1239.
132. G.Malakondaiah and P.Rama Rao,  
Proc. of 4th Int. Conf. on Fracture, Waterloo,  
Canada 2B (1977) 741.
133. R.Hauenstein and W.Epprecht,  
Scripta Met. 15(1981) 67.
134. I.Ferreira and R.G.Stang,  
Acta Met.31 (1983) 585.
135. C.S.Harendranath and A.K. Mallik,  
Trans.I.I.M. 35 (1982) 415.
136. Neal L.Person,  
Metal Progress 120 (1981) 33.
137. A.R.Krause and C.Laird,  
Mater. Sci. Eng.2 (1967) 331.
138. D.Broek and C.O.Bowles,  
J.Inst. Metals 99 (1971) 255.
139. J.O.Lyst,  
J.Materials 3 (1968) 996.
140. K.R.L. Thompson and J.V.Craig,  
Met. Trans. 1A (1970) 1047.
141. C.Calabrese and C.Laird,  
Met. Trans. 5A (1974) 1785.



142. G.G.Garrett and J.F.Knott,  
Acta Met. 23 (1975) 841.
143. S.Purushothaman and John K.Tien,  
Scripta Met., 9 (1975) 923.
144. Morris E.Fine and Joseph S.Santner,  
Met. Trans. 7A (1976) 583.
145. S.J. Brett, B.Cantor and R.D.Doherty,  
Proc. of 4th Int. Conf. on Fracture, Waterloo,  
Canada, 2B(1977) 719.
146. K.S.Chan and J.Lankford,  
Scripta Met. 17 (1983) 529.
147. David Sigler, Michael C.Montpetit and W.L.Haworth,  
Met. Trans. 14A (1983) 931.
148. J.Polák and M.Klesnil,  
Matr. Sci. Eng. 63 (1984) 189.
149. P.Lukáš and L.Kunz,  
Matr. Sci. Eng. 62 (1984) 149.
150. W.Ruch and V.Gerold,  
Proc. of 4th ECF Conference, Leoben, Austria (1982)383.
151. V.Weiss and S.Yukawa,  
ASTM STP 381, Amer.Soc. for Testing and Materials(1965)1.
152. V.Z.Parton and E.M. Morozov,  
'Elastic-Plastic Fracture Mechanics', Mir Publishers,  
Moscow(1978).
153. Joseph E.Shigley and Larry D. Mitchell,  
'Mechanical Engg. Design', McGraw-Hill Book Company,  
Tokyo, Japan(1983).
154. George E.Dieter,  
'Mechanical Metallurgy', McGraw-Hill Kogakusha Ltd.,  
Tokyo, Japan(1976).

155. Howard E. Boyer (Ed.),  
'Failure Analysis and Prevention', Metals Handbook,  
ASM, Metals Park, Ohio 10 (1975).
156. H.J. Saxton, A.T. Jones, A.J. West and T.C. Mamaros,  
ASTM STP 563, Amer. Soc. for Testing and Materials (1974) 30.
157. R.A. Wullaert, D.R. Ireland and A.S. Tetelman,  
Symp. on Fracture Prevention and Control, ASM (1974) 255.
158. R.I. Jaffee,  
Proc. of 2nd Int. Conf. on Titanium, Cambridge 3 (1973) 1665.
159. J.R. Rice,  
J. Appl. Mech. 35 (1968) 379.
160. T. Kawabata and O. Izumi,  
Acta Met. 29 (1981) 229.
161. Taylor Lyman (Ed.),  
'Properties and Selection of Metals, Metals Handbook,  
ASM, Metals Park, Ohio 1 (1969).
162. M.V. Hyatt and W.E. Quist,  
AFML Tech. Rept. TR-67-329 (1967).
163. J.T. Staley,  
Tech. Rept. Naval Air Systems Command Contract  
M000019-71-C-0131 (May 1972).
164. J.G. Kaufman,  
'Design of Al-alloys for high toughness and high  
fatigue strength', Proc. of 40th meeting of Structures  
and materials Panel NATO, Brussels, Belgium, (April 1975).
165. J.T. Staley,  
'Microstructure and Toughness of High strength Al-alloys',  
Proc. of ASTM Symposium on properties related to  
toughness, Montreal, Canada (June 1975).

166. A.Ewing and L.Raymond,  
ASTM STP 563, Amer.Soc. for Testing and Materials  
(1974) 180.
167. T.J.Koppelaar,  
ASTM STP 563, Amer.Soc. for Testing and Materials  
(1974) 92.
168. U.Köster and E.Hornbogen,  
Z.Metallkunde 59(1968) 787.
169. J.K.Park and A.J.Ardell,  
Met.Trans.15A(1984) 1531.
170. H.Wilsdorf and D.Kuhlmann-Wilsdorf,  
'Defects in crystalline solids', Physical Society  
(1955) 175.
171. R.Castaing and A.Guinier,  
Comptes Rendus 228 (1949) 2033.
172. A.H.Cottrell,  
'Vacancies and other point defects in metals and  
alloys', Inst. Metals (1958) 1.
173. G.Thomas and J.Nutting,  
'The mechanism of phase transformations in metals',  
Inst. Metals (1956) 57.
174. T.V.Rajan and M.N.Saxena,  
Trans. I.I.M. 23 (1970) 64.
175. G.Sauthoff,  
Scripta Met. 10 (1976) 557.
176. H.Tamler, O.Kanert, W.H.M. Alsem and J.Th.M.DeHosson,  
Acta Met. 30 (1982) 1523.
177. R.Roberge, K.Krishna Rao and H.Herman,  
J.Inst. Metals 97 (1969) 53.

178. U.Köster and E.Hornbogen,  
Z.Metallkunde 59 (1968) 792.
179. H.Ahlborn, E.Hornbogen and U.Köster,  
J.Mater. Sci. 4 (1969) 944.
180. R.B.Nicholson,  
'Electron microscopy and strength of crystals',  
Interscience, New York(1963).
181. Vincent C.Nardone and John K. Tien,  
Scripta Met.17(1983) 467.
182. U.Köster,  
'Recrystallisation of metallic materials',  
Dr.Riederer Verlag, Stuttgart (1970).
183. D.B.Goel, P.Furrer and H.Warlimont,  
Aluminium 50 (1974) 641.
184. M.R.Staker and D.L. Holt,  
Acta Met.20 (1972) 569.
185. R.D.Doherty and J.W.Martin,  
J.Inst. Metals 91(1963) 332.
186. J.S.Santner and D.Eylon,  
Met. Trans. 10A (1979) 841.
187. C.Y.Kung and M.E.Fine,  
Met. Trans.10A (1979) 603.
188. H.Abdel-Raouf, T.H.Topper and A.Plumtree,  
Met.Trans.10A (1979) 449.
189. W.Vogel, M.Wilhelm and V.Gerold,  
Acta Met.30 (1982) 21 and 31.
190. K.J.Nix and H.M.Flower,  
Acta Met.30 (1982) 1549.

191. M.Wilhelm, M.Nageswararao and R.Meyer,  
ASTM STP 675, Amer. Soc. for Testing and Materials  
(1979) 214.
192. T.Broom, J.H.Molineux and V.N.Whittaker,  
J.Inst. Metals 84 (1955) 357.
193. S.Pilecki,  
Proc. of 4th Int. Conf. on Fracture, Waterloo,  
Canada 2 (1977) 687.
194. J.M.Papazian, R.J.DeIasi and P.N.Adler,  
Met. Trans. 11A(1980) 135.
195. C.Calabrese and C.Laird,  
Mater. Sci.Eng.13(1974) 141.
196. R.E.Stoltz and R.M.Pelloux,  
Met. Trans. 7A(1976) 1295.
197. T.H.Sanders, Jr. and E.A. Strake, Jr.,  
Met. Trans.7A(1976) 1407.
198. R.G.Pahl, Jr. and J.B.Cohen,  
Met. Trans. 15A (1984) 1519.
199. R.J.H.Wanhill,  
Met.Trans.6A(1975) 1587.
200. J.H.Mulherin and H.Rosenthal,  
Met. Trans.2A(1971) 427.
201. C.J.Peel and P.J.E.Forsyth,  
Metal Sci. J.7 (1973) 121.
202. B.J.Dunwoody, D.M.Moore and A.T.Thomas,  
J.Inst.Metals 101(1973) 172.
203. G.T.Hahn and A.R.Rosenfield,  
Met. Trans.6A (1975) 653.

204. B.Lou and B.L. Averbach,  
Met. Trans. 14A(1983) 1889.
205. A.N.Kumar and R.K.Pandey,  
Mater. Sci. Eng. 63(1984)121.
206. G.T.Hahn,  
Met. Trans. 15A(1984) 947.
207. R.O.Ritchie and A.W.Thompson,  
Met. Trans. 16A (1985) 233.

\*\*\*\*\*  
APPENDIX

TABLES OF EXPERIMENTAL RESULTS  
\*\*\*\*\*

## APPENDIX

Table-1  
Hardness and tensile properties during ageing at 160°C

S.N.	Time (hrs)	Hardness (VHN)	UTS (N/mm <sup>2</sup> )	YS (N/mm <sup>2</sup> )	Elongation (Pct.)
1	0.00	59.33	245.18	198.10	22.00
2	0.25	61.40	-	-	-
3	0.40	63.50	-	-	-
4	0.75	66.00	-	-	-
5	1.00	69.40	272.63	216.73	21.05
6	1.50	72.00	-	-	-
7	2.00	74.70	286.36	230.46	20.10
8	2.50	79.70	-	-	-
9	3.00	82.20	302.06	245.18	18.90
10	3.50	84.10	-	-	-
11	4.00	86.20	311.86	254.98	18.20
12	4.50	91.00	-	-	-
13	5.00	95.30	322.65	274.56	17.40
14	5.75	100.40	-	-	-
15	6.00	-	339.32	289.30	16.60
16	6.50	106.10	-	-	-
17	7.50	112.10	369.72	305.98	15.90
18	8.50	114.00	375.12	313.82	15.00
19	9.50	110.10	361.88	304.02	16.00
20	10.50	105.10	348.15	289.30	16.50
21	13.00	102.00	-	-	-
22	16.00	96.30	-	-	-



Table-2

Hardness and tensile properties during TMA Ia treatment

S.No	Condition	Hardness (VHN)	UTS (N/mm <sup>2</sup> )	YS (N/mm <sup>2</sup> )	Elonga- tion (Pct.)
1.	25 pct. preaged	73.10	284.40	254.98	18.50
2.	25 pct. preaged and 10 pct. deformed	94.50	320.68	286.36	17.30
	25 pct. preaged, 10 pct. deformed and further aged for (hrs):				
3.	0.50	100.20	-	-	-
4.	1.00	105.50	338.34	305.00	16.20
5.	2.00	113.50	349.13	316.76	15.00
6.	3.00	119.20	360.90	323.63	14.00
7.	3.50	123.00	-	-	-
8.	4.00	-	374.62	334.42	13.40
9.	4.50	130.50	-	-	-
10.	5.00	-	388.36	341.28	12.70
11.	5.50	134.10	-	-	-
12.	6.00	137.20	404.05	347.16	12.00
13.	7.00	131.50	392.28	343.24	12.50
14.	8.00	126.10	378.55	336.38	13.20
15.	9.00	120.20	-	-	-

Table-3

Hardness and tensile properties during TMA Ib treatment:

S.No.	Condition	Hardness (VHN)	UTS (N/mm <sup>2</sup> )	YS (N/mm <sup>2</sup> )	Elonga- tion (Pct.)
1.	25 pct. preaged	73.10	284.40	254.98	18.50
2.	25 pct. preaged and 20 pct. def- ormed	97.90	333.44	304.02	15.90
	25 pct. preaged, 20 pct. deformed and further aged for (hrs):				
3.	0.50	105.10	344.22	324.61	14.00
4.	1.00	110.20	-	-	-
5.	1.50	-	358.94	335.40	13.10
6.	2.00	121.40	-	-	-
7.	2.50	-	372.66	344.22	12.30
8.	3.00	128.10	-	-	-
9.	3.50	132.30	388.36	355.01	11.10
10.	4.50	136.10	402.08	363.84	10.70
11.	5.00	139.00	-	-	-
12.	5.50	144.80	426.10	372.66	10.00
13.	6.00	139.70	-	-	-
14.	6.50	131.70	411.90	365.80	10.50
15.	7.50	125.20	400.12	355.01	11.00
16.	8.00	120.20	-	-	-
17.	8.50	-	392.28	354.03	11.00
18.	9.00	117.20	-	-	-

Table 4

Hardness and tensile properties during TMA IIa treatment

S.No.	Condition	Hardness (VHN)	UTS (N/mm <sup>2</sup> )	YS (N/mm <sup>2</sup> )	Elongation (Pct.)
1.	50 pct. preaged	87.00	313.82	284.40	15.00
2.	50 Pct. Preaged and 10 pct. deformed	98.60	341.28	305.00	13.00
	50 Pct. Preaged, 10 pct. deformed and further aged for (hrs.):				
3.	0.50	110.20	355.01	321.67	12.50
4.	1.00	117.30	370.70	334.42	11.90
5.	1.50	119.30	-	-	-
6.	2.00	126.30	386.40	346.18	11.40
7.	2.50	134.00	-	-	-
8.	2.75	141.20	416.80	364.82	10.50
9.	3.50	132.60	390.32	348.15	11.20
10.	4.00	129.10	-	-	-
11.	4.50	-	372.66	335.40	11.50
12.	5.00	119.20	-	-	-
13.	5.50	-	357.96	323.63	12.20
14.	6.00	114.00	-	-	-
15.	8.00	110.40	-	-	-
16.	10.00	107.50	-	-	-

Table-5

Hardness and tensile properties during TMA IIb treatment

S.No.	Condition	Hardness (VHN)	UTS (N/mm <sup>2</sup> )	YS (N/mm <sup>2</sup> )	Elongation (Pct.)
1.	50 pct. Preaged	87.00	313.82	284.40	15.00
2.	50 pct. preaged and 20 Pct. deformed	123.00	370.70	345.20	13.50
	50 pct. preaged, 20 pct. deformed and further aged for (hrs):				
3.	0.50	130.70	387.38	362.86	11.50
4.	1.00	135.50	413.85	381.50	10.60
5.	1.50	142.10	-	-	-
6.	2.00	148.00	431.50	392.28	9.50
7.	2.50	137.10	-	-	-
8.	3.00	130.70	390.32	363.84	11.30
9.	4.00	126.20	372.66	348.15	12.90
10.	5.00	-	362.86	338.34	13.20
11.	6.00	117.20	-	-	-
12.	8.00	114.30	-	-	-

Table-6

Hardness values during ageing at 160°C  
after 75 pct. preageing and 10 pct. deformation

S.No.	Condition	Hardness (VHN)
1.	75 pct. preaged	101.00
2.	75 pct. preaged and 10 pct. deformed	116.20
	75 pct. preaged, 10 pct. deformed and further aged for (hrs.):	
3.	0.50	121.50
4.	0.75	124.30
5.	1.00	127.60
6.	1.25	129.90
7.	1.50	132.50
8.	1.75	131.60
9.	2.00	129.80
10.	2.50	126.20

Table-6

Hardness values during ageing at 160°C  
after 75 pct. preageing and 10 pct. deformation

S.No.	Condition	Hardness (VHN)
1.	75 pct. preaged	101.00
2.	75 pct. preaged and 10 pct. deformed	116.20
	75 pct. preaged, 10 pct. deformed and further aged for (hrs.):	
3.	0.50	121.50
4.	0.75	124.30
5.	1.00	127.60
6.	1.25	129.90
7.	1.50	132.50
8.	1.75	131.60
9.	2.00	129.80
10.	2.50	126.20

Table -7

Hardness values during ageing at  
160°C after 75 pct.preageing and 20 pct.  
deformation

S.No.	Condition	Hardness (VHN)
1.	75 pct. preaged	101.00
2.	75 pct.preaged and 20 pct.deformed	122.80
	75 pct.preaged, 20 pct. deformed and further aged for (hrs.):	
3.	0.50	128.50
4.	0.75	132.60
5.	1.00	138.80
6.	1.25	137.60
7.	1.50	137.00
8.	2.00	135.10
9.	2.50	133.20

Table-8

Hardness values on subsequent ageing after peak ageing and 10 pct. deformation

S.No.	Condition	Hardness (VHN)
1.	Peak aged	114.00
2.	Peak aged and 10 pct. deformed	130.10
	Peak aged, 10 pct. deformed and further aged for (hrs):	
3.	0.50	129.40
4.	1.00	129.00
5.	1.50	128.30
6.	2.00	127.80

Table-9

Hardness values on subsequent ageing after peak ageing and 20 pct. deformation

S.No.	Condition	Hardness (VHN)
1.	Peak aged	114.00
2.	Peak aged and 20 pct. deformed	137.20
	Peak aged, 20 pct. deformed and further aged for (hrs.):	
3.	0.50	136.80
4.	1.00	136.30
5.	1.50	135.80
6.	2.00	135.20



Table-10

Peak age values of hardness and tensile properties after different treatments

S.No.	Treatment	Hardness (VHN)	UTS (N/mm <sup>2</sup> )	YS (N/mm <sup>2</sup> )	Elongation (Pct.)
1.	As quenched	59.33	245.18	198.10	22.00
2.	Peak Aged	114.00	375.12	313.82	15.00
3.	TMA Ia	137.10	404.05	347.16	12.00
4.	TMA Ib	144.80	426.10	372.66	10.00
5.	TMA IIa	141.20	416.80	364.82	10.50
6.	TMA IIb	148.00	431.50	392.28	9.50

Table -11

Room temperature tensile properties of peak aged alloy after 100 hour exposure at various temperatures

S.No.	Temperature (°C)	UTS (N/mm <sup>2</sup> )	YS (N/mm <sup>2</sup> )	Elongation (Pct.)
1.	Room temp.	375.12	313.82	15.00
2.	100	347.16	289.30	17.00
3.	150	306.96	254.98	21.00
4.	200	250.08	201.04	26.00
5.	250	178.48	147.10	32.00

Table-12

Room temperature tensile properties of TMA Ia treated alloy after 100 hour exposure at various temperatures

S.N.	Temperature °C	UTS (N/mm <sup>2</sup> )	Y.S. (N/mm <sup>2</sup> )	Elonga- tion (pct.)
1.	Room temp.	404.04	347.16	12.00
2.	100	372.66	320.68	13.00
3.	150	323.63	279.50	15.00
4.	200	274.60	235.36	19.00
5.	250	225.56	191.24	25.40

Table-13

Room temperature tensile properties of TMA Ib treated alloy after 100 hour exposure at various temperatures

S.No.	Temperature °C	UTS (N/mm <sup>2</sup> )	YS (N/mm <sup>2</sup> )	Elongation (Pct.)
1.	Room temp.	426.11	372.66	10.00
2.	100	392.28	357.96	11.00
3.	150	348.15	323.63	13.00
4.	200	318.73	282.44	15.00
5.	250	294.21	264.78	19.20

Table-14

Room temperature tensile properties of TMA IIa treated alloy after 100 hour exposure at various temperatures

S.No.	Temperature °C	UTS (N/mm <sup>2</sup> )	YS (N/mm <sup>2</sup> )	Elongation (pct.)
1.	Room temp.	416.80	364.82	10.50
2.	100	382.47	343.24	11.60
3.	150	337.36	304.02	12.80
4.	200	294.21	264.78	16.00
5.	250	254.98	225.56	21.00

Table-15

Room temperature tensile properties of TMA IIb treated alloy after 100 hour exposure at various temperatures

S.No.	Temperature °C	UTS (N/mm <sup>2</sup> )	YS (N/mm <sup>2</sup> )	Elongation (Pct.)
1	Room Temp.	431.50	392.28	9.50
2	100	416.80	382.47	10.60
3	150	392.28	362.86	12.00
4	200	376.58	348.15	14.20
5	250	346.18	318.72	18.00

Table-16

Fatigue properties of as quenched alloy at various levels

S.No.	Stress (s) N/mm <sup>2</sup>	Number of cycles to failure (N)	Fatigue ratio ( $\sigma_1$ /UTS)
1	98	4.00x10 <sup>6</sup>	0.40
2	118	2.80x10 <sup>6</sup>	0.48
3	137	7.00x10 <sup>5</sup>	0.56
4	157	3.60x10 <sup>5</sup>	0.64
5	177	7.50x10 <sup>4</sup>	0.72

Table-17

Fatigue properties of peak aged alloy at various stress levels

S.No.	Stress (S) N/mm <sup>2</sup>	Number of cycles to failure (N)	Fatigue ratio ( $\sigma_1$ /UTS)
1.	98	2.36x10 <sup>6</sup>	0.261
2.	118	0.80x10 <sup>6</sup>	0.313
3.	137	4.20x10 <sup>5</sup>	0.366
4.	157	1.30x10 <sup>5</sup>	0.418
5.	177	6.60x10 <sup>4</sup>	0.470

Table-18-

Fatigue properties of TMA Ia treated alloy at various stress levels

S.No.	Stress (S) N/mm <sup>2</sup>	Number of cycles to failure (N)	Fatigue ratio ( $\sigma_1$ /UTS)
1.	118	10 <sup>7</sup> (did not fail)	0.291
2.	137	1.20x10 <sup>6</sup>	0.339
3.	157	3.50x10 <sup>5</sup>	0.388
4.	177	1.30x10 <sup>5</sup>	0.437

Table-19

Fatigue properties of TMA Ib treated alloy at various stress levels

S.No.	Stress (S) N/mm <sup>2</sup>	Number of cycles to failure (N)	Fatigue ratio ( $\sigma_1$ /UTS)
1	118	10 <sup>7</sup> (did not fail)	0.276
2	137	1.70x10 <sup>6</sup>	0.322
3	157	5.00x10 <sup>5</sup>	0.368
4	177	1.70x10 <sup>5</sup>	0.414

Table-20

Fatigue properties of TMA IIa treated alloy at various stress levels

S.No.	Stress(S) N/mm <sup>2</sup>	Number of Cycles to failure(N)	Fatigue ratio ( $\sigma_1$ /UTS)
1.	118	$1.80 \times 10^6$	0.282
2.	137	$6.00 \times 10^5$	0.329
3.	157	$2.50 \times 10^5$	0.376
4.	177	$9.40 \times 10^4$	0.423

Table-21

Fatigue properties of TMA IIb treated alloy at various stress levels

S.No.	Stress(S) N/mm <sup>2</sup>	Number of cycles to failure(N)	Fatigue ratio ( $\sigma_1$ /UTS)
1.	118	$3.00 \times 10^6$	0.272
2.	137	$1.00 \times 10^6$	0.318
3.	157	$3.20 \times 10^5$	0.363
4.	177	$1.00 \times 10^5$	0.409

Table-22

Fatigue life at various endurance limits (derived from Fig.4.11)

S.No.	Treatment	Fatigue life (cycles)			
		120 N/mm <sup>2</sup>	140 N/mm <sup>2</sup>	160 N/mm <sup>2</sup>	180 N/mm <sup>2</sup>
1	As quenched	1.50x10 <sup>6</sup>	4.80x10 <sup>5</sup>	1.80x10 <sup>5</sup>	7.00x10 <sup>4</sup>
2	Peak aged	8.00x10 <sup>5</sup>	2.90x10 <sup>5</sup>	1.10x10 <sup>5</sup>	5.00x10 <sup>4</sup>
3	TMA Ia	6.00x10 <sup>6</sup>	1.00x10 <sup>6</sup>	3.20x10 <sup>5</sup>	1.10x10 <sup>5</sup>
4	TMA Ib	8.00x10 <sup>6</sup>	1.50x10 <sup>6</sup>	4.50x10 <sup>5</sup>	1.40x10 <sup>5</sup>
5	TMA IIa	1.80x10 <sup>6</sup>	5.30x10 <sup>5</sup>	2.20x10 <sup>5</sup>	8.40x10 <sup>4</sup>
6	TMA IIb	2.60x10 <sup>6</sup>	8.20x10 <sup>5</sup>	2.70x10 <sup>5</sup>	9.40x10 <sup>4</sup>

Table -23

## Plane strain fracture toughness data

S.No.	Treatment	Notch-tensile strength (N/mm <sup>2</sup> )	$K_{Ic}$ (N/mm <sup>3/2</sup> )
1.	As quenched	202.44	401.32
2.	Peak aged	323.64	641.58
3.	TMA Ia	353.05	699.88
4.	TMA Ib	416.80	826.26
5.	TMA IIa	388.85	770.85
6.	TMA IIb	417.78	828.20



Table-24

## Dynamic fracture toughness data

S.No.	Treatment	Energy absorbed per unit area CVN/A (J/mm <sup>2</sup> )	$K_{Id}$ (N/mm <sup>3/2</sup> )	Dynamic fracture toughness parameters $K_{Id}^2/E$ (N/mm)
1.	As quenched	0.1420	754.00	7.78
2.	Peak aged	0.1296	720.00	7.10
3.	TMA Ia	0.2143	926.00	11.74
4.	TMA Ib	0.2809	1060.00	15.38
5.	TMA IIa	0.2284	956.00	12.56
6.	TMA IIb	0.3410	1168.00	18.68

Table-25

Space-to-size ratio ( $\lambda/d$ ) of dispersoids  
after various treatments

S.No.	Treatment	Average diameter d ( $\mu$ )	Average inter-particle spacing $\lambda$ ( $\mu$ )	Space-to-size ratio $\lambda/d$
1.	As quenched	1.05	2.75	2.67
2.	Peak aged	2.60	3.70	1.42
3.	TMA Ia	1.30	4.60	3.54
4.	TMA Ib	1.15	5.80	4.90
5.	TMA IIa	1.40	5.15	3.72
6.	TMA IIb	1.70	9.00	5.30

Table-26

Increase in various properties from peak age value after different TMA treatments

S.No.	Properties	Peak Age	Increase (pct.)			
			TMA Ia	TMA Ib	TMA IIa	TMA IIb
1.	Hardness (VHN)	114.00	20.26	27.00	23.86	29.82
2.	UTS (N/mm <sup>2</sup> )	375.12	7.71	13.60	11.11	15.03
3.	Room temp. UTS after 100 hour exposure at 250°C (N/mm <sup>2</sup> )	178.48	26.38	64.84	42.86	93.96
4.	Endurance limit for 10 <sup>6</sup> cycles (N/mm <sup>2</sup> )	116.00	20.70	26.72	12.94	18.10
5.	K <sub>Ic</sub> (N/mm <sup>3/2</sup> )	641.58	9.09	28.78	20.15	29.09
6.	K <sub>Ia</sub> (N/mm <sup>3/2</sup> )	720.00	28.61	47.22	32.77	62.22